Nonlocal Neumann volume-constrained problems and their application to local-nonlocal coupling

Yunzhe Tao

Submitted in partial fulfillment of the
requirements for the degree
of Doctor of Philosophy
in the Graduate School of Arts and Sciences

COLUMBIA UNIVERSITY

2019

ABSTRACT

Nonlocal Neumann volume-constrained problems and their application to local-nonlocal coupling

Yunzhe Tao

As alternatives to partial differential equations (PDEs), nonlocal continuum models given in integral forms avoid the explicit use of conventional spatial derivatives and allow solutions to exhibit desired singular behavior. As an application, peridynamic models are reformulations of classical continuum mechanics that allow a natural treatment of discontinuities by replacing spatial derivatives of stress tensor with integrals of force density functions.

The thesis is concerned about the mathematical perspective of nonlocal modeling and local-nonlocal coupling for fracture mechanics both theoretically and numerically. To this end, the thesis studies nonlocal diffusion models associated with "Neumann-type" constraints (or "traction conditions" in mechanics), a nonlinear peridynamic model for fracture mechanics with bond-breaking rules, and a multi-scale model with local-nonlocal coupling.

In the computational studies, it is of practical interest to develop robust numerical schemes not only for the numerical solution of nonlocal models, but also for the evaluation of suitably defined derivatives of solutions. This leads to a posteriori nonlocal stress analysis for structure mechanical models.

Table of Contents

List of Figures

List of Tables

Acknowledgments

I would like to express my great appreciation to Professor Qiang Du, my research advisor and role model, for his patient guidance, enthusiastic encouragement and useful critiques of the thesis work, and for his priceless suggestions and active support of my career. His sober, honest, and curious personality and high sense of responsibility have strongly influenced me for years. I am grateful to having such a mentor in my Ph.D. study and my life.

In addition, I would also like to thank my committee members, Professors Michael Weinstein, Kyle Mandli, Kui Ren, and Steve Sun for their constructive comments, and my colleagues during my internship in Oak Ridge National Lab, especially Dr. Pablo Seleson, who provided me insightful ideas and research directions.

My deep thanks are also extended to my group members Xiaochuan Tian, Jiang Yang, Zhi Zhou, Qi Sun, Dong Wang, and Hwi Lee, and my friends Tingkai Liu, Wei Liu, and Ju Sun for their support both academically and personally.

I am particularly grateful to my parents for their unremitting help and encouragement in the past 27 years. I always remember the words that my father told me, "Do your best and leave the rest", which become the attitude how I treat my work and potential opportunities.

Finally, I would like to offer my special thanks to Wen. Without her support and suggestions, I cannot finish my graduate study and set up my career so smoothly.

Chapter 1

Introduction

Nonlocal peridynamic (PD) models initially proposed by Silling [Silling, 2000] have been subjects of recent studies. Such models are reformulations of classical continuum mechanics that allow a natural treatment of discontinuities by replacing spatial derivatives of stress tensors with integrals of force density functions. As an alternative to classical partial differential equation (PDE) based models, PD models have been shown to be effective in modeling cracks and materials failure as well as other mechanical properties and physical processes [Askari *et al.*, 2008; Silling and Lehoucq, 2010; Silling *et al.*, 2010; Palatucci *et al.*, 2013]. A distinct feature of PD models (also shared among other nonlocal models) is that the range of nonlocal interactions is bounded by a positive parameter, the so called horizon parameter δ [Silling, 2000]. For suitably defined nonlocal interaction kernels, as $\delta \to 0$, interactions can become localized so that the zero-horizon limit of the nonlocal operators, when it exists, becomes a local differential operator. That is, a nonlocal model gets reduced to a conventional differential equation model in the local limit.

Although more refined models, such as [Silling *et al.*, 2007; Aguiar and Fosdick, 2014], have been proposed in the literature, the models proposed in [Silling, 2000] are simple enough for the purpose of mathematical analysis and are still physically meaningful. Let $\mathbf{u} = \mathbf{u}(t, \mathbf{x})$ denote the displacement field and ρ be the constant density, the bond-based PD equation of motion [Silling, 2000] is given by an integro-

differential equation of the form

$$\rho\ddot{\mathbf{u}}(t,\mathbf{x}) = \int_{B_\delta(\mathbf{x})} \mathbf{f}(t,\mathbf{u}(t,\hat{\mathbf{x}}) - \mathbf{u}(t,\mathbf{x}), \hat{\mathbf{x}} - \mathbf{x}) d\hat{\mathbf{x}} + \mathbf{b}(t,\mathbf{x}) \,, \tag{1.1}$$

where $\mathbf{b} = \mathbf{b}(t,\mathbf{x})$ denotes the body force, and $\mathbf{f}$ is the pairwise force density. $B_\delta(\mathbf{x})$ is the ball of radius δ centered at $\mathbf{x}$ and specifies the extent of nonlocal interactions. Each pair $(\hat{\mathbf{x}}, \mathbf{x})$ for $\hat{\mathbf{x}} \in B_\delta(\mathbf{x})$ is called a bond. The constitutive model, previously used in the PD model for prototype microelastic brittle (PMB) materials [Lehoucq *et al.*, 2008], is defined as

$$\mathbf{f}(t,\boldsymbol{\eta}(t),\boldsymbol{\xi}) = \omega_\delta(|\boldsymbol{\xi}|)\mathcal{S}(\boldsymbol{\eta}(t),\boldsymbol{\xi})\mathbf{e}(\boldsymbol{\eta}(t),\boldsymbol{\xi}) \,, \tag{1.2}$$

where $\boldsymbol{\eta}(t)$ and $\boldsymbol{\xi}$ are used to denote $\mathbf{u}(t,\hat{\mathbf{x}}) - \mathbf{u}(t,\mathbf{x})$ and $\hat{\mathbf{x}} - \mathbf{x}$ respectively (see Figure 1.1). The unit vector $\mathbf{e}$ for bond direction and the bond relative elongation (stretch) $\mathcal{S}$ are given by

$$\mathbf{e}(\boldsymbol{\eta},\boldsymbol{\xi}) = \frac{\boldsymbol{\eta}+\boldsymbol{\xi}}{|\boldsymbol{\eta}+\boldsymbol{\xi}|} \quad \text{and} \quad \mathcal{S}(\boldsymbol{\eta},\boldsymbol{\xi}) = \frac{|\boldsymbol{\eta}+\boldsymbol{\xi}| - |\boldsymbol{\xi}|}{|\boldsymbol{\xi}|} \,, \tag{1.3}$$

where $|\cdot|$ denotes the Euclidean norm. When the bond-breaking rule (more detailed discussion can be found in Chapter 3) is incorporated in order to model the cracks, the force density $\mathbf{f}$ also takes on history dependence, so the dynamic system is in fact a distributed system of spatially nonlocal functional differential equations. Many numerical simulations based on the PD theory have been carried out thereafter [Askari *et al.*, 2008; Oterkus and Madenci, 2012; Ha and Bobaru, 2010; Hu *et al.*, 2012].

Due to the nonlocality and nonlinearity involved in the PD models, rigorous theoretical and numerical analysis is challenging. Therefore, recent studies usually focus on the linearized models [Aksoylu and Parks, 2011; Andreu-Vaillo *et al.*, 2010; Du *et al.*, 2013b; Du *et al.*, 2012; Mengesha and Du, 2014a; Mengesha and Du, 2014b; Emmrich *et al.*, 2007; Mengesha and Du, 2016]. When $|\boldsymbol{\eta}(t)|$ is uniformly small, the force density function can be linearized as

$$\mathbf{f}(t,\boldsymbol{\eta}(t),\boldsymbol{\xi}) = \omega_\delta(|\boldsymbol{\xi}|)\frac{\boldsymbol{\xi}\otimes\boldsymbol{\xi}}{|\boldsymbol{\xi}|^3}\boldsymbol{\eta}(t) \,. \tag{1.4}$$

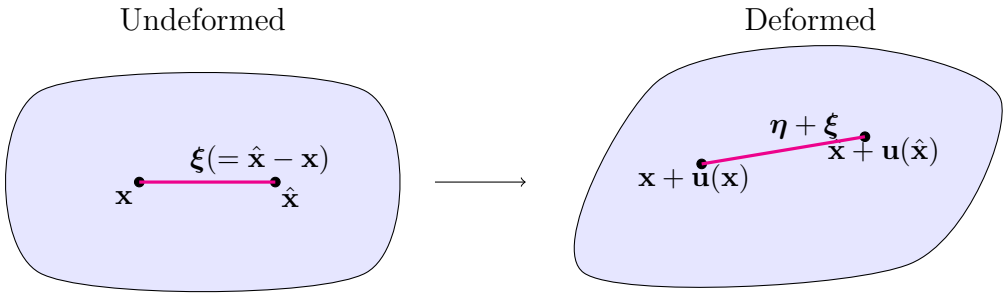

Figure 1.1: Undeformed bond and deformed bond.

For an isotropic system, the PD equation of motion takes the form

$$\rho\ddot{\mathbf{u}}(t,\mathbf{x}) = \int_{B_\delta(\mathbf{x})} \mathbb{C}_\delta(\hat{\mathbf{x}}-\mathbf{x})(\mathbf{u}(t,\hat{\mathbf{x}})-\mathbf{u}(t,\mathbf{x}))d\hat{\mathbf{x}} + \mathbf{b}(t,\mathbf{x})\,, \tag{1.5}$$

where the micromodulus tensor $\mathbb{C}_\delta(\boldsymbol{\xi})$ is given by

$$\mathbb{C}_\delta(\boldsymbol{\xi}) = \gamma_\delta(|\boldsymbol{\xi}|)\frac{\boldsymbol{\xi}\otimes\boldsymbol{\xi}}{|\boldsymbol{\xi}|^2}\,, \tag{1.6}$$

with $\gamma_\delta(|\boldsymbol{\xi}|) = \omega_\delta(|\boldsymbol{\xi}|)/|\boldsymbol{\xi}|$, the so-called kernel function in our study.

In order to systematically study the mathematical and numerical issues of PD models, we are particularly interested in the equilibrium system in the scalar field, namely

$$-\int_{B_\delta(\mathbf{x})} \gamma_\delta(|\hat{\mathbf{x}}-\mathbf{x}|)(\mathbf{u}(\hat{\mathbf{x}})-\mathbf{u}(\mathbf{x}))d\hat{\mathbf{x}} = \mathbf{b}(\mathbf{x})\,. \tag{1.7}$$

The kernel function γ_δ of our interest in the thesis is assumed to be symmetric, non-negative, and compactly supported in $B_\delta(\mathbf{0})$. In addition, we also assume that γ_δ has finite second moment, namely

$$\int_{\mathbb{R}^d} \gamma_\delta(|\hat{\mathbf{x}}-\mathbf{x}|)|\hat{\mathbf{x}}-\mathbf{x}|^2 d\hat{\mathbf{x}} = \int_{B_\delta(\mathbf{0})} \gamma_\delta(|\boldsymbol{\xi}|)|\boldsymbol{\xi}|^2 d\boldsymbol{\xi} < \infty\,. \tag{1.8}$$

A popular case to study is given by the following rescaled form:

$$\gamma_\delta(|\boldsymbol{\xi}|) = \frac{1}{\delta^{d+2}}\gamma(\frac{|\boldsymbol{\xi}|}{\delta})\,, \tag{1.9}$$

with γ being a non-increasing function having compact support in a unit ball. The rescaled form (1.9) helps us study the limit case as $\delta \to 0$ since $|\boldsymbol{\xi}|^2\gamma_\delta(|\boldsymbol{\xi}|)$ reduces to the Dirac-Delta measure in the zero limit so that local models can be recovered.

In addition, a feature of nonlocal models, different from the local PDEs, is the treatment of interfaces and domain boundaries. Unlike local boundary conditions, the nonlocal analog may be attributed to how the law of nonlocal interactions gets modified in the presence of physical boundary. Therefore, the condition of volumetric constraint [Du *et al.*, 2012] is proposed as the nonlocal boundary condition, which is imposed on a δ-neighborhood of the domain. In the thesis, we are interested in the Neumann type volumetric constraints since most works that simulate PD systems use traction boundary conditions [Oterkus and Madenci, 2012; Ha and Bobaru, 2010; Hu *et al.*, 2012; Bobaru and Zhang, 2015], which is mathematically equivalent to the Neumann conditions. Nonlocal Neumann problems are not only interesting on their own but also play important roles in interface problems, free boundary problems, the coupling and domain decomposition of nonlocal problems. It is known that Neumann type problems present substantial differences from that on Dirichlet type problems for nonlocal equations [Alali and Gunzburger, 2015; Andreu-Vaillo *et al.*, 2010; Barles *et al.*, 2014a; Barles *et al.*, 2014a; Cortazar *et al.*, 2008; Dipierro *et al.*, 2014; Mengesha and Du, 2016; Zhou and Du, 2010]. Moreover, we are particularly interested in the convergence analysis of the nonlocal models to their local limit in the horizon parameter δ as $\delta \to 0$, both theoretically and numerically.

Given the mathematical and numerical understanding on linear nonlocal models with Neumann type conditions, we are also interested in the numerical simulation and convergence study of the nonlinear PD model for brittle fracture. As mentioned above, the PD model that incorporates the bond-breaking rule leads to a dynamic system of time dependent differential integral equations having both spatial nonlocal/nonlinear interactions and temporal memory/history dependence. By incorporating the nonlocal Neumann conditions, we want the PD model to not only capture the crack propagation and branching patterns, but also present the convergence phenomenon in the discrete level.

Another aspect of nonlocal formulations of mechanics is that the equations are

posed in terms of displacement or displacement field. In applications like structure analysis, the primary interest might be in the deformation gradient or, through appropriate constitutive relation, the stress, rather than the deformation itself. Therefore, the development of accurate and robust numerical schemes is needed for not only nonlocal solutions but also their suitably defined nonlocal spatial derivatives. For traditional PDEs models, various numerical techniques have been developed in order to achieve accurate evaluations of solution derivatives, *e.g.*, local gradient recovery (mostly done by a posteriori error estimation [Zienkiewicz and Zhu, 1992]). Although the PD stress tensor has been introduced [Silling, 2000], gradient recovery techniques for nonlocal models remain largely unexplored in the literature.

While nonlocal modeling has its advantage on complex physical processes, nonlocal model based numerical simulations often incur higher computational cost than those based on traditional local models. Therefore, local-nonlocal coupling is a natural approach in practice and various strategies have been proposed [D'Elia *et al.*, 2016; Du *et al.*, 2018a; Du *et al.*, 2016a; Mitchell *et al.*, 2015; Seleson *et al.*, 2015]. On the other hand, while the horizon parameter is often chosen as a positive constant over the spatial domain in most of the earlier studies, in [Silling *et al.*, 2015], models with a variable horizon having a positive lower bound over the domain have also been examined. In [Tian and Du, 2017], the variable horizon adopted there is allowed to vanish as the material points approach a co-dimension one hyper-surface. With a vanishing horizon, nonlocal models get localized heterogeneously. Unlike nonlocal models with a constant horizon that are generically accompanied by volumetric constraints, models with heterogeneous localization allow conventional boundary conditions to be imposed [Tian and Du, 2017]. This is the topic that we like to further explore. We want to see if there is any difference on the nonlocal Neumann problems, and the convergence on the nonlocal and local-nonlocal coupling problems.

Motivated by the above issues in nonlocal modeling, we study the following mathematical and numerical questions in the thesis (more general discussion of the nonlocal

modeling, analysis and computation can be found in [Du, 2018; Du, 2019]). First, we aim to provide the proper formulation of Neumann conditions in Chapter 2 and the numerical approximations for the nonlocal Neumann problems. The discussion can also be found in [Tao *et al.*, 2017]. Secondly, we present in Chapter 3 the numerical simulation and convergence study of a PD model for brittle fracture with bond breaking rules. We aim to carry out numerical simulations based on the modified PD model in [Tian, 2017], which have been shown as a portion of [Du *et al.*, 2017a]. In addition, in Chapter 4, most of which can also be found in [Du *et al.*, 2016b], we make some preliminary investigations on the nonlocal gradient recovery. At last, we discuss a couple of remedies in Chapter 5 to address the nonlocal problems and local-nonlocal coupling problems with variable horizon. The methods have also been studied in [Du *et al.*, 2018b].

Chapter 2

Nonlocal diffusion models with Neumann type constraints

This chapter studies nonlocal diffusion models associated with Neumann type constraints and their numerical approximations (also in [Tao *et al.*, 2017]). The study here is parallel to the traditional analysis of local second order elliptic equations as well as the analysis of nonlocal diffusion models with Dirichlet type constraints, but with necessary modifications. We refer to [Du *et al.*, 2012] for more discussions on the differences and connections between local and nonlocal steady-state diffusion problems.

Moreover, for nonlocal models characterized by the parameter δ, it has been known in the literature that as $\delta \to 0$, one often encounter consistency issues at both continuum and discrete levels between the nonlocal models and the local PDEs, when the latter remain valid. On the continuum level, the consistency has been established either formally using Taylor expansions of sufficiently smooth solutions [Silling, 2000; Silling and Lehoucq, 2010], or more rigorously via functional analytic means without extra regularity assumptions [Mengesha and Du, 2013; Mengesha and Du, 2016; Tian and Du, 2014]. With the increasing interests in developing efficient codes for nonlocal models, it is often asked if numerical schemes developed for nonlocal models

would produce results consistent with that produced by the local limit models when the horizon is small and with sufficient numerical resolution. Answering such questions on the discrete level is an important task of code validation and verification. In [Tian and Du, 2014], a theory of asymptotically compatible schemes was developed. It was successfully applied to nonlocal models with Dirichlet type nonlocal volumetric constraints. Given the extra complications involved in the nonlocal Neumann type problems, we then discuss the numerical approximations including standard finite element methods and quadrature based finite difference methods in this chapter. We study their convergence in the nonlocal setting and in the local limit.

2.1 The variational problem

We first introduce a nonlocal variational problem with Neumann type volume constraints. Let $\Omega \subset \mathbb{R}^d$ denote a bounded, open domain with a piecewise planar boundary. Consider the nonlocal energy functional

$$E(u) = \frac{1}{2}\int_\Omega \int_\Omega \gamma_\delta(\mathbf{x}', \mathbf{x}) \left(u(\mathbf{x}') - u(\mathbf{x})\right)^2 d\mathbf{x}' d\mathbf{x}\,, \tag{2.1}$$

where $\gamma_\delta(\mathbf{x}', \mathbf{x}) = \gamma_\delta(\mathbf{x}, \mathbf{x}')$ is a symmetric, nonnegative kernel, and satisfies, for all $\mathbf{x}, \mathbf{x}' \in \mathbb{R}^d$,

$$\gamma_\delta(\mathbf{x}', \mathbf{x}) = \begin{cases} \gamma_\delta(|\mathbf{x}' - \mathbf{x}|) \geq 0, & \text{if } |\mathbf{x}' - \mathbf{x}| \leq \delta, \\ 0, & \text{if } |\mathbf{x}' - \mathbf{x}| > \delta, \end{cases} \tag{2.2}$$

Here $|\mathbf{x}' - \mathbf{x}|$ denotes the distance between $\mathbf{x}'$ and $\mathbf{x}$. Moreover, as mentioned in the introduction, we assume that the kernel function γ_δ satisfies the second moment condition. For simplicity, we assume that

$$\int_{\mathbb{R}^d} \gamma(\mathbf{x}, \mathbf{x}')|\mathbf{x}' - \mathbf{x}|^2 d\mathbf{x}' = \int_{|\mathbf{x}'-\mathbf{x}|\leq\delta} \gamma(\mathbf{x}, \mathbf{x}')|\mathbf{x}' - \mathbf{x}|^2 d\mathbf{x}' = 1\,. \tag{2.3}$$

Without loss of generality, for given data $f = f(\mathbf{x})$ defined on Ω, with the total net-flux assumed to be zero, the following compatibility condition is assumed:

$$\int_\Omega f(\mathbf{x}) d\mathbf{x} = 0\,. \tag{2.4}$$

This type of compatibility is also present in Neumann type problems associated with local elliptic operators. We then define the total energy

$$E_f(u) = \frac{1}{2}\int_\Omega\int_\Omega \gamma_\delta(\mathbf{x}',\mathbf{x})\left(u(\mathbf{x}')-u(\mathbf{x})\right)^2 d\mathbf{x}'d\mathbf{x} - \int_\Omega f(\mathbf{x})u(\mathbf{x})d\mathbf{x}\,. \tag{2.5}$$

The space of interest to us, denoted by $\mathcal{S}(\Omega)$, is a subspace of $L^2(\Omega)$ given by

$$\mathcal{S}(\Omega) = \{u \in L^2(\Omega) : \int_\Omega\int_\Omega \gamma_\delta(\mathbf{x},\mathbf{x}')|u(\mathbf{x}')-u(\mathbf{x})|^2 d\mathbf{x}'d\mathbf{x} < \infty\}.$$

$\mathcal{S}(\Omega)$ is often called the nonlocal energy space. Furthermore, with the compatibility condition (2.4), the nonlocal constrained energy space is defined by

$$\mathcal{S}_\delta(\Omega) = \{u \in \mathcal{S}(\Omega) : \int_\Omega u d\mathbf{x} = 0\}.$$

which is a real inner product space with the inner product $(\cdot,\cdot)_s$ defined as

$$(u,w)_s = B_\delta(u,w).$$

We use $\|u\|_s$ to denote the induced norm $\sqrt{(B_\delta(u,u))}$ of u in $\mathcal{S}_\delta(\Omega)$. For $\{S_\delta\}$ defined earlier, $\|\cdot\|_s$ is equivalent to a full norm, as demonstrated by the Poincaré inequality given later. Following the same argument as in [Mengesha and Du, 2013], it can be established that, for any nonnegative, radial kernel with a constant horizon δ, the constrained energy space $\mathcal{S}_\delta(\Omega)$ is a Hilbert space with the norm $\|\cdot\|_s$.

Consider the constrained minimization problem

$$\min_{u\in\mathcal{S}(\Omega)} E_f(u) \quad \text{subject to} \quad E_c(u) = 0,$$

where $E_c = E_c(u)$ denotes a constraint functional. For example, let

$$E_c(u) := \int_\Omega u(\mathbf{x})\,d\mathbf{x} = 0\,. \tag{2.6}$$

We then have the equivalent formulation as $\min_{u\in\mathcal{S}_\delta(\Omega)} E_f(u)$.

With the compatibility condition (2.4), the Euler-Lagrange equations for (2.5) becomes

$$B_\delta(u,v) = \int_\Omega\int_\Omega \gamma_\delta(\mathbf{x}',\mathbf{x})\left(u(\mathbf{x}')-u(\mathbf{x})\right)\left(v(\mathbf{x}')-v(\mathbf{x})\right)d\mathbf{x}'d\mathbf{x} = (f,v) \tag{2.7}$$

where

$$(f, v) = \int_\Omega f(\mathbf{x}) v(\mathbf{x}) d\mathbf{x}$$

and $B_\delta(\cdot, \cdot)$ defines a symmetric bilinear form. The Lagrange multiplier for the constraint on u vanishes for compatible f. Thus, by defining the nonlocal operator

$$u \mapsto \mathcal{L}_\delta u := -2 \int_\Omega \gamma_\delta(\mathbf{x}', \mathbf{x}) \left(u(\mathbf{x}') - u(\mathbf{x})\right) d\mathbf{x}', \tag{2.8}$$

we end up with a nonlocal integral equation

$$\begin{cases} \mathcal{L}_\delta u = f \quad \text{in } \Omega \,, \\ \int_\Omega u = 0 \end{cases} \tag{2.9}$$

for data f satisfying

$$\int_\Omega f(\mathbf{x}) d\mathbf{x} = 0 \,.$$

One can see that the compatibility condition on f is a consequence of the anti-symmetry of $\gamma_\delta(\mathbf{x}', \mathbf{x}) \left(u(\mathbf{x}') - u(\mathbf{x})\right)$ in $\mathbf{x}$ and $\mathbf{x}'$ so that

$$\int_\Omega f(\mathbf{x}) d\mathbf{x} = \int_\Omega \mathcal{L}_\delta u(\mathbf{x}) d\mathbf{x} = -2 \int_\Omega \int_\Omega \gamma_\delta(\mathbf{x}', \mathbf{x}) \left(u(\mathbf{x}') - u(\mathbf{x})\right) d\mathbf{x}' d\mathbf{x} = 0 \,.$$

We note that the difference between the above problem (2.9) with those corresponding to the Dirichlet type volumetric constraints is that no values of the solution u is specified in any subdomain of Ω, this is consistent to the nature of Neumann conditions which are natural conditions implied by the variational principle. Moreover, for nonlocal models, the information of the Neumann type conditions is encoded in the equations themselves, see [Du *et al.*, 2013a; Du *et al.*, 2013b] for detailed accounts on how one may symbolically rewrite (2.9) as a combination of balance laws in a subset of Ω and a (nonlocal) flux condition in its complement.

2.2 Well-posedness of nonlocal Neumann problems

Well-posedness of nonlocal Neumann volume-constrained problems has been shown in many previous studies with some conditions imposed on the kernel. see for instance

[Andreu-Vaillo *et al.*, 2010; Barles *et al.*, 2014a; Barles *et al.*, 2014b; Du *et al.*, 2013a; Mengesha and Du, 2013]. For completeness, we include a brief discussion on Neumann type problems here. The study utilizes extensions of the ideas in [Bourgain *et al.*, 2001]. A key is the following nonlocal Poincaré-type inequality that holds over all subspaces of functions in $L^2(\Omega)$ satisfying certain compatible constraints. We begin with Proposition 1 of [Mengesha and Du, 2013].

Proposition 2.2.1. *[Mengesha and Du, 2013, Proposition 1] Suppose that γ_δ satisfies* (2.2) *and* (2.3) *and V is a closed subspace of $L^2(\Omega)$ that intersects $\mathbb{R}^d$ trivially. Then there exists $C = C(\gamma_\delta, V, \Omega)$ such that*

$$\|u\|^2 \leq C \int_\Omega \int_\Omega \gamma_\delta(\mathbf{x}', \mathbf{x})|\mathbf{x}' - \mathbf{x}|^2 (u(\mathbf{x}') - u(\mathbf{x}))^2 d\mathbf{x}' d\mathbf{x}\,, \quad \forall u \in V. \tag{2.10}$$

A strengthened nonlocal Poincaré inequality is given later with a sharper constant C independent of the horizon δ. A consequence of the nonlocal Poincaré-type inequality is the coercivity of the bilinear form $B = B_\delta(u, v)$. A standard application of Lax-Milgram theory or Riesz representation theorem then yields the well-posedness of the variational problem.

Proposition 2.2.2. *Suppose that γ_δ satisfies* (2.2) *and* (2.3) *and V is a closed subspace of $L^2(\Omega)$ that intersects $\mathbb{R}^d$ trivially. Then there exists $\kappa = \kappa(\gamma_\delta, V, \Omega)$ such that*

$$\|u\|_s^2 \leq \kappa B_\delta(u, u), \quad \textit{for all } u \in V \cap \mathcal{S}(\Omega).$$

Consequently, for a given $f \in L^2$ satisfying (2.4)*, by taking $\mathcal{V} = \mathcal{S}_\delta(\Omega)$, we see that there exists a unique $u \in \mathcal{S}_\delta(\Omega)$ such that*

$$B_\delta(u, v) = (f, v), \quad \forall v \in \mathcal{S}_\delta(\Omega). \tag{2.11}$$

Moreover, $|u|_s = |f|_{\mathcal{S}_\delta^*(\Omega)}$ where $\mathcal{S}_\delta^*(\Omega)$ denote the dual space of $\mathcal{S}_\delta(\Omega)$.

It follows then that the operator $\mathcal{L}_\delta$ restricted on $\mathcal{S}_\delta(\Omega)$, that is, $\mathcal{L}_\delta : \mathcal{S}_\delta(\Omega) \to \mathcal{S}_\delta^*(\Omega)$ is an isometry. In addition, the restriction of the inverse operator $\mathcal{L}_\delta^{-1}$ to $L^2(\Omega)$,

that is, $\mathcal{L}_\delta^{-1} : L^2(\Omega) \to \mathcal{S}_\delta(\Omega)$ and satisfies the inequality $|\mathcal{L}_\delta^{-1} f|_s \leq C\|f\|_{L^2}$. This follows from the continuous embedding of $L^2(\Omega)$ into $\mathcal{S}_\delta^*(\Omega)$ and $\|f\|_{\mathcal{S}_\delta^*(\Omega)} \leq \|f\|_{L^2(\Omega)}$ for any $f \in L^2(\Omega)$.

2.3 The local limit with vanishing horizon

Although we are interested in studying nonlocal models, it is important to get consistency with classical local models when the latter are valid and applicable. For suitably defined kernels, limiting local models of nonlocal models are indeed well-defined. While there have been existing studies on similar limiting process for Dirichlet type volume constraints, the case for Neumann type problem presents some different issues.

For a point $\mathbf{x} \in \Omega_\delta = \{\mathbf{x} \in \Omega \mid \mathrm{d}ist(\mathbf{x}, \partial\Omega) > \delta\}$, we know that

$$\int_\Omega \gamma_\delta(\mathbf{x}', \mathbf{x})(\mathbf{x}' - \mathbf{x}) d\mathbf{x}' = 0\,, \tag{2.12}$$

and

$$\int_\Omega \gamma_\delta(\mathbf{x}', \mathbf{x})|\mathbf{x}' - \mathbf{x}|^2 d\mathbf{x}' = 1\,, \quad \int_\Omega \gamma_\delta(\mathbf{x}', \mathbf{x})(\mathbf{x}' - \mathbf{x})^k d\mathbf{x}' = o(1) \quad \forall k > 2\,. \tag{2.13}$$

With these assumptions, for any smooth enough function u we have formally that $\mathcal{L}_\delta$ represents a nonlocal diffusion operator with a local limit

$$\mathcal{L}_\delta u(\mathbf{x}) \to \mathcal{L}_0 u(\mathbf{x}) := -\Delta u(\mathbf{x})$$

for $\mathbf{x} \in \Omega_\delta$, which is a fact widely stated in many earlier studies. What concerns us is, when taking into account the modifications in the layer around the boundary of Ω, the formal order of convergence rate as $\delta \to 0$.

To better illustrate our idea, we let Ω be a finite bar in $\mathbb{R}$. Without loss of generality, we can let $\Omega = (0, 1)$. Given data $f = f(x)$, we introduce a modified body force

$$\begin{aligned} f_\delta(x) =& f(x) - \frac{1}{2}\left(\int_\Omega \gamma_\delta(x + y)(y^2 - x^2)(f(x) + f(y))dy \right. \\ &\left. + \int_\Omega \gamma_\delta(x + y - 2)(x + y - 2)(y - x)(f(x) + f(y))dy\right)\,. \end{aligned} \tag{2.14}$$

It is simple to check that:

Lemma 2.3.1. *The modified function f_δ satisfies the compatibility condition* (2.4) *and $f_\delta(x) = f(x)$ for $x \in \Omega_\delta$.*

Instead of (2.9), we consider the following nonlocal equation

$$\begin{cases} \mathcal{L}_\delta u = f_\delta \quad \text{on } \Omega \ , \\ \displaystyle\int_\Omega u = 0 \ . \end{cases} \tag{2.15}$$

The limiting local model of (2.15) is given by

$$\begin{cases} \mathcal{L}_0 u = f \quad \text{in } \Omega \ , \ \ u'(0) = u'(1) = 0 \ , \\ \displaystyle\int_\Omega u(x)dx = 0 \ . \end{cases} \tag{2.16}$$

Let

$$\mathcal{S}_0 = \{u \in H^1(\Omega) : \int_\Omega u(x)dx = 0\}$$

with an inner product and norm

$$(u, v)_{\mathcal{S}_0} = \int_\Omega u'(x)v'(x)dx, \quad \|u\|_{\mathcal{S}_0} = \left(\int_\Omega |u'(x)|^2 dx\right)^{\frac{1}{2}},$$

and a bilinear form

$$B_0(u, v) = (u, v)_{\mathcal{S}_0} = \int_\Omega u'(x)v'(x)dx \ , \tag{2.17}$$

for $u, v \in \mathcal{S}_0$. The weak formulation of (2.16) can be cast in the same form as (2.11) with $\delta = 0$.

2.3.1 Convergence of variational solutions

To study the asymptotic property of the nonlocal model as $\delta \to 0$, we need a "sharper" version of Poincaré inequality, that is, the Poincaré constant in the inequality should be independent of the horizon δ. This can be worked out by following

[Mengesha and Du, 2015] to consider a sequence of radial kernels $\gamma_n (n \geq 1)$ satisfying:

$$\xi^{-2}\gamma_n(\xi) \text{ is nonnegative and nonincreasing in } |\xi|, \tag{2.18}$$

$$\int_{\mathbb{R}} \gamma_n(|\xi|)d\xi = 1, \tag{2.19}$$

$$\text{and } \lim_{n\to\infty} \int_{|\xi|\geq r} \gamma_n(|\xi|)d\xi = 0, \quad \forall r > 0. \tag{2.20}$$

Note that in our case, if we let $\gamma_\delta(|\xi|) = \xi^{-2}\gamma_n(|\xi|)$ and $\delta = \frac{1}{n}$, then the kernel satisfies all the assumptions above. So we have the following variant of the Poincaré-type inequality:

Lemma 2.3.2. *[Mengesha and Du, 2015, Lemma 4.1] There exists $C > 1$ and $\delta_0 \leq 1$ such that*

$$\|u\|^2 \leq C \int_\Omega \int_\Omega \gamma_\delta(x', x)(u(x') - u(x))^2 dx'dx \tag{2.21}$$

for all $u \in \mathcal{S}_\delta$ and all $\delta \leq \delta_0$.

From the lemma, we can get that

$$\|u\|^2 \leq C B_\delta(u, u)\,,$$

with the same constant C for all $u \in \mathcal{S}_\delta$, independent of δ. The uniform boundedness of $\mathcal{L}_\delta^{-1}$ in L^2 norm then follows from the uniform Poincaré inequality (Theorem 2.3.2).

Theorem 2.3.3. *There exists a constant C which is independent of the horizon δ such that*

$$\|\mathcal{L}_\delta^{-1}\|_{L^2} \leq C,$$

To study the limiting behavior of the nonlocal solution, we also need a compactness lemma that can be found in [Mengesha and Du, 2015, Proposition 4.2].

Lemma 2.3.4. *Suppose $u_n \in \mathcal{S}_{\delta_n}$ with $\delta_n \to 0$. If*

$$\sup_n \int_\Omega \int_\Omega \gamma_{\delta_n}(x', x)(u_n(x') - u_n(x))^2 dx'dx \leq \infty,$$

then u_n is precompact in $L^2(\Omega)$. Moreover, any limit point $u \in \mathcal{S}_0$.

Now we state some convergence results for the solutions of the parametrized variational problems as $\delta \to 0$. We consider the original problem (2.9) first and the same result for (2.15) with data f_δ is given in the subsequent Corollary.

Theorem 2.3.5. *Suppose u_δ is the weak solution of (2.9) and u_0 is the weak solution of (2.16). Then we have*

$$\|u_\delta - u_0\|_{L^2} \to 0 \quad as\ \delta \to 0.$$

Proof. Since $B_\delta(u_\delta, v) = (f, v)_{L^2}$ for any $v \in \mathcal{S}_\delta$, by uniform Poincaré inequality (2.21), for some constants C_1 and C_2 we have

$$C_1\|u_\delta\|^2_{\mathcal{S}_\delta} \le B_\delta(u_\delta, u_\delta) = (f, u_\delta)_{L^2} \le \|f\|_{L^2}\|u_\delta\|_{L^2} \le C_2\|f\|_{L^2}\|u_\delta\|_{\mathcal{S}_\delta},$$

which leads to the uniform boundedness of $\{u_\delta \in \mathcal{S}_\delta\}$. Thus by the asymptotically compact embedding property, we get the convergence of a subsequence of $\{u_\delta\}$ in L^2 to a limit point $u_* \in \mathcal{S}_0$. For notational convenience, we use the same $\{u_\delta\}$ to denote the subsequence. We claim that

$$B_0(u_*, v) = (f, v)_{L^2}, \quad \forall v \in C^\infty(\Omega).$$

Moreover, since $C^\infty(\Omega)$ is dense in $H^1(\Omega)$, we see that u_* is the unique weak solution u_0 of (2.16) and the convergence of the whole sequence also follows.

Indeed, let ϕ_ϵ be standard mollifiers so

$$\int_{B(0,\epsilon)} \phi_\epsilon(x)dx = 1\,.$$

Let

$$u_{\delta,\epsilon} = u_\delta * \phi_\epsilon = \int_{B(0,\epsilon)} u_\delta(x-y)\phi_\epsilon(y)dy\,.$$

Define $\Omega_\epsilon = \{x \in \Omega : \mathrm{dist}(x, \partial\Omega) > \epsilon\}$. Then for all $v \in C^\infty(\Omega)$,

$$\begin{aligned}
&\int_{\Omega_\epsilon}\int_{\Omega_\epsilon} \gamma_\delta(x,x')(u_{\delta,\epsilon}(x') - u_{\delta,\epsilon}(x))(v(x') - v(x))dx'dx \\
&= \int_{B(0,\epsilon)} \phi_\epsilon(y)\left(\int_{\Omega_\epsilon}\int_{\Omega_\epsilon} \gamma_\delta(x,x')(u_\delta(x'-y) - u_\delta(x-y))(v(x') - v(x))dx'dx\right)dy.
\end{aligned}$$

Denote

$$B_\delta^\epsilon(u,v) = \int_{\Omega_\epsilon}\int_{\Omega_\epsilon} \gamma_\delta(x,x')(u(x')-u(x))(v(x')-v(x))dx'dx\,,$$

$$B_0^\epsilon(u,v) = \int_{\Omega_\epsilon} u'(x)v'(x)dx$$

and $u_\delta^y(x) = u_\delta(x-y)$, we have

$$B_\delta^\epsilon(u_{\delta,\epsilon},v) = \int_{B(0,\epsilon)} \phi_\epsilon(y) B_\delta^\epsilon(u_\delta^y,v)dy. \tag{2.22}$$

We want to show that by letting $\delta \to 0$ first and then letting $\epsilon \to 0$, the left hand side of (2.22) goes to $B_0(u_*,v)$ and the right hand side goes to $(f,v)_{L^2}$.

Consider the left hand side of (2.22), for fixed ϵ and small enough δ, $\Omega_\epsilon \subset \Omega_\delta$. Then

$$\begin{aligned} B_\delta^\epsilon(u_{\delta,\epsilon},v) = &\int_{\Omega_\epsilon}\int_{\Omega} \gamma_\delta(x,x')(u_{\delta,\epsilon}(x')-u_{\delta,\epsilon}(x))(v(x')-v(x))dx'dx \\ &- \int_{\Omega_\epsilon}\int_{\Omega\setminus\Omega_\epsilon} \gamma_\delta(x,x')(u_{\delta,\epsilon}(x')-u_{\delta,\epsilon}(x))(v(x')-v(x))dx'dx. \end{aligned}$$

For the first term, by the fact $u_{\delta,\epsilon} \to u_{*,\epsilon}$ in $C^\infty(\Omega)$ and Dominated Convergence Theorem, we have

$$\begin{aligned} &\lim_{\epsilon\to 0}\lim_{\delta\to 0} \int_{\Omega_\epsilon}\int_{\Omega} \gamma_\delta(x,x')(u_{\delta,\epsilon}(x')-u_{\delta,\epsilon}(x))(v(x')-v(x))dx'dx \\ &= \lim_{\epsilon\to 0} B_0^\epsilon(u_{*,\epsilon},v) = B_0(u_*,v). \end{aligned}$$

For the second term, since the integrand is uniformly bounded, we have

$$\begin{aligned} &\lim_{\epsilon\to 0}\lim_{\delta\to 0} \Big| \int_{\Omega_\epsilon}\int_{\Omega\setminus\Omega_\epsilon} \gamma_\delta(x,x')(u_{\delta,\epsilon}(x')-u_{\delta,\epsilon}(x))(v(x')-v(x))dx'dx\Big| \\ &\le C\lim_{\epsilon\to 0} |\Omega_\epsilon||\Omega\setminus\Omega_\epsilon| = 0. \end{aligned}$$

Thus we have

$$B_\delta^\epsilon(u_{\delta,\epsilon},v) \to B_0(u_*,v).$$

For the right hand side of (2.22), define

$$\Delta_\epsilon = |B_\delta^\epsilon(u_\delta^y,v) - B_\delta(u_\delta,v)|.$$

Since $B_\delta(u_\delta, v) = (f, v)_{L^2}$ for all smooth v, it suffices to show that Δ_ϵ is bounded by some constant which is independent of δ and $\Delta_\epsilon \to 0$ as $\epsilon \to 0$. Now define $\Omega_\epsilon^y = \{x \in \Omega : x - y \in \Omega_\epsilon\}$, since the kernel is translation invariant, i.e. $\gamma_\delta(x+y, x'+y) = \gamma_\delta(x, x')$ if $x + y$ and $x' + y$ are in Ω, we have

$$\begin{aligned}&\int_{\Omega_\epsilon}\int_{\Omega_\epsilon} \gamma_\delta(x, x')(u_\delta(x' - y) - u_\delta(x - y))(v(x') - v(x))dx'dx \\ &= \int_{\Omega_\epsilon^y}\int_{\Omega_\epsilon^y} \gamma_\delta(x, x')(u_\delta(x') - u_\delta(x))(v(x' + y) - v(x + y))dx'dx.\end{aligned}$$

Therefore,

$$\Delta_\epsilon \le I + II,$$

where

$$\begin{aligned}I = |&\int_{\Omega_\epsilon^y}\int_{\Omega_\epsilon^y} \gamma_\delta(x, x')(u_\delta(x') - u_\delta(x))(v(x') - v(x))dx'dx \\ &- \int_\Omega\int_\Omega \gamma_\delta(x, x')(u_\delta(x') - u_\delta(x))(v(x') - v(x))dx'dx|\end{aligned}$$

and

$$II = |\int_{\Omega_\epsilon^y}\int_{\Omega_\epsilon^y} \gamma_\delta(x, x')(u_\delta(x') - u_\delta(x))(v(x' + y) - v(x') - (v(x + y) - v(x)))dx'dx|.$$

Note that

$$\begin{aligned}I &= 2|\int_{\Omega\setminus\Omega_\epsilon^y}\int_\Omega \gamma_\delta(x, x')(u_\delta(x') - u_\delta(x))(v(x') - v(x))dx'dx| \\ &\le 2\|u_\delta\|_{\mathcal{S}_\delta}\left(\int_{\Omega\setminus\Omega_\epsilon^y}\int_\Omega \gamma_\delta(x, x')(v(x') - v(x))^2dx'dx\right)^{\frac{1}{2}} \\ &\le C\left(\int_{\Omega\setminus\Omega_{2\epsilon}}\int_\Omega \gamma_\delta(x, x')(v(x') - v(x))^2dx'dx\right)^{\frac{1}{2}}.\end{aligned}$$

The last inequality holds because of $\Omega_{2\epsilon} \subset \Omega_\epsilon^y$. Since v is also in $\mathcal{S}_\delta$, by Bounded Convergence Theorem, we can get $I \to 0$ as $\epsilon \to 0$.

Consider II, since v is smooth, we have

$$II \le \|u_\delta\|_{\mathcal{S}_\delta}\|v(x + y) - v(x)\|_{\mathcal{S}_\delta(\Omega_\epsilon^y)} \le C\|u_\delta\|_{\mathcal{S}_\delta}\|v(x + y) - v(x)\|_{\mathcal{S}_0(\Omega_\epsilon^y)},$$

which also goes to 0 when $\epsilon \to 0$ since $|y| < \epsilon$. □

Corollary 2.3.6. *Suppose u_δ is the weak solution of* (2.15) *and u_0 is the weak solution of* (2.16)*. Then we have*

$$\|u_\delta - u_0\|_{L^2} \to 0 \quad as\ \delta \to 0\,.$$

Proof. Let us assume that $\tilde{u_\delta}$ is the weak solution of (2.9). By the theorem stated above, it suffices to show that $\|\tilde{u_\delta} - u_\delta\|_{L^2} \to 0$ as $\delta \to 0$, which can be derived from Theorem 2.3.3 and the fact that

$$\|f - f_\delta\|_{L^2} \to 0 \quad as\ \delta \to 0\,.$$

Indeed, denote by $\phi_\delta(x) = \int_\Omega \gamma_\delta(x+y)(y^2-x^2)dy$, then ϕ_δ is compactly supported in $x \in [0,\delta]$ and

$$|\phi_\delta(x)| \le \int_\Omega \gamma_\delta(x+y)|y^2-x^2|dy \le \int_\Omega \gamma_\delta(x+y)(x+y)^2 dy\,,$$

which is bounded for any $x \in [0,\delta]$. Moreover, we also have

$$\int_\Omega \gamma_\delta(x+y-2)(x+y-2)(y-x)dy = \phi_\delta(1-x)\,,$$

which is compactly supported in $x \in [1-\delta, 1]$ and is also bounded. Therefore, when $x \in [0,\delta]$,

$$|f(x) - f_\delta(x)| \le \frac{|f(x)|}{2}\left|\int_\Omega \gamma_\delta(x+y)(y^2-x^2)dy\right| + \frac{1}{2}\left|\int_\Omega \gamma_\delta(x+y)(y^2-x^2)f(y)dy\right|\,.$$

The first integral is bounded and by Schwarz's inequality,

$$\begin{aligned}\left|\int_\Omega \gamma_\delta(x+y)(y^2-x^2)f(y)dy\right|^2 &\le \int_\Omega \gamma_\delta(x+y)(y-x)^2dy \int_\Omega \gamma_\delta(x+y)(x+y)^2 f(y)^2 dy\\ &\le \int_\Omega \gamma_\delta(x+y)(x+y)^2 dy \int_\Omega f(y)^2 dy\\ &\le \|f\|_{L^2}\,.\end{aligned}$$

Then we can get that

$$\|f - f_\delta\|_{L^2[0,\delta]} \le C_1\|f\|_{L^2[0,\delta]} + C_2\delta\,,$$

which vanishes as $\delta \to 0$. Similarly, we also have

$$\|f - f_\delta\|_{L^2[1-\delta,1]} \to 0$$

as $\delta \to 0$. Then the claim is true since $f(x) - f_\delta(x) = 0$ for $x \in [\delta, 1-\delta]$. □

2.3.2 Order of convergence

Our next aim is to estimate the formal order of convergence rate as $\delta \to 0$, in the presence of Neumann type constraints. Towards this goal, we consider an even more general setting by imposing a mixed type of volume constraints. For simplicity in presentation, we consider the case $\Omega = (0, 1)$ with a Neumann type volume constraint at $x = 0$ and a nonlocal Dirichlet type constraint at $\Omega_D = [1, 1 + \delta]$. In this case, the nonlocal operator given by (2.8) should be properly modified as

$$u \mapsto \mathcal{L}_\delta u := -2 \int_{\Omega \cup \Omega_D} \gamma_\delta(x', x) \left(u(x') - u(x)\right) dx', \tag{2.23}$$

Then the nonlocal equation to be solved is

$$\begin{cases} \mathcal{L}_\delta u = f_\delta^L \quad \text{on } \Omega \,, \\ \quad u = 0 \quad \text{on } \Omega_D \,, \end{cases} \tag{2.24}$$

where the one-sided modified body force f_δ^L is given by

$$f_\delta^L(x) = f(x) - \frac{1}{2} \int_{\Omega \cup \Omega_D} \gamma_\delta(x + y)(y^2 - x^2)(f(x) + f(y))dy$$

for any $x \in \Omega$. The corresponding limiting local model of (2.24) is given by

$$\begin{cases} \mathcal{L}_0 u = f \quad \text{in } \Omega \,, \\ u'(0) = 0 \,, \quad u(1) = 0 \,. \end{cases} \tag{2.25}$$

Note that we always choose f such that the exact solution u_0 of the local problem (2.25) decays smoothly to zero on the Dirichlet side and therefore we can zero extend u_0 to Ω_D smoothly. We first remark that the use of the nonlocal δ-layer (such as $\Omega_D = [1, 1 + \delta]$ for the 1-D case) for imposing Dirichlet type of constraints is a feature of nonlocal interaction that has been discussed in many previous works [Du *et al.*, 2013a]. Effectively, we are now treating $\Omega \cup \Omega_D = [0, 1 + \delta]$ as the material body but assuming that $u = 0$ over $[1, 1 + \delta]$, the δ neighborhood on the right end, which is a typical feature of nonlocal interaction that has been discussed in [Du *et al.*, 2013a]. Due to mixed volume constraints, we have the nonlocal maximum principle stated below.

Lemma 2.3.7 (Maximum principle)**.** *Let γ_δ satisfy* (2.12)*. If $u \in C(\overline{\Omega})$ and $\mathcal{L}_\delta u(x) \leq 0$ for all $x \in \Omega$, then*

$$\sup_{x\in\Omega} u(x) \leq \sup_{x\in\Omega_D} u(x)\,.$$

Proof. Step 1. We are going to show that the claim is true if $\mathcal{L}_\delta u(x) \leq -\epsilon$ for $x \in \Omega$, where $\epsilon > 0$. Assume that $\sup_{x\in\Omega} u(x) > \sup_{x\in\Omega_D} u(x)$. Then since $u \in C(\overline{\Omega})$, we can find $x^* \in \Omega$ such that $u(x^*) = \sup_{x'\in\Omega} u(x') \geq u(x)$ for any $x \in \Omega \cup \Omega_D$. Thus

$$\mathcal{L}_\delta u(x^*) = -\int_{\Omega\cup\Omega_D} \gamma_\delta(|x-x'|)(u(x') - u(x^*))dx' \geq 0\,,$$

which contradicts with $\mathcal{L}_\delta u(x) \leq 0, \forall x \in \Omega$. So it must be true that $\sup_{x\in\Omega} u(x) \leq \sup_{x\in\Omega_D} u(x)$.

Step 2. Now we show that the claim is true if $\mathcal{L}_\delta u(x) \leq 0$. Let $w(x) = u(x) + \epsilon x^2$, then one can show that

$$\mathcal{L}_\delta w(x) \leq -\epsilon \int_{\Omega\cup\Omega_D} \gamma_\delta(|x-x'|)(x'^2 - x^2)dx' \leq -\epsilon\,.$$

Therefore, from step 1 we know that for any $\epsilon > 0$

$$\sup_{x\in\Omega} w(x) = \sup_{x\in\Omega} u(x) + \epsilon \leq \sup_{x\in\Omega_D} w(x) = \sup_{x\in\Omega_D} u(x) + \epsilon(1+\delta)^2\,.$$

So we have the claim verified by letting $\epsilon \to 0$. □

Assume that u_δ and u_0 are the solutions to (2.24) and (2.25) respectively. Let us denote $e_\delta(x) = u_\delta(x) - u_0(x)$ and $T_\delta(x) = (\mathcal{L}_0 u_0 - \mathcal{L}_\delta u_0) + (f_\delta^L - f)$, then $\mathcal{L}_\delta e_\delta(x) = \mathcal{L}_\delta u_\delta(x) - \mathcal{L}_\delta u_0(x) = T_\delta(x)$. By Taylor expansion and the symmetry of the kernels, we can get the following truncation error estimate.

Lemma 2.3.8. *[Truncation error] Suppose u_0 is the solution to local problem* (2.25)*. Then*

$$T_\delta(x) = \begin{cases} O(\delta^2) \quad \text{for } x \in [\delta, 1)\,, \\ \left(\displaystyle\int_x^\delta \left(2s^2x - \frac{s^3}{6} - 3x^2 s\right)\gamma_\delta(s)ds\right) u_0'''(0) + O(\delta^2) \quad \text{for } x \in (0,\delta)\,. \end{cases}$$

To get the formal order of convergence, we need the following important lemma.

Lemma 2.3.9. *Suppose that a nonnegative continuous function* $\Phi(x)$ *is defined on* $\Omega \cup \Omega_D$, *and*

$$-\mathcal{L}_\delta \Phi(x) \geq G(x) > 0 \,.$$

Then

$$\sup_{x\in\Omega} |e_\delta(x)| \leq \sup_{x\in\Omega_D} \Phi(x) \cdot \sup_{x\in\Omega} \frac{|T_\delta(x)|}{G(x)}$$

Proof. Let $K_\delta = \sup_{x\in\Omega} \frac{|T_\delta(x)|}{G(x)}$. Then consider $K_\delta\Phi(x)+e_\delta(x)$, we have $\mathcal{L}_\delta(K_\delta\Phi+e_\delta) \leq 0$. By applying the maximum principle Lemma 2.3.7 (noticing that it can be applied since $u_\delta \in C(\overline{\Omega})$ if $f_\delta^L \in C(\overline{\Omega})$ which implies $e_\delta \in C(\overline{\Omega})$), we have

$$\sup_{x\in\Omega} e_\delta(x) \leq \sup_{x\in\Omega}(K_\delta\Phi(x) + e_\delta(x)) \leq \sup_{x\in\Omega_D} (K_\delta\Phi(x) + e_\delta(x)) = K_\delta \sup_{x\in\Omega_D} \Phi(x)\,,$$

where $e_\delta(x) = 0$ for $x \in \Omega_D$ is used. Similarly, we can also get

$$\sup_{x\in\Omega} -e_\delta(x) \leq K_\delta \sup_{x\in\Omega_D} \Phi(x)\,,$$

which completes the proof. □

Now to find $\Phi(x)$, the so-called barrier function (as in the PDE literature), we suppose that it is of the form

$$\Phi(x) = x^2 + 2x\,.$$

Then $\Phi(x)$ is nonnegative on Ω_D. Moreover, let

$$G(x) = -\mathcal{L}_\delta\Phi(x) = \begin{cases} 2 \quad \text{for } x \in (\delta, 1)\,, \\ 2\displaystyle\int_{-x}^{\delta} \gamma_\delta(s)\left(s^2 + 2sx + 2s\right) ds \quad \text{for } x \in [0,\delta]\,. \end{cases}$$

Therefore, $G(x) > 0$ for $x \in \Omega$ since when $x \in [0,\delta]$,

$$G(x) = 2\int_{-x}^{\delta} \gamma_\delta(s)s^2 ds + 4(1+x)\int_x^{\delta} \gamma_\delta(s)s ds > 0\,.$$

Now if we pick a specific kernel, namely (1.9) with γ being the characteristic function on $(0,1)$:

$$\gamma_\delta(x,x') = \frac{3}{2\delta^3}\chi_{[0,1]}(\frac{|x-x'|}{\delta}) \text{ for all } x, x' \in \mathbb{R}. \tag{2.26}$$

Then we have

$$K_\delta = \sup\left\{ \sup_{x\in(0,\delta)} \frac{|\delta^4 - 16\delta^3 x - 36\delta^2 x^2 + 51x^4||u_0'''(0)| + O(\delta^4)}{16\left(\delta^3 + 3\delta^2(1+x) - x^2(3+2x)\right)}, O(\delta^2)\right\},$$

where the first term can be proved to be $O(\delta^2)$. Indeed, let $x = \alpha\delta$, $\alpha \in (0,1)$, then the first term is equivalent to

$$\frac{(1-\alpha)|1 - 15\alpha - 51\alpha^2 - 51\alpha^3||u_0'''(0)|\delta^4 + O(\delta^5)}{48\left(1-\alpha^2\right)\delta^2 + \mathcal{O}(\delta^3)} = O(\delta^2)\,.$$

Combining Lemma 2.3.9 and the above calculations, we have the desired $O(\delta^2)$ estimate.

More generally, for rescaled kernels (1.9), we have

$$K_\delta = \sup\left\{ \sup_{x\in(0,\delta)} \frac{\left|\int_x^\delta \gamma_\delta(s)\left(2s^2x - \frac{s^3}{6} - 3x^2s\right)ds\right|}{\int_{-x}^\delta \gamma_\delta(s)(2s + 2sx + s^2)ds}|u_0'''(0)|, O(\delta^2)\right\}.$$

Let $x = \alpha\delta$ where $\alpha \in (0,1)$. We can simplify the fraction in the above equation by plugging (1.9) into it and apply a change of variable $t = s/\delta$ to get:

$$\frac{\left|\int_x^\delta \gamma_\delta(s)\left(2s^2x - \frac{s^3}{6} - 3x^2s\right)ds\right|}{\int_{-x}^\delta \gamma_\delta(s)(2s + 2sx + s^2)ds} = \delta^2 \cdot \frac{\left|\int_\alpha^1 \gamma(s)\left(2\alpha s^2 - \frac{s^3}{6} - 3\delta\alpha^2 s^2\right)ds\right|}{\int_{-\alpha}^1 \gamma(s)(2s + 2\alpha\delta s + \delta s^2)ds},$$

which can be proved to be $O(\delta^2)$. Indeed, by (2.13) we can get

$$\int_{-\alpha}^1 \delta s^2\gamma(s)ds = O(\delta)\,.$$

Moreover, the numerator on the right hand side

$$\begin{aligned}\left|\int_\alpha^1 \gamma(s)\left(2\alpha s^2 - \frac{s^3}{6} - 3\delta\alpha^2 s^2\right)ds\right| &\le (2\alpha + 3\delta\alpha^2)\int_\alpha^1 \gamma(s)s^2ds + \frac{1}{6}\int_\alpha^1 \gamma(s)s^3ds \\ &\le \left(2\alpha + 3\delta\alpha^2 + \frac{1}{6}\right)\int_\alpha^1 \gamma(s)sds\,.\end{aligned}$$

and the denominator can be simplified to

$$\int_{-\alpha}^{1} \gamma(s)(2s + 2\alpha\delta s + \delta s^2)ds = (2 + 2\alpha\delta) \int_{\alpha}^{1} \gamma(s)sds + O(\delta)\,.$$

Then there exists a constant C independent of δ and α, such that

$$\frac{\left|\int_{\alpha}^{1} \gamma(s) \left(2\alpha s^2 - \frac{s^3}{6} - 3\delta\alpha^2 s^2\right) ds\right|}{\int_{-\alpha}^{1} \gamma(s)(2s + 2\alpha\delta s + \delta s^2)ds} \leq C\,,$$

which again gives the $O(\delta^2)$ convergence order. We summarize into the following key result of this chapter.

Theorem 2.3.10. *Suppose u_δ solves the nonlocal problem (2.24) and u_0 is the solution to local problem (2.25). Then when $\delta < \delta_0$ for some constant δ_0, there exists a constant $C > 0$ independent of δ such that*

$$\sup_{x\in\Omega} |u_\delta(x) - u_0(x)| \leq C\delta^2\,.$$

2.3.3 Inhomogeneous Neumann conditions

Now we discuss the nonlocal analog to the classical diffusion problem with inhomogeneous Neumann boundary conditions. The latter is given by

$$\begin{cases} \mathcal{L}_0 u = f \quad \text{in } \Omega\,, \\ u'(0) = a\,, \quad u(1) = 0\,, \end{cases} \tag{2.27}$$

where $a \neq 0$.

We aim to impose Neumann type volume constraint at the left end point $x = 0$. In order to have the consistency, we assume in addition that the first moment of γ exists for any $\delta > 0$, namely

$$\int_{0}^{1} \gamma(s)s\,ds < \infty\,. \tag{2.28}$$

Note that (2.28) is not always true for kernels given by (1.9), for example, $\gamma(s) = 1/s^2$. We note however that among practical choices of the kernels, one often takes γ to be integrable itself, then (2.28) is automatically satisfied.

Instead of (2.24), the nonlocal equation to be solved is

$$\begin{cases} \mathcal{L}_\delta u = \tilde{f}_\delta^L & \text{on } \Omega\,, \\ \quad u = 0 & \text{on } \Omega_D\,, \end{cases} \tag{2.29}$$

where $\mathcal{L}_\delta$ remains the same as (2.23) but

$$\tilde{f}_\delta^L(x) = f_\delta^L(x) + 2a\int_{-\delta}^{0} \gamma_\delta(x,x')(x'-x)dx'\,. \tag{2.30}$$

By (2.28), it is easy to check that the extra integration in (2.30) is well defined since $\gamma(s)$ does not have singularities when $x \neq 0$. Moreover, Lemma 2.3.8 and Lemma 2.3.9 still hold in this case since the last term in (2.30) cancels the new terms of truncation errors due to the inhomogeneous conditions. Therefore, we still have:

Theorem 2.3.11. *Suppose u_δ solves the nonlocal problem* (2.29) *and u_0 is the solution to local problem* (2.27)*. Then when $\delta < \delta_0$ for some constant δ_0, there exists a constant C independent of δ such that*

$$\sup_{x\in\Omega} |u_\delta(x) - u_0(x)| \leq C\delta^2\,.$$

***Remark* 2.3.12.** *We can generalize the last term in* (2.30)*. Indeed, to solve for inhomogeneous Neumann boundary conditions, we introduce an auxiliary function u_b which is supported on $(-\delta, 0)$. Define*

$$\mathcal{L}_\delta^N u_b = -2\int_{-\delta}^{0} \gamma_\delta(x,x')(u_b(y) - u_b(x))dy\,.$$

Then (2.30) *can be written as*

$$\tilde{f}_\delta^L(x) = f_\delta^L(x) + 2\mathcal{L}_\delta^N u_b\,,$$

where $u_b(x) = -ax$ for $x \in (-\delta, 0)$. Here $a \neq 0$ is the local Neumann boundary data and the negative sign comes from the outward normal direction at $x = 0$.

In general, u_b does not have to be a linear function and the kernel in $\mathcal{L}_\delta^N$ does not have to be the same as that in $\mathcal{L}_\delta$. It is sufficient to choose the kernel ρ_δ for $\mathcal{L}_\delta^N$ and the auxiliary function u_b such that

$$\int_{-\delta}^{0} \rho_\delta(x,x')(u_b(x') - u_b(x))dx' = a\int_{-\delta}^{0} \gamma_\delta(x,x')(x'-x)dx' + \mathcal{O}(\delta)\,, \tag{2.31}$$

where $\mathcal{O}(\delta)$ is some higher order term that is at least uniformly bounded by a constant multiple of δ.

2.4 Numerical schemes

In this section, two classes of discrete schemes for (2.15) are studied, including the quadrature/collocation schemes which are analogous to the ones presented in [Tian and Du, 2013], and conforming finite element Galerkin approximations with piecewise constant and piecewise linear finite element spaces. We refer to [Bessa *et al.*, 2014; Chen and Gunzburger, 2011; Tian and Du, 2014; Wang and Tian, 2012] for more discussions on different numerical schemes and additional references. In this and the followed section we still use the kernel (2.26) which provides a good illustration of the more general case without messy notations.

2.4.1 Geometric discretization

We consider a uniform mesh (grid) in this section. For a positive integer N, we set $h = 1/N$ and let $\delta = rh$ for an integer $r \geq 1$. Furthermore, we assume $\delta < \frac{1}{3}$. Introduce grid points on Ω as $\{x_i = (i-1)h\}_{i\in\Omega_N}$ where the index set is defined by $\Omega_N = \{1, 2, \ldots, N+1\}$. Denote by $I_j = ((j-1)h, jh)$ for $1 \leq j \leq r$. We also define the standard piecewise constant basis functions by

$$\phi_i^0(x) = \begin{cases} 1 & \text{for } x \in (x_{i-1}, x_i), \\ 0 & \text{otherwise,} \end{cases} \qquad \text{for } i \in \Omega_N, \tag{2.32}$$

and the standard continuous piecewise linear *hat* basis functions by

$$\phi_i^1(x) = \begin{cases} (x - x_{i-1})/h & \text{for } x \in (x_{i-1}, x_i), \\ (x_{i+1} - x)/h & \text{for } x \in [x_i, x_{i+1}), \\ 0, & \text{otherwise} \end{cases} \qquad \text{for } i \in \Omega_N. \tag{2.33}$$

2.4.2 Quadrature based finite difference discretization

For $x \in \Omega_\delta$, since the integrating interval is symmetric with respect to x, we can follow [Tian and Du, 2013] to get

$$\begin{aligned}\mathcal{L}_\delta u(x) &= \int_0^\delta \gamma_\delta(s)(u(x-s) - 2u(x) + u(x+s))ds \\ &= \int_0^\delta \frac{u(x-s) - 2u(x) + u(x+s)}{s^\alpha} s^\alpha \gamma_\delta(s) ds.\end{aligned} \tag{2.34}$$

We consider the discrete operator $\mathcal{L}^h_{\delta,\alpha}$ given by

$$\mathcal{L}^h_{\delta,\alpha} u_i = \sum_{m=1}^{r} \frac{u_{i-m} - 2u_i + u_{i+m}}{(mh)^\alpha} \int_{I_m} s^\alpha \phi_i^1(s)\gamma_\delta(s)ds. \quad i = r+1, ..., N-r, \tag{2.35}$$

where $\{u_i\}$ are approximations of $\{u(x_i)\}$.

If we take α to be 1, then the discrete operator above can be written by

$$\mathcal{L}^h_{\delta,0} u_i = -\frac{3h}{\delta^3} \sum_{m=1}^{r-1} (u_{i-m} - 2u_i + u_{i+m}) - \frac{h^2(3r-1)}{2\delta^4} (u_{i-r} - 2u_i + u_{i+r}), \tag{2.36}$$

for $i = r+1, ..., N-r$.

In [Tian and Du, 2013], it was shown that such quadrature-based schemes are asymptotically compatible for linear nonlocal equations with Dirichlet-type constraints. We now demonstrate in our numerical experiments that it is also true for Neumann volume-constrained problems.

A distinction from [Tian and Du, 2013] is that we also need to discuss here the case that $x \in \Omega \setminus \Omega_\delta$, for which the integrating interval is no longer symmetric. We can either directly use the composite trapezoid rule to approximate the integral, or separate the interval into a symmetric part where we can again exploit the quadrature scheme mentioned above and the remainder where we can consider other quadratures.

Given the above discrete nonlocal difference operators, the proposed quadrature based finite difference scheme of (2.15) is

$$-\mathcal{L}^h_{\delta,0} u_i = f_\delta(x_i) \quad i \in \{1, ..., N+1\} \tag{2.37}$$

Let $\boldsymbol{U}$ be a column vector with entries $\{u_i\}_{i=1}^{N+1}$, and $\mathbf{F}$ be that with entries $\{f_\delta(x_i)\}_{i=1}^{N+1}$, we may rewrite the corresponding linear systems as

$$\mathbb{A}_D\mathbf{U} = \mathbf{F} \tag{2.38}$$

Note that the above stiffness matrix is obtained without any compatibility constraints, so the matrix is singular and the solution of corresponding linear system is not unique. This issue is to be discussed in section 2.5.

2.4.3 Finite element discretization

Given the constrained energy space $\mathcal{S}_\delta(\Omega)$ and the bilinear form, the associated weak formulation of (2.15) is given by: finding $u \in \mathcal{S}_\delta(\Omega)$ such that $\forall v \in \mathcal{S}_\delta(\Omega)$,

$$B_\delta(u, v) = (f_\delta, v)_\Omega.$$

Let $\mathcal{S}_\delta^h \subset \mathcal{S}_c$ be a family of finite element spaces corresponding to a uniform mesh $\{x_i\}$ parameterized by the mesh size h, as described earlier, with $\{\phi_i^k\}_{i=1}^{N_h}$ being the nodal basis. Let $u_h \in \mathcal{S}_\delta^h$ be the Galerkin approximation of u given by

$$B_\delta(u_h, v_h) = (f_\delta, v_h)_\Omega \quad \forall v_h \in \mathcal{S}_\delta^h \ . \tag{2.39}$$

Now suppose $u_h = \sum_{i=1}^{N_h} u_i\phi_i^k(x)$, we pay particular attention to the cases $k = 0$ and 1 with the case $k = 0$ corresponding to piecewise constant basis functions (2.32) (if the energy space admits such functions, which is guaranteed if ρ_δ has finite first order moment), and the case $k = 1$ corresponding to standard continuous piecewise linear elements with *hat* basis functions given by (2.33) (which works for γ_δ that has finite second order moment).

Similar to difference approximations, let $\mathbf{U}$ be the column vector composed of the nodal values $\{u_i\}_{i=1}^{N_h}$, and $\mathbf{F}^k$ being the vector with entries $\{(f_\delta, \phi_i^k)_\Omega/h\}_{i=1}^{N_h}$ that represent the weighted average of f_δ around x_i. Then (2.39) gives linear systems $\mathbb{A}_{E,k}\mathbf{U} = \mathbf{F}^k$ with $\{\mathbb{A}_{E,k}\}_{k=0}^1$ being the nonlocal stiffness matrices for the finite element approximation. The issue of uniqueness of solution will again be discussed later.

2.5 Numerical studies

We now report results of numerical experiments which substantiate the analysis given earlier and offer quantitative pictures to the behavior of numerical solutions especially in the local limit. We first discuss how to impose the Neumann constraint numerically in order to ensure the uniqueness of the numerical solution. The order of convergence for some limiting processes are also examined. Through the numerical experiments, we can recover results analogous to those in [Tian and Du, 2013] for pure Dirichlet constraints.

2.5.1 Numerically imposing the compatibility constraints

After numerical discretization, we get the stiffness matrices $\mathbb{A}$ that can be $\mathbb{A}_D$, $\mathbb{A}_{E,0}$ or $\mathbb{A}_{E,1}$. However, they all have a one-dimensional kernel due to the non-uniqueness. We may impose the constraint that the average of the solution being zero. Or we may modify the stiffness matrix obtained from numerical discretization. Let $\mathbb{E}$ be the column vector with entries all 1. Then $\mathbb{E}$ is in the kernel of stiffness matrix $\mathbb{A}$. Let $\mathbb{B} = \mathbb{A} + \mathbb{E}\mathbb{E}^T$, we solve the linear system $\mathbb{B}\mathbf{U}' = \mathbf{F}$ instead of solving $\mathbb{A}\mathbf{U} = \mathbf{F}$, where $\mathbf{F}$ is the right hand side corresponding to different stiffness matrices. Then the vector $\mathbf{U}'$ has the property of mean zero. For homogeneous nonlocal Neumman condition, $\mathbf{U}'$ is the numerical solution we want. If the compatibility constraint is that average of u in $(0, 1)$ is C_n but not zero, we need to set $\mathbf{U}^h = \mathbf{U}' + C_h\mathbb{E}$, where $C_h \to C_n$ as $h \to 0$ (h is the mesh size).

In our experiments, we adopt the second approach for the following reasons: 1) the order of convergence with mixed type volume constraints is derived theoretically in Section 2.3.2. We want to see if there is any difference for pure Neumann volume constraints; 2) previous studies in [Tian and Du, 2013] contained a set of experiments with Dirichlet volume constraints, it is desirable to impose pure Neumann type constraints numerically as in the model here in order to compare with the results shown

in [Tian and Du, 2013].

We note that the compatibility constraint can be avoided if we impose Dirichlet type volume constraint on one end of the nonlocal boundary region ($\Omega_D = [1, 1+\delta]$, for instance) and consider Neumann type constraint on the other end. In other words, we discretize and solve (2.24) with the nonlocal operator given by (2.23). This also ensures the uniqueness of the numerical solution without the need for imposing the compatibility constraint.

2.5.2 Example 1

We first fix the horizon δ. In order to get simpler benchmark solutions, we calculate the right hand side of the nonlocal equation based on an exact solution $u(x) = x^2(1-x)^2$. This naturally leads to a δ-dependent right hand side $f = \tilde{f}_\delta(x)$. Meanwhile, we need to modify our nonlocal constraints to match with $u(x)$, which leads to our target inhomogeneous volume constrained equation:

$$\begin{cases} \mathcal{L}_\delta u = \tilde{f}_\delta \quad \text{on } \Omega \ , \\ \int_\Omega u = C_n \ . \end{cases} \tag{2.40}$$

We solve the nonlocal problem on a uniform mesh and take δ to be constant and reduce h to check the convergence properties. As an illustration we choose $\delta = \frac{1}{4}$ and refine the mesh with decreasing h. For each h, we use the second approach discussed above to numerically impose the compatibility conditions and the constant C_h is chosen as $C_h = C_n = \frac{1}{30}$ which is the integral of u over Ω.

Table 2.1 shows errors and error orders of the finite difference (columns 2 and 3) and the piecewise linear finite element (columns 4 and 5) approximations to limiting solution $x^2(1-x)^2$ with a fixed $\delta = \frac{1}{4}$ while refining mesh with a decreasing h, where $\mathcal{R}_h$ denotes the restriction to the quadrature points $\{x_i = ih\}_{i=0}^N$ and $\mathcal{I}_h$ denotes the piecewise linear interpolant operator. From the data in the table, we see that the convergence rate for fixed δ is $\mathcal{O}(h^2)$ for both finite difference and finite element

	quadrature collocation		p.w. linear fem	
h	$\|\mathbf{U}^h - \mathcal{R}_h u\|_\infty$	Order	$\|u^h - \mathcal{I}_h u\|_\infty$	Order
2^{-3}	4.59×10^{-3}	$--$	8.23×10^{-3}	$--$
2^{-4}	1.19×10^{-3}	1.95	3.85×10^{-3}	1.10
2^{-5}	3.00×10^{-4}	1.98	1.22×10^{-3}	1.66
2^{-6}	7.53×10^{-5}	1.99	3.37×10^{-4}	1.85
2^{-7}	1.88×10^{-5}	2.00	8.82×10^{-5}	1.93
2^{-8}	4.71×10^{-6}	2.00	2.25×10^{-5}	1.97
2^{-9}	1.18×10^{-6}	2.00	5.69×10^{-6}	1.98
2^{-10}	2.94×10^{-7}	2.00	1.43×10^{-6}	1.99

Table 2.1: Errors of quadrature collocation and piecewise finite element approximations for fixed $\delta = \frac{1}{4}$ to solution $x^4 - 2x^3 + x^2$.

approximations. We remark that the piecewise constant finite element approximation has the same convergence behavior and the data is omitted.

2.5.3 Example 2

We now report numerical experiments to show the order of convergence at continuum level as $\delta \to 0$, which was discussed analytically in Section 2.3. We discretize and solve the following equation:

$$\begin{cases} \mathcal{L}_\delta u_\delta = f_\delta \quad \text{on } \Omega \,, \\ \displaystyle\int_\Omega u_\delta = C_\delta \,. \end{cases} \tag{2.41}$$

f_δ is the modified body force given in (2.14). The constant C_δ in the above equation is dependent of δ, and goes to some constant C_n when δ goes to zero, which means

that the limiting local equation is

$$\begin{cases} \mathcal{L}_0 u = f \quad \text{on } \Omega \,, \\ u'(0) = u'(1) = 0 \,, \\ \displaystyle\int_\Omega u = C_n \,. \end{cases} \tag{2.42}$$

We specify the local limit of the nonlocal solution as $u(x) = x^3/3 - x^6/6$, hence the right hand side of the local PDE would be $f(x) = 5x^4 - 2x$. Denote by $\mathbf{U}_\delta^h$ the numerical solution of (2.41) with horizon δ and mesh size h. Then from example 1, with fixed δ, $\mathbf{U}_\delta^h$ are known to converge to the interpolant of nonlocal solution u_δ with decreasing h. Therefore, when we keep δ decreasing and pick a relative small enough h as our limit case, the result we get can approximate the limiting process which we discussed in section 2.3. In this example, since we only care about the limiting behavior of the numerical solution of u_δ, we can directly choose C_δ as $\frac{5}{84}$ which is the exact integral of the local limit u. Moreover, we impose such a constraint on the numerical solution $\mathbf{U}_\delta^h$ as well by setting

$$h\left(\mathbf{U}_\delta^h[1]/2 + \mathbf{U}_\delta^h[2] + \cdots + \mathbf{U}_\delta^h[N] + \mathbf{U}_\delta^h[N+1]/2\right) = 5/84\,.$$

Table 2.2 shows errors and error orders to the local limit of the quadrature collocation (columns 2 and 3) and piecewise linear finite element (columns 4 and 5) approximations as δ goes to 0 while fixing a small enough mech size h. From the data in the table, we can see that the convergence rate to the local limit is $O(\delta^2)$, which is same as what we showed in earlier analysis. We remark that the piecewise constant finite element approximations also converge to the local limit with the same rates. We also want to check the asymptotic compatibility of the model. Table 2.3 shows that the error order as $h \to 0$ with fixed $r = \delta/h$ remain $\mathcal{O}(h^2)$.

Furthermore, we now confirm that the nonlocal solution recovers the Neumann boundary conditions as $\delta \to 0$ and the derivatives also converge. For $\mathbf{U}_\delta^h$ with different δ and h small enough, we have that

$$u_\delta'(0) \approx D_h^+ \mathbf{U}_\delta^h[1] := (\mathbf{U}_\delta^h[2] - \mathbf{U}_\delta^h[1])/h$$

	quadrature collocation		p.w linear fem	
δ	$\|\mathbf{U}_\delta^h - \mathcal{R}_h u\|_\infty$	Order	$\|u_\delta^h - \mathcal{I}_h u\|_\infty$	Order
2^{-2}	3.03×10^{-2}	$--$	2.80×10^{-2}	$--$
2^{-3}	7.26×10^{-3}	2.06	5.07×10^{-3}	2.47
2^{-4}	1.79×10^{-3}	2.02	9.50×10^{-4}	2.41
2^{-5}	4.45×10^{-4}	2.01	1.92×10^{-4}	2.31
2^{-6}	1.08×10^{-4}	2.04	4.13×10^{-5}	2.21
2^{-7}	2.59×10^{-5}	2.06	8.48×10^{-6}	2.27

Table 2.2: Errors and error orders of finite difference and piecewise linear finite element approximations as $\delta \to 0$ to solution $x^3/3 - x^6/6$.

	quadrature collocation		p.w linear fem	
h	$\|\mathbf{U}_\delta^h - \mathcal{R}_h u\|_\infty$	Order	$\|u_\delta^h - \mathcal{I}_h u\|_\infty$	Order
2^{-3}	4.97×10^{-3}	$--$	1.13×10^{-2}	$--$
2^{-4}	1.20×10^{-3}	2.04	2.86×10^{-3}	1.98
2^{-5}	2.96×10^{-4}	2.02	7.21×10^{-4}	1.99
2^{-6}	7.34×10^{-5}	2.01	1.81×10^{-4}	2.00
2^{-7}	1.83×10^{-5}	2.01	4.53×10^{-5}	2.00
2^{-8}	4.55×10^{-6}	2.00	1.13×10^{-5}	2.00

Table 2.3: Errors and error orders of finite difference and piecewise linear finite element approximations as $h \to 0$ with fixed $r = 2$ to solution $x^3/3 - x^6/6$.

and

$$u'_\delta(1) \approx D_h^- \mathbf{U}_\delta^h[N+1] := (\mathbf{U}_\delta^h[N+1] - \mathbf{U}_\delta^h[N])/h \ ,$$

where $D_h^\pm$ are the difference quotient operators associated to forward and backward differences respectively. Central difference quotient is used for other nodes, namely

$$u'_\delta((j-1)h) \approx D_h \mathbf{U}_\delta^h[j-1] := (\mathbf{U}_\delta^h[j] - \mathbf{U}_\delta^h[j-2])/2h \ ,$$

where $j = 2, 3, \cdots, N$. Take the finite difference approximation as illustration, Table 2.4 shows that as $\delta \to 0$, the derivatives of nonlocal solutions converge with an order of $\mathcal{O}(\delta)$. For more studies on nonlocal gradient recovery, we refer to [Du *et al.*, 2016b], and also Chapter 4 in the thesis.

δ	$\|D_h \mathbf{U}_\delta^h - \mathcal{R}_h u'\|_\infty$	Order
2^{-2}	4.51×10^{-1}	$--$
2^{-3}	2.24×10^{-1}	1.01
2^{-4}	1.17×10^{-1}	0.93
2^{-5}	6.09×10^{-2}	0.95
2^{-6}	3.11×10^{-2}	0.97
2^{-7}	1.57×10^{-2}	0.98

Table 2.4: Errors and error orders of numerical derivatives of finite difference approximations as $\delta \to 0$.

2.5.4 Example 3

In this example, we study another limit process. Recall in [Tian and Du, 2013; Tian and Du, 2014] that in the case with asymptotically compatible finite difference and piecewise linear finite element discretization, the numerical solutions give the correct local limit but not the case with piecewise constant finite element. For $\delta = rh$

with a fixed integer $r \geq 1$, the continuous piecewise linear finite element approximation provides a consistent difference approximation to the local limit as $h \to 0$. Moreover, for problems with sufficiently smooth solutions, the order of truncation error is still $\mathcal{O}(h^2)$. However, for the piecewise constant finite element approximation, it goes to a different and wrong local limit as $h \to 0$, confirming that the conclusions in [Tian and Du, 2013; Tian and Du, 2014] remain valid for the Neumann case. We take $r = 1$ and start with $\delta = 2^{-4}$ and choose the local limit as $u(x) = x^2(1-x)^2$. Figure 2.1 shows that with fixed $r = 1$, the piecewise constant finite element approximation converges to a local limit which is no longer u.

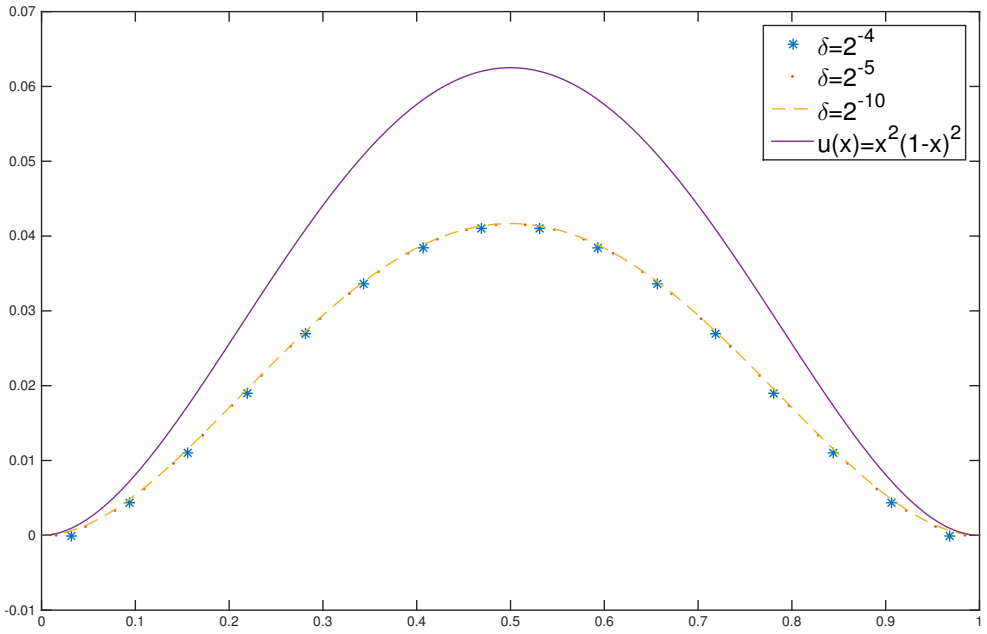

Figure 2.1: The local limit of piecewise constant finite element approximation with fixed r as $h \to 0$.

2.6 Discussion

In this chapter, we have analyzed a linear nonlocal diffusion model which is posed as a nonlocal boundary value problem of Neumann type. We have considered a class of kernels associated with the some variational problems. Basic structural properties of the associated nonlocal energy spaces, such as completeness and compactness, are established, leading to well-posedness for the variational problems. We refer to [Mengesha and Du, 2014a; Mengesha and Du, 2014b; Mengesha and Du, 2013; Mengesha and Du, 2016] for more properties of the energy space.

One of our main focuses is a study of the limiting processes of both the nonlocal diffusion models and the discrete approximations, including the quadrature based finite difference and conforming finite element discretizations. These are representatives of two classes of methods which can be applied to problems with very general nonlocal interaction kernels having a finite second order moment. Note that much of the previous studies on Dirichlet type constrained nonlocal diffusion problems have now been extended to problems with Neumann type volume constraints. We establish the local limit of the nonlocal diffusion model as the horizon goes to zero, and estimate the convergence rate of such a limiting process, which is confirmed by numerical experiments. In particular, we are able to numerically recover most of the results presented in [Tian and Du, 2013] of the problems with Dirichlet volume constraints. In section 2.5, we discuss the similarities and differences between the limiting behavior of numerical methods. These methods are all convergent with the same rate when applied to the nonlocal problem with a fixed horizon δ. However, they behave differently depending on the ratio of horizon and mesh size (δ/h) being fixed. The piecewise constant finite element approximation converges to a different local limit, which is a scalar multiple of the local limit of other approximations. The surprising findings are again consistent to the results given for models with homogeneous Dirichlet conditions.

Finally, the current study is largely based on a simple one-dimensional linear model

for the sake of offering insight without being impeded by tedious calculations. One can find in [Du *et al.*, 2018c] the asymptotically compatible quadrature-based finite difference schemes for general-dimensional spaces. In our analysis here, the computational mesh is taken to be uniform and the horizon parameter δ is also assumed to be a constant. While these serve the purpose of illustration well, additional complications may arise in practical implementations. In addition, later in Chapter 5 we will extend the results obtained in here to the linear peridynamic model with a spatially varying horizon which mimics a spatial change of scales in nonlocal interactions. The present work also serves as a useful step towards the study of nonlocal interface problems and the development of domain decomposition strategies for nonlocal problems.

Chapter 3

A peridynamic model of fracture mechanics with bond-breaking

As mentioned in Chapter 1, the PD model that incorporates the bond-breaking rule leads to a dynamic system of time dependent differential integral equations having both spatial nonlocal/nonlinear interactions and temporal memory/history dependence. A few recent studies have touched upon the rigorous mathematical theory of nonlinear models [Emmrich and Puhst, 2013; Lipton, 2014; Mengesha and Du, 2016; Emmrich and Puhst, 2016]. Notably, [Tian, 2017] presents rigorous results on the existence, uniqueness and continuous dependence on the initial data of solutions to the nonlinear PD model with a properly defined bond-breaking rule.

In this chapter, we aim to carry out numerical simulations based on the modified PD model in [Tian, 2017] which serve several purposes. For example, they offer demonstrations on how to mathematically impose inhomogeneous traction loading conditions properly in the numerical simulations of nonlocal models like peridynamics, which is an interesting and important practical issue. Moreover, numerical convergence can be observed in the test cases and the simulations also illustrate the effectiveness of the well-posed PD models for crack propagation. In particular, they are able to capture propagation and branching patterns that are consistent to those

presented in earlier simulations. The full discussion can be found in [Du *et al.*, 2017a].

3.1 A new mathematical formulation

As introduced in Chapter 1, the bond-based peridynamic equation of motion is given by

$$\rho\ddot{\mathbf{u}}(t,\mathbf{x}) = \int_{B_\delta(\mathbf{x})} \mathbf{f}(t,\mathbf{u}(t,\hat{\mathbf{x}}) - \mathbf{u}(t,\mathbf{x}), \hat{\mathbf{x}} - \mathbf{x}) d\hat{\mathbf{x}} + \mathbf{b}(t,\mathbf{x})\,, \tag{3.1}$$

where ρ is the constant density, $\mathbf{u} = \mathbf{u}(t,\mathbf{x})$ is the displacement field, $\mathbf{b} = \mathbf{b}(t,\mathbf{x})$ denotes the body force, and $\mathbf{f}$ is the pairwise force density. We let $\boldsymbol{\eta}(t)$ and $\boldsymbol{\xi}$ denote $\mathbf{u}(t,\hat{\mathbf{x}}) - \mathbf{u}(t,\mathbf{x})$ and $\hat{\mathbf{x}} - \mathbf{x}$ respectively. [Du *et al.*, 2017a; Tian, 2017] reformulates the original form via a rigorously defined mathematical relation where the force density $\mathbf{f}$ is specified by a single scalar equation given by

$$\mathbf{f}(t,\mathbf{x},\hat{\mathbf{x}},\mathbf{u}) = \omega_\delta(|\boldsymbol{\xi}|) f(\mathcal{S}(t,\mathbf{x},\hat{\mathbf{x}},\mathbf{u}) \mu(\mathcal{S}^*(t,\mathbf{x},\hat{\mathbf{x}},\mathbf{u})) \mathbf{e}(t,\mathbf{x},\hat{\mathbf{x}},\mathbf{u})\,. \tag{3.2}$$

Here, the unit vector $\mathbf{e}$ for bond direction and the bond relative elongation (stretch) $\mathcal{S}$ are given by

$$\mathbf{e}(t,\mathbf{x},\hat{\mathbf{x}},\mathbf{u}) = \mathbf{e}(\boldsymbol{\eta},\boldsymbol{\xi}) = \frac{\boldsymbol{\eta}+\boldsymbol{\xi}}{|\boldsymbol{\eta}+\boldsymbol{\xi}|} \quad \text{and} \quad \mathcal{S}(t,\mathbf{x},\hat{\mathbf{x}},\mathbf{u}) = \mathcal{S}(\boldsymbol{\eta},\boldsymbol{\xi}) = \frac{|\boldsymbol{\eta}+\boldsymbol{\xi}| - |\boldsymbol{\xi}|}{|\boldsymbol{\xi}|}\,. \tag{3.3}$$

Moreover, $\mathcal{S}^*$ is defined as

$$\mathcal{S}^*(t,\mathbf{x},\hat{\mathbf{x}},\mathbf{u}) = \max_{0\le s\le t} \mathcal{S}(s,\mathbf{x},\hat{\mathbf{x}},\mathbf{u})\,.$$

The kernel function ω_δ is assumed to be compactly supported. In particular,

$$\omega_\delta(|\boldsymbol{\xi}|) = 0 \quad \text{if } |\boldsymbol{\xi}| > \delta\,,$$

with the constant $\delta > 0$ representing the horizon parameter measuring the range of nonlocal interaction. An additional assumption on ω_δ used in this paper is that

$$\int \frac{\omega_\delta(|\boldsymbol{\xi}|)}{|\boldsymbol{\xi}|} d\boldsymbol{\xi} < \infty\,. \tag{3.4}$$

The modification reflects on two scalar functions, f and μ, in order to have desired continuous history dependence of the force field, which could be a physically sensible feature as well. To this end, we define some constant parameters

$$-1 < \mathcal{S}_1^- < \mathcal{S}_0^- < 0 \leq \mathcal{S}_0^+ < \mathcal{S}_1^+ < \infty,$$

and scalar functions $f, \mu \in C([-1, \infty])$ such that

$$f(x) = \begin{cases} \mathcal{S}_0^- \dfrac{x - \mathcal{S}_1^-}{\mathcal{S}_0^- - \mathcal{S}_1^-}, & \text{if } x \in (\mathcal{S}_1^-, \mathcal{S}_0^-), \\ x, & \text{if } x \in [\mathcal{S}_0^-, \mathcal{S}_0^+], \\ \mathcal{S}_0^+ \dfrac{\mathcal{S}_1^+ - x}{\mathcal{S}_1^+ - \mathcal{S}_0^+}, & \text{if } x \in (\mathcal{S}_0^+, \mathcal{S}_1^+), \\ 0, & \text{elsewhere,} \end{cases} \quad \text{and} \quad \mu(x) = \begin{cases} 1, & \text{if } x \in [-1, \mathcal{S}_0^+), \\ \dfrac{\mathcal{S}_1^+ - x}{\mathcal{S}_1^+ - \mathcal{S}_0^+}, & \text{if } x \in [\mathcal{S}_0^+, \mathcal{S}_1^+], \\ 0, & \text{if } x \in (\mathcal{S}_1^+, \infty). \end{cases} \tag{3.5}$$

A pictorial illustration of f and μ is shown in Fig. 3.1.

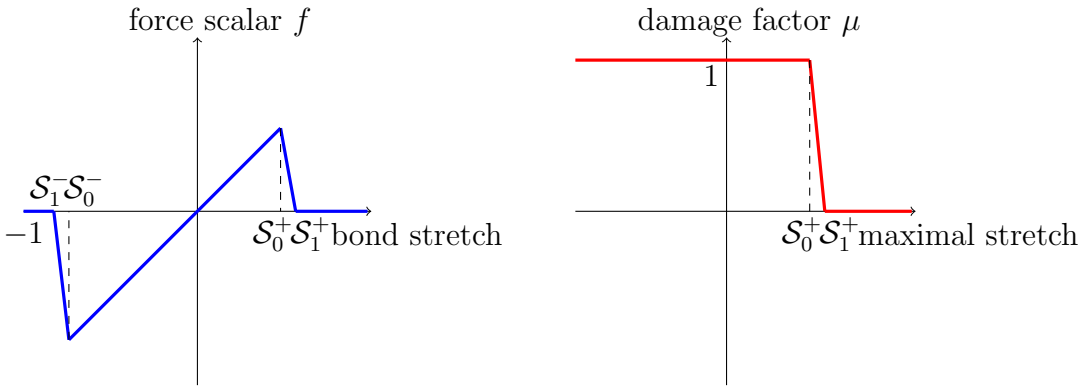

Figure 3.1: Modified force scalar and damage factor.

The study of mathematical properties of the new formulation, such as well-posedness of the new PD model and energy decay of the underlying dynamics, is omitted here since we aim to focus on the numerical simulation in this chapter. We refer to [Du *et al.*, 2017a] for more detailed discussions.

3.2 Numerical simulations

In this section, we present a set of numerical experiments to demonstrate the effectiveness of the new peridynamic model when applied to the numerical simulations of dynamic brittle fracture. For comparison purposes, we mainly focus on the crack branching process in a model of soda-lime glass as documented in [Bobaru and Zhang, 2015].

3.2.1 Discretization

The numerical solution to nonlocal peridynamic models has been a popular research subject. Various methods have been implemented including particle/meshfree discretization, finite difference and finite element methods as well as Fourier spectral methods (for spatially periodic problems). We refer to [Du, 2016] for a brief review. Although we have studied the notion of asymptotically compatible schemes in the previous chapters, we only focus on solving PD models with a fixed horizon in this chapter. We therefore adopt a more popular quadrature based discretization developed in [Lehoucq *et al.*, 2008]. For the integrals in (3.1), the discretization uses a midpoint quadrature rule. We denote by $\mathbf{x}_i$ (the reference position of the node i) and V_i (the nodal volume of the node i) the quadrature point and weight respectively. The spatially discrete dynamic systems are then given by

$$\rho\ddot{\mathbf{u}}_i = \sum_{j\in\mathcal{F}_i} \mathbf{f}_{ij} V_j^{(i)} + \mathbf{b}_i \,,$$

where $\mathbf{f}_{ij}$ denotes the discrete pairwise force function as defined by (3.2) and (3.5). For time discretization of the dynamic system, we use the standard Velocity Verlet scheme. As in [Bobaru and Zhang, 2015], we use the 2D conical micromodulus as the nonlocal interaction kernel:

$$\omega_\delta(|\boldsymbol{\xi}|) = \frac{24E}{\pi\delta^3(1-\nu)}\left(1-\frac{|\boldsymbol{\xi}|}{\delta}\right) \,,$$

where E is Young's modulus and ν is Poisson ratio (fixed to 1/3 in this 2D plane stress case). It is easy to see that in 2D, the above defined ω_δ satisfies (3.4) so our mathematical theory does apply. For the conical micromodulus function, the critical relative elongation used in the original PMB model is given by

$$\mathcal{S}_c = \sqrt{\frac{5\pi G_0}{9E\delta}},$$

where G_0 is the material fracture energy. In our simulations, $\mathcal{S}_1^-$ and $\mathcal{S}_0^-$ are simply set to be -0.99 and -0.98 respectively, which are thought to be close enough to -1 so that it will not affect bond breaking when the bonds are in compression. Indeed, we see from the simulations that making them closer to -1 do not change the solution at all. Meanwhile, we consider several choices of $\mathcal{S}_0^+$ and $\mathcal{S}_1^+$ as they get closer together and the results will be discussed in more details later. We also use the algorithms stated in [Bobaru and Zhang, 2015] to approximate the nodal areas covered by the horizon and to compute the conical micromodulus function.

3.2.2 Modeling dynamic fracture of soda-lime glass

Similar to the problem setup in [Bobaru and Zhang, 2015], let us consider a central-crack thin rectangular plate of dimensions 10cm×4cm (see Fig. 3.2). Along the top and bottom edges a spatially uniform and constant-in-time tensile load σ is applied. The implementation details for such a loading boundary condition will be given later. The material used here is the soda-lime glass with its elastic and fracture properties given in Table 3.1. Rather than the Poisson ratio 0.22, we note that the corresponding 2D bond-based peridynamic model takes on a Poisson ratio 1/3.

In [Bobaru and Zhang, 2015], loading traction boundary conditions are imposed on a single layer of discrete nodal points by the upper and lower boundary edge, which is a practice that may lead to some issues as the mesh get refined, see Chapter 2 for more extensive discussions. The more suitable and mathematically rigorous approach, which is implemented in our experiments here, is to impose "Neumann"-type nonlocal

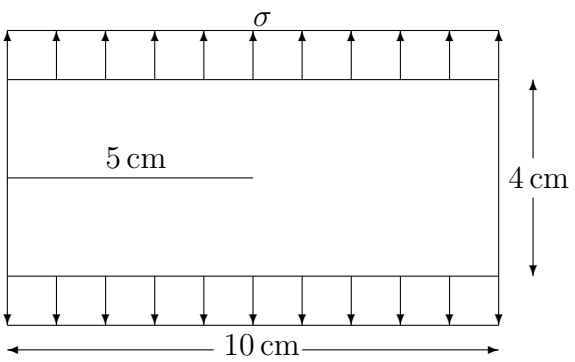

Figure 3.2: Two-dimensional rectangular pre-cracked plate under traction loading.

Material Property	Value
Young's modulus E (GPa)	72
Density ρ (kg/m^3)	2440
Fracture energy G_0 (J/m^2)	3.8

Table 3.1: Material and model parameters for the crack propagation simulation in Fig. 3.2.

boundary conditions through a body force $\mathbf{b} = \mathbf{b}(t, \mathbf{x})$ on a δ-layer inside the boundary edges, or discretely, on m layers of nodal points near the boundary where m is the ratio between horizon and mesh size: $m = \delta/h$. Initially in discretization, if a node, indexed by n_i, is close to the upper boundary with a distance less than δ, then the traction on this node is defined as

$$\mathbf{b}(n_i) = \frac{\sigma \cdot \Delta x}{m \cdot V(n_i)} \boldsymbol{e}\,,$$

where $\boldsymbol{e}$ is the unit vector pointing up, i.e $\boldsymbol{e} = (0, 1)$, Δx is the grid spacing in the x-direction and $V(n_i)$ is the area of the node n_i. Similarly, if the node is close enough to the lower boundary, that traction on this node is computed by the same formula but in an opposite direction $-\boldsymbol{e}$.

3.2.3 Crack branching in soda-lime glass

We first perform an experiment to see how the cracks propagate subject to different loading amplitudes. A uniform grid spacing, namely $\Delta x = \Delta y = h$ is used. We choose the tensile load σ to be 0.2 MPa, 2 MPa and 4 MPa respectively. The results in terms of the damage maps with a horizon of $\delta = 1$mm and a sufficiently small time stepping $\Delta t = 0.02\ \mu s$ are shown in Fig. 3.3.

In this example we choose $\mathcal{S}_0^+ = 0.95\mathcal{S}_c$ and $\mathcal{S}_1^+ = 1.05\mathcal{S}_c$ first. To assure the numerical accuracy of all of our reported simulation results, we focus on the propagation of the pre-existing central crack and the first branching process. We stop the time evolution roughly around the time of a secondary crack branching. Reliable simulations after such a point in time are feasible but demand much higher numerical resolution, which is beyond the scope of this work.

The damage index ϕ for a node is a number between 0 and 1 whose definition is given by

$$\phi(\boldsymbol{x}, t) = 1 - \frac{\displaystyle\int_{B_\delta(\mathbf{x})} \mu dV_{\hat{\mathbf{x}}}}{\displaystyle\int_{B_\delta(\mathbf{x})} dV_{\hat{\mathbf{x}}}},$$

where μ is the modified damage factor as defined by (3.5). We plot the damage index ϕ (using a threshold of 0.4 to highlight the damage area and crack path) in Fig. 3.3. By comparing the results in Fig. 3.3 with that in [Bobaru and Zhang, 2015, Fig. 5], we can see that our new model does not alter the damage maps much for all the different loading amplitudes.

We now discuss the effect of the choice of $\mathcal{S}_0^+ = 0.95\mathcal{S}_c$ and $\mathcal{S}_1^+ = 1.05\mathcal{S}_c$ on the simulation results. In fact, the crack profile has little change when we make perturbations to values $\mathcal{S}_0^+$ and $\mathcal{S}_1^+$. Fig. 3.4 presents the damage index maps with three sets of values to demonstrate the numerical convergence as $\mathcal{S}_0^+$ and $\mathcal{S}_1^+$ go to $\mathcal{S}_c$. In order to see the convergence more quantitatively, we look into the displacement fields and damage indices at the final time step. We compute the differences between the solutions

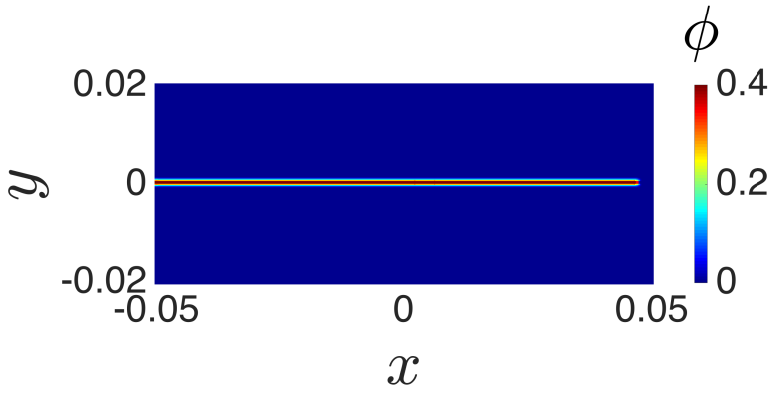

(a)

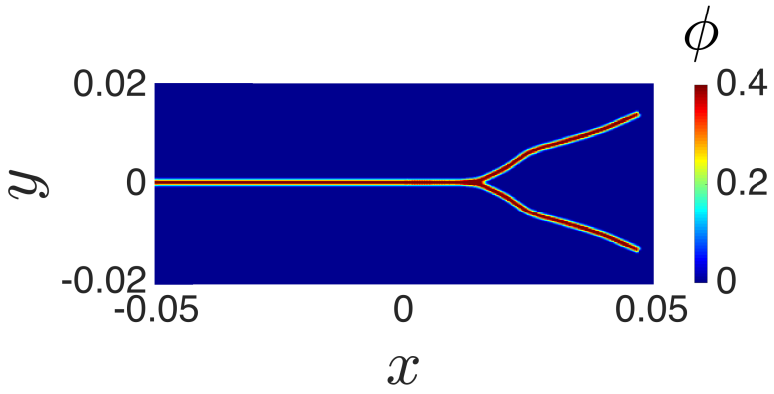

(b)

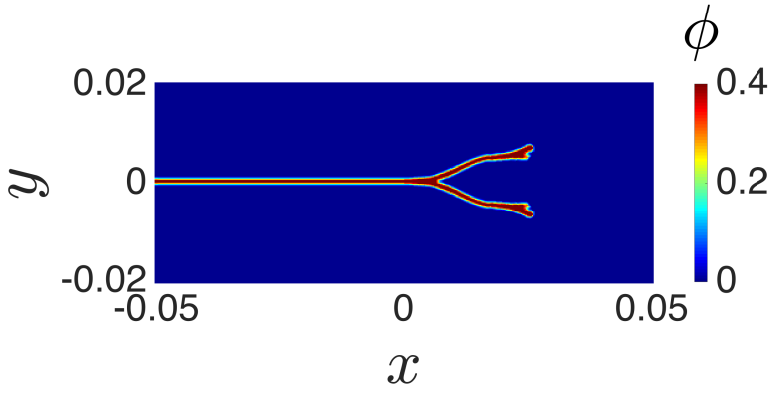

(c)

Figure 3.3: Damage index maps (or crack paths) computed with different amplitudes. From top to bottom: **(a)** $\sigma = 0.2$ MPa at 150 μs; **(b)** $\sigma = 2$ MPa at 43 μs; **(c)** $\sigma = 4$ MPa at 20 μs.

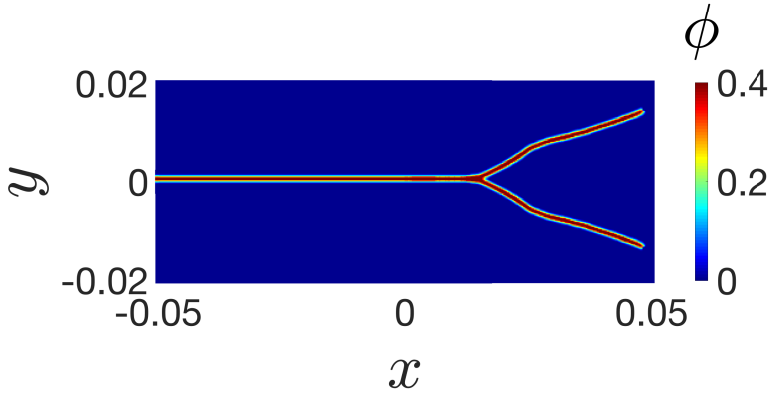

(a)

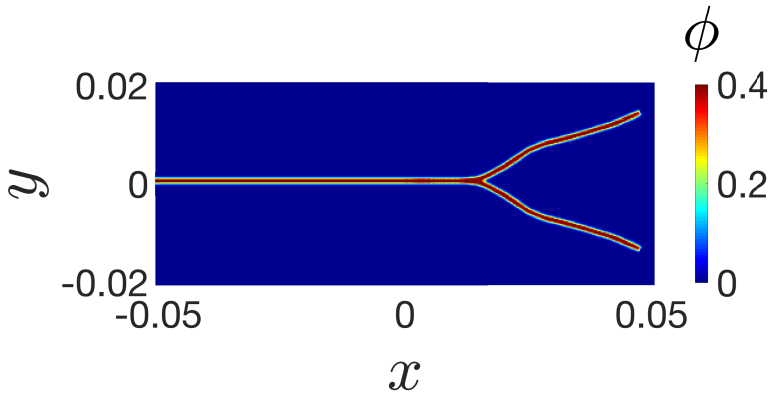

(b)

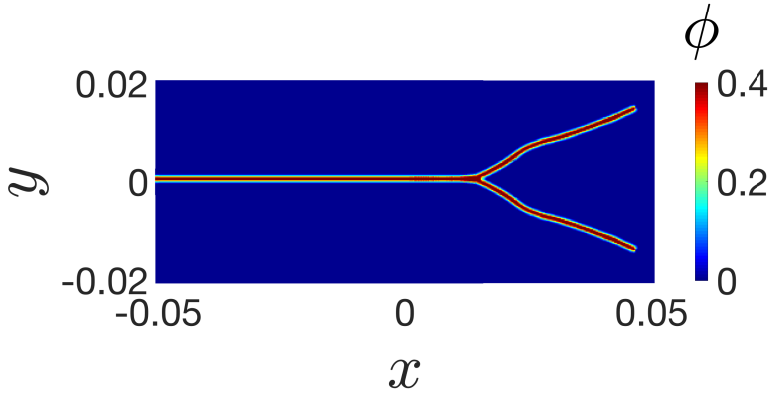

(c)

Figure 3.4: Damage index maps (or crack paths) computed with different $\mathcal{S}_0^+$ and $\mathcal{S}_1^+$ for $\delta = 1$ mm, $m = 4$ and $\sigma = 2$ MPa at 43 μs. From top to bottom: **(a)** $\mathcal{S}_0^+ = 0.85\mathcal{S}_c$ and $\mathcal{S}_1^+ = 1.15\mathcal{S}_c$; **(b)** $\mathcal{S}_0^+ = 0.9\mathcal{S}_c$ and $\mathcal{S}_1^+ = 1.1\mathcal{S}_c$; **(c)** $\mathcal{S}_0^+ = 0.98\mathcal{S}_c$ and $\mathcal{S}_1^+ = 1.02\mathcal{S}_c$.

of $\{\mathcal{S}_0^+, \mathcal{S}_1^+\} = \{0.85\mathcal{S}_c, 1.15\mathcal{S}_c\}$, $\{0.9\mathcal{S}_c, 1.1\mathcal{S}_c\}$ and $\{0.95\mathcal{S}_c, 1.05\mathcal{S}_c\}$ and the solution of $\{\mathcal{S}_0^+, \mathcal{S}_1^+\} = \{0.98\mathcal{S}_c, 1.02\mathcal{S}_c\}$ in the L^2 norm. We denote by $\{e_i^x, e_i^y, e_i^p, i = 1, 2, 3\}$ these norms of the differences in the components of the displacement field in the x-direction and the y-direction, and the damage index respectively. In Table 3.2, we present the differences at the final time $t = 43\,\mu$s. The results imply that the errors are relatively quite small and the convergence is evident as both $\mathcal{S}_0^+$ and $\mathcal{S}_1^+$ go to $\mathcal{S}_c$. Based on this observation, in the remaining experiments, we retain the choice of $\mathcal{S}_0^+ = 0.95\mathcal{S}_c$ and $\mathcal{S}_1^+ = 1.05\mathcal{S}_c$.

x-Direction	e_1^x	e_2^x	e_3^x
	8.87×10^{-8}	5.52×10^{-8}	2.52×10^{-8}
y-Direction	e_1^y	e_2^y	e_3^y
	1.07×10^{-6}	6.74×10^{-7}	3.05×10^{-7}
Damage index	e_1^p	e_2^p	e_3^p
	4.59×10^{-3}	3.49×10^{-3}	2.48×10^{-3}

Table 3.2: Differences between displacements and damage indices computed with different $\mathcal{S}_0^+$ and $\mathcal{S}_1^+$ for $\delta = 1$ mm, $m = 4$ and $\sigma = 42$ MPa at $43\,\mu$s, showing convergence as $\mathcal{S}_0^+$ and $\mathcal{S}_1^+$ go to $\mathcal{S}_c$.

Let us next conduct a numerical convergence test, which is important but has not been carefully performed in the literature especially for crack growth simulations. The convergence is checked by refining meshes with a fixed horizon ($\delta = 1$mm) and a constant loading amplitude ($\sigma = 4$ MPa). We refine the spatial mesh by taking the ratio between horizon and mesh size to be $m = 2$, 3, 6 and 12. The case $m = 1$ is also performed but it produces nonphysical results and is thus discarded. We take a sufficiently small time step $\Delta t = 0.02\,\mu$s to assure that the time-integration error is negligible.

Fig. 3.5 shows the damage maps and plots of energies with different values of m,

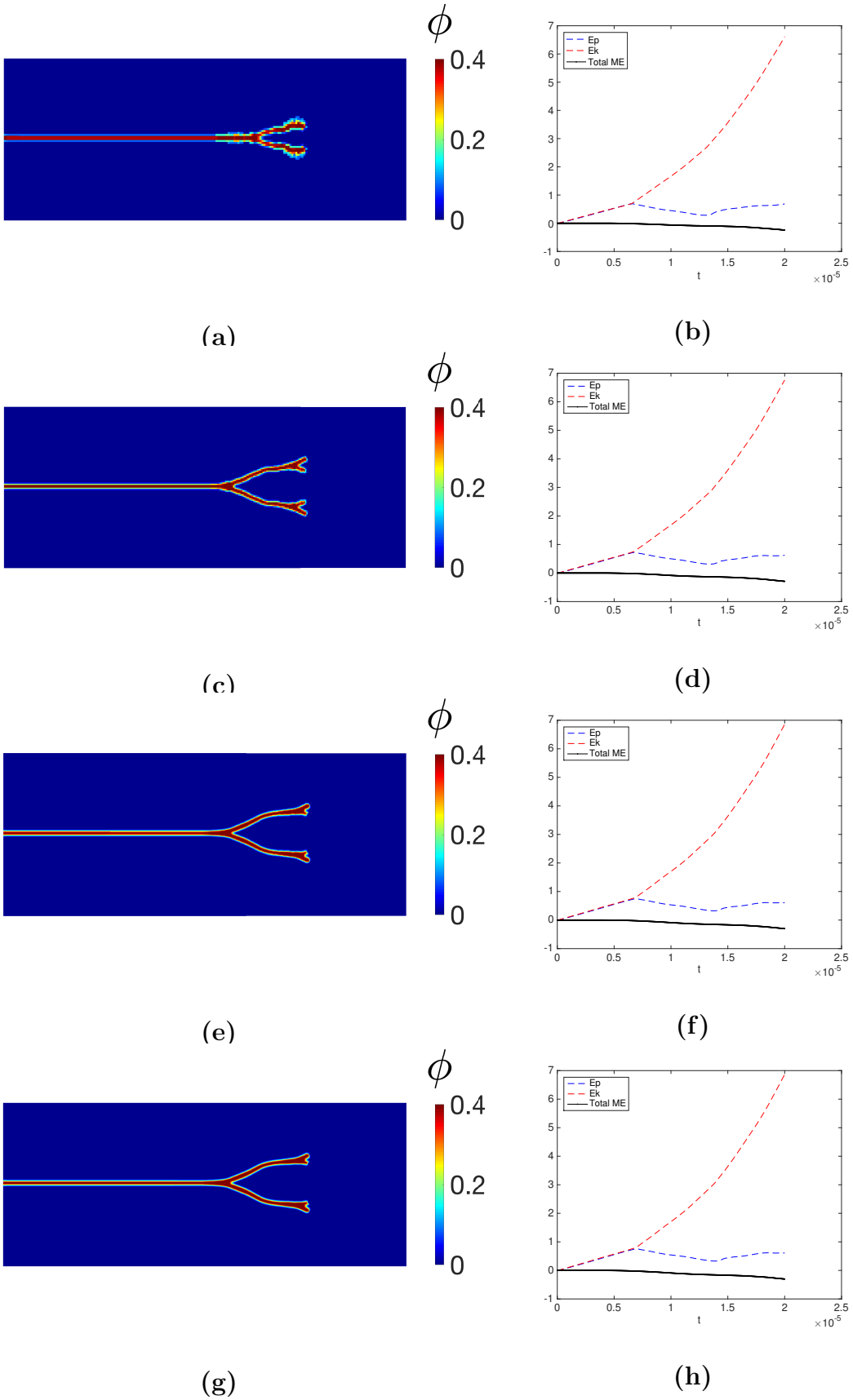

Figure 3.5: Damage index maps (or crack paths) and energies computed with different m for $\delta = 1$ mm and $\sigma = 4$ MPa at 20 μs. Left from top to bottom: damage maps of **(a)** $m = 2$, **(c)** $m = 3$, **(e)** $m = 6$, and **(g)** $m = 12$; Right from top to bottom: the plots of energies of **(b)** $m = 2$, **(d)** $m = 3$, **(f)** $m = 6$, and **(h)** $m = 12$.

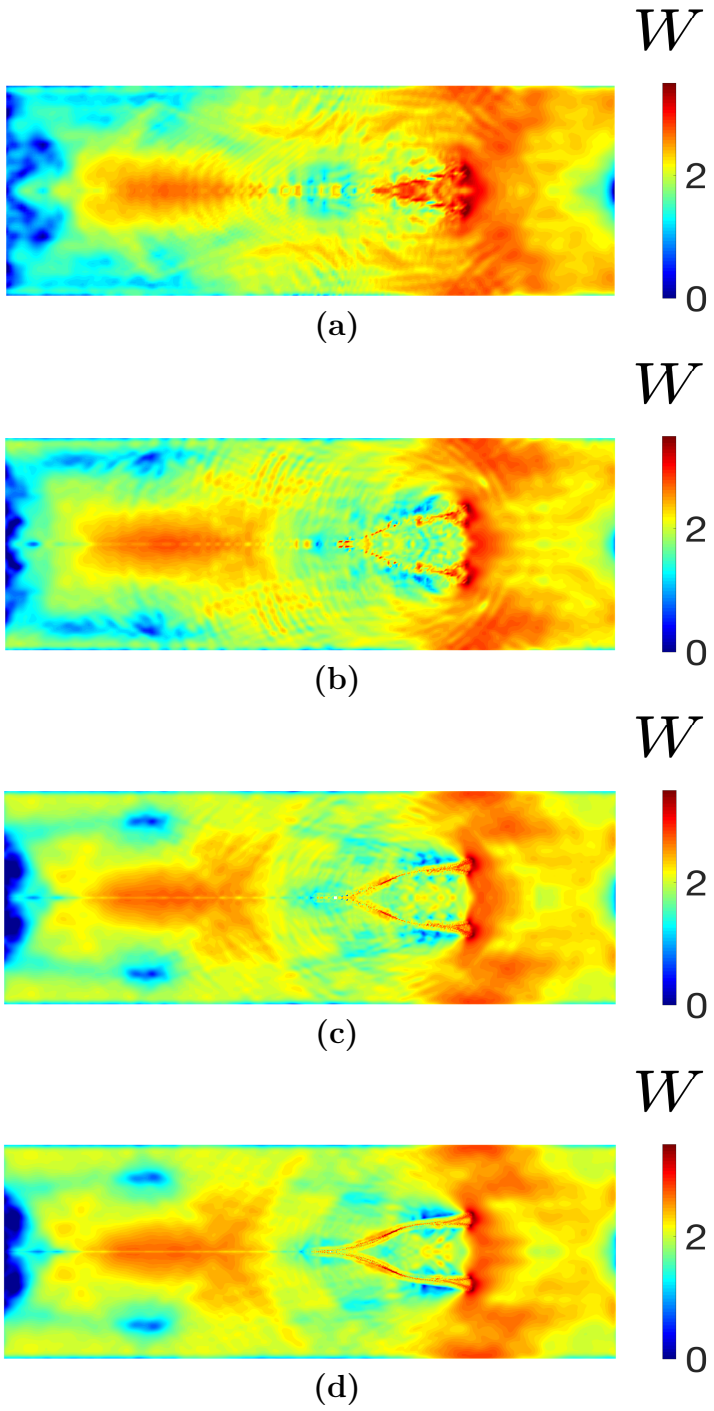

Figure 3.6: Strain energy computed with different m for $\delta = 1$mm and $\sigma = 4$ MPa at 20 μs. From top to bottom: **(a)** $m = 2$; **(b)** $m = 3$; **(c)** $m = 6$; **(c)** $m = 12$.

where Ep and Ek denote the potential and kinetic energy respectively, and Total ME is the total energy $E(t)$ defined as

$$\begin{aligned} E(t) =& \frac{1}{2}\int_{\Omega\cup\Omega_{\mathcal{I}}}\int_{\Omega\cup\Omega_{\mathcal{I}}} |\hat{\mathbf{x}}-\mathbf{x}|\omega_\delta(|\hat{\mathbf{x}}-\mathbf{x}|)p(\mathcal{S}(t,\mathbf{x},\hat{\mathbf{x}},\mathbf{u}))\mu(\mathcal{S}^*(t,\mathbf{x},\hat{\mathbf{x}},\mathbf{u}))d\hat{\mathbf{x}}d\mathbf{x} \\ &+ \frac{1}{2}\int_\Omega |\dot{\mathbf{u}}(t,\mathbf{x})|^2 d\mathbf{x} - \int_\Omega \mathbf{u}(t,\mathbf{x})\cdot\mathbf{b}(\mathbf{x})d\mathbf{x}\,, \end{aligned} \tag{3.6}$$

which consists of the contributions from the stored nonlocal elastic energy, kinetic energy and the work done by external force. Here p is the antiderivative of the force scalar function f. More specifically, we can let $p(0) = 0$ and $p'(x) = f(x)$. By the definition of f in (3.5), we can see that $p(x) \geq 0$ for any x. See Fig. 3.7 for a sketch of $p(x)$.

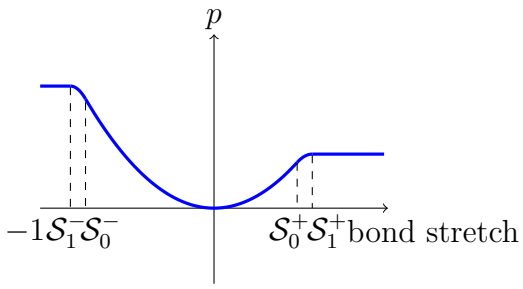

Figure 3.7: Sketch of $p(x)$. $p'(x) = f(x)$, $p(0) = 0$.

From the figure we can see that the total energy is a nonincreasing function over time (energy decay property). Moreover, Fig. 3.6 also shows convergence results with mesh refinement where the plots of strain energy density (in logarithmic scale) are given at the final time. From Fig. 3.5 and Fig. 3.6, the convergence can be visually observed.

Moreover, in Fig. 3.8, the convergence can also be seen from the plots of the differences, between the coarse meshes ($m = 2$, $m = 3$ and $m = 6$) and the finest mesh ($m = 12$), of the potential energy, kinetic energy and total mechanical energy including the work done by the external body force (tensile loading). As time increases, the crack propagates and branches so that the increased complexity in the solutions and

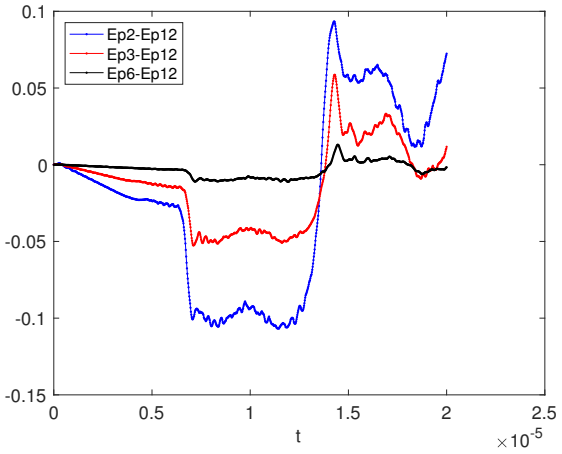

(a)

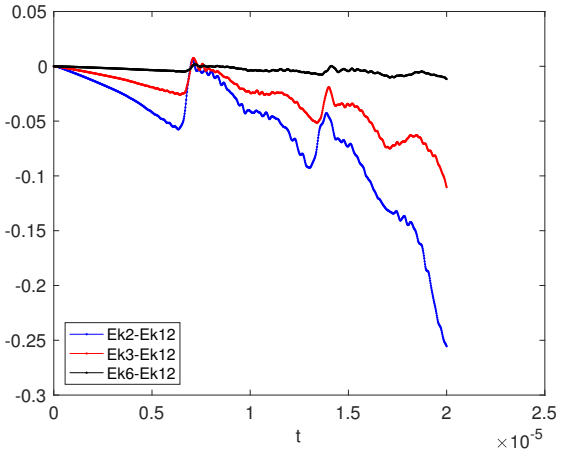

(b)

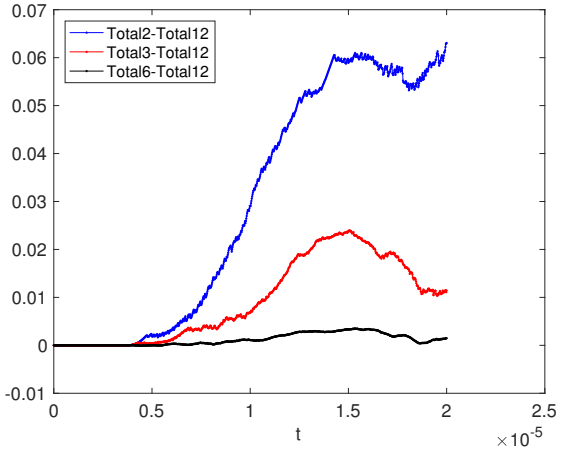

(c)

Figure 3.8: Convergence of energy differences with different m for $\delta = 1$mm and $\sigma = 4$ MPa. From top to bottom: **(a)** Potential energy; **(b)** Kinetic energy; **(c)** Total ME.

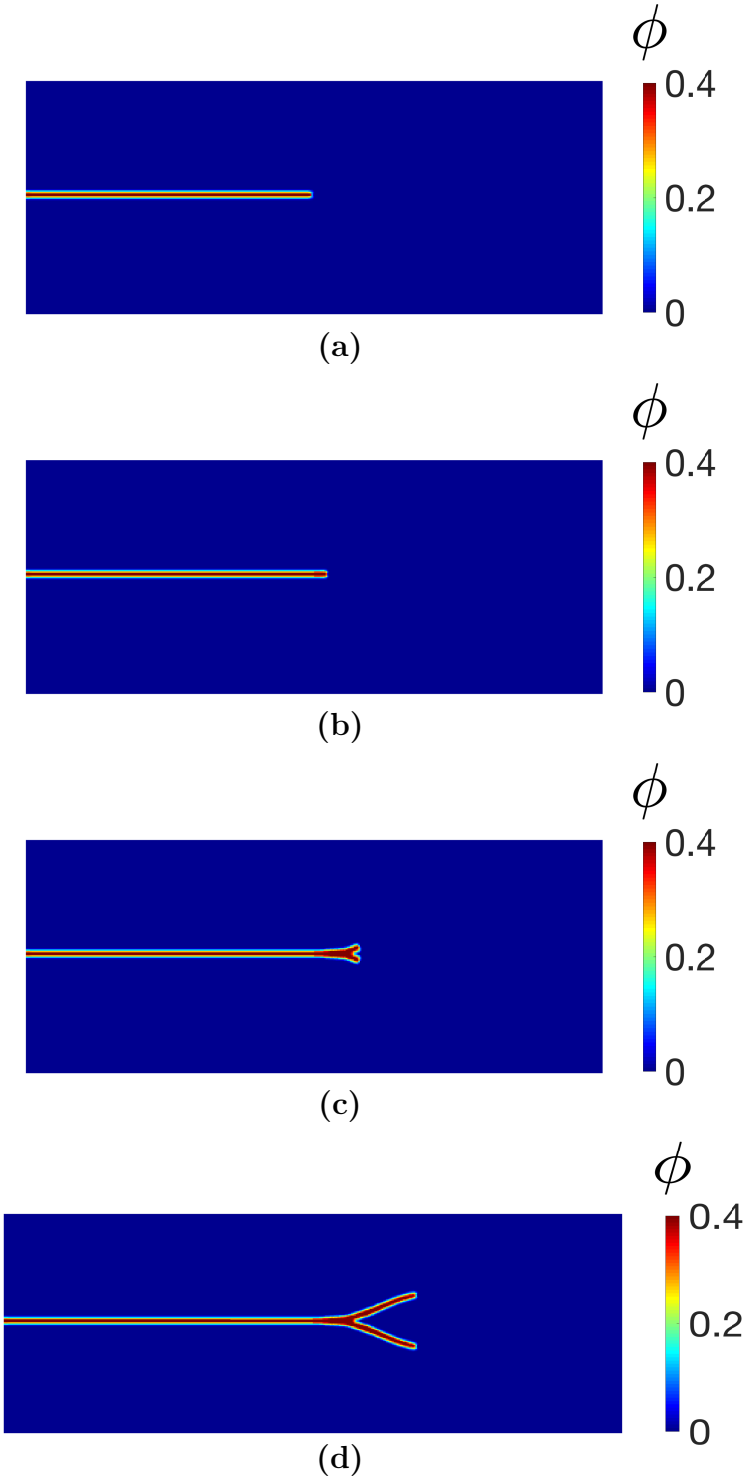

Figure 3.9: Different phases of crack propagation and branching for $\delta = 1$ mm and $\sigma = 4$ MPa. From top to bottom: **(a)** $t = 0$ μs; **(b)** $t = 6$ μs; **(c)** $t = 9$ μs; **(d)** $t = 15$ μs.

accumulations of errors generally leads to increases in the absolute differences. This is particularly evident in the plots of the total mechanical energy in Fig. 3.8. The plots of errors of potential energy and kinetic energy (differences between solutions on different meshes), however, show oscillations, which may be correlated with the variations in numerical resolutions of the different phases of the underlying process (including the growth of cracks, branching of cracks as well as effects of wave reflections from the boundary). More details on the different phases of crack evolution can be visualized in Fig. 3.9. Nevertheless, all of the results show diminishing differences between numerical solutions on different meshes as the mesh gets refined.

$x-direction$			$y-direction$		
$error_2^x$	$error_3^x$	$error_6^x$	$error_2^y$	$error_3^y$	$error_6^y$
1.62×10^{-7}	8.73×10^{-8}	1.36×10^{-8}	4.43×10^{-7}	3.50×10^{-7}	2.21×10^{-7}

Table 3.3: Differences between displacements computed with different m for $\delta = 1$mm and $\sigma = 4$ MPa at $20\,\mu$s.

In order to see the convergence more quantitatively, we look into the displacement fields for different m. We interpolate displacement fields computed on coarse meshes ($m = 2$, $m = 3$ and $m = 6$) to the finest mesh ($m = 12$). Then we compute the differences between the interpolated solutions on the coarse meshes and the solution on the finest mesh in the L^2 norm. We denote by $\{error_m^x, error_m^y, m = 2, 3, 6\}$ these norms for the components of the displacement field in the x-direction and y-direction respectively. In Table 3.3, we present $\{error_m^x, error_m^y, m = 2, 3, 6\}$ at the final time $t = 20\,\mu$s. We note that the relatively larger errors (differences) produced in the $\{error_m^y\}$ are consistent with the larger displacement fields in the y-direction.

Chapter 4

Robust nonlocal gradient recovery for quadrature collocation approximations

As alternatives to partial differential equations (PDEs), nonlocal continuum models given in integral forms avoid the explicit use of conventional spatial derivatives and allow solutions to exhibit desired singular behavior. It is of practical interest to develop robust numerical schemes not only for the numerical solution of nonlocal models but also for the evaluation of suitably defined derivatives of solutions. The latter motivates the development of a nonlocal analog of gradient recovery for numerical solution of PDEs. For structure mechanical models, this leads to a posteriori nonlocal stress analysis. We illustrate in this chapter that when smooth solutions are found in nonlocal models, one may compute local gradients of nonlocal solutions using conventional techniques like that for PDEs. More generically however, we present a framework for stress analysis of nonlocal solutions based on nonlocal gradient operators and their asymptotically compatible discretization. We demonstrate that the nonlocal gradient recovery is consistent in the local limit and is more advantageous than using local gradients of nonlocal solutions. Superconvergence properties of some special nonlocal

gradient operators are identified for nonlocal continuum models. Moreover, methods are presented to preserve such features in the numerical discretization. Both computational observations and theoretical insights are provided to substantiate our findings. The study here can also be found in [Du *et al.*, 2016b].

4.1 Nonlocal gradient operator and quadrature collocation approximation

In this section, we discuss how nonlocal gradient operators can offer a more robust tool for nonlocal stress analysis, in comparison with the use of conventional local gradients and local differential operators. Our discussion here is focused on quadrature/collocation approximations of nonlocal models, though much of the analysis works for other approximation methods as well.

To illustrate the key concepts, we still present the study for a linear nonlocal model defined on a finite bar Ω in $\mathbb{R}$. However in this chapter, to further avoid unnecessary complications due to nonlocal boundary conditions, periodic condition is imposed with the periodic cell given by $\Omega = (0, 1)$. The simple setting allows us to compare with results of their well-defined limiting local models. It is expected that our approach works also for systems of equations in multi-dimensional spaces.

Let $u = u(x)$ denote a scalar deformation field. Same to Chapter 2, the nonlocal operator $\mathcal{L}_\delta$ is defined by

$$\mathcal{L}_\delta u(x) = -2 \int_{-\delta}^{\delta} \gamma_\delta(s) \left(u(x+s) - u(x)\right) ds \,, \tag{4.1}$$

where $\delta > 0$ denotes the nonlocal horizon parameter and $\gamma_\delta(s)$ is a nonnegative nonincreasing kernel function with a compact support in $[0, \delta]$ and a normalized second moment. The nonlocal balance law is prescribed by

$$\mathcal{L}_\delta u = f \quad \text{in } \Omega \,, \tag{4.2}$$

for a given external force f satisfying the compatibility condition

$$\int_\Omega f(x)dx = 0\,.$$

An additional constraint is needed to make the solution unique. We take

$$\int_\Omega u(x)dx = 0 \tag{4.3}$$

for simplicity. The limiting local model of (4.2) is then given by

$$\mathcal{L}_0 u = f \quad \text{in } \Omega = (0,1)\,, \tag{4.4}$$

for $\mathcal{L}_0 = -\frac{d^2}{dx^2}$, again with the periodic condition and uniqueness condition imposed in (4.3).

4.1.1 Nonlocal gradient operator

The operator $\mathcal{L}_\delta$ can be seen as the nonlocal analog of the second order derivative $\mathcal{L}_0$. It is natural to introduce a nonlocal analog of the first order derivative, or the nonlocal gradient operator in multidimensions. Detailed studies of these operators are the subject of recently developed nonlocal vector calculus and we refer to [Du *et al.*, 2012] for formal derivations and [Mengesha and Du, 2016] for more extended functional analysis. Nonlocal analog of integration by parts formula has also been rigorously derived [Du *et al.*, 2017b; Mengesha and Du, 2016].

Here, to recall the necessary definitions, we limit ourselves to the nonlocal gradient operators defined below:

$$\mathbb{G}_\delta u(x) = \int_{-\delta}^{\delta} s\beta_\delta(s)(u(x+s) - u(x))ds\,, \tag{4.5}$$

where $\beta_\delta = \beta_\delta(s)$ is a nonnegative kernel with a bounded second moment. In particular, it may be taken as a rescaled form $\beta_\delta(s) = \delta^{-3}\beta(s/\delta)$, the same as (1.9), with β

sharing the same properties. Another way of looking at $\mathbb{G}_\delta$ is to rewrite (4.5) as

$$\begin{aligned}\mathbb{G}_\delta u(x) &= \int_{-\delta}^{\delta} s^2\beta_\delta(s)\frac{u(x+s)-u(x)}{s}ds \\ &= \int_{-\delta}^{\delta} s^2\beta_\delta(s)\frac{u(x)-u(x-s)}{s}ds \\ &= \int_{-\delta}^{\delta} s^2\beta_\delta(s)\frac{u(x+s)-u(x-s)}{2s}ds\,.\end{aligned}$$

With the assumptions on $\beta_\delta(s)$, we may view $s^2\beta_\delta(s)$ as a density function, so that $\mathbb{G}_\delta$ is effectively a continuum weighted average of some discrete first order difference operators up to the scale δ. If $\delta \to 0$, $s^2\beta_\delta(s)$ gets localized and behaves like a Dirac-delta measure at the origin, thus, we indeed have $\frac{d}{dx}$ as the local limit of $\mathbb{G}_\delta$.

The above definition is a scalar version of a specialized case of nonlocal gradient operators defined in [Du *et al.*, 2012] and [Mengesha and Du, 2016]. There are also the one sided versions (see [Du *et al.*, 2017b; Tian *et al.*, 2015] for related discussions)

$$\mathbb{G}_\delta^{\pm} u(x) = \pm 2\int_0^{\delta} s\beta_\delta(s)(u(x\pm s)-u(x))ds\,, \tag{4.6}$$

that one may also consider, in particular in the presence of geometric boundary or potential discontinuities.

We note that there have been much discussions on nonlocal peridynamic stresses and nonlocal strains in the literature, see [Silling, 2000; Lehoucq and Silling, 2008; Bessa *et al.*, 2014; Tupek and Radovitzky, 2014]. For the one dimensional nonlocal operator $\mathcal{L}_\delta$ associated with a kernel γ_δ, a particular nonlocal gradient operator $\mathbb{G}_\delta^p$ is given by

$$\mathbb{G}_\delta^p u(x) = \int_{-\delta}^{\delta} s\rho_\delta(s)(u(x+s)-u(x))ds\,, \tag{4.7}$$

for any scalar field $u = u(x)$, and

$$\rho_\delta(s) = \frac{2}{s}\int_s^{\delta} \gamma_\delta(z)\, dz, \quad \text{for } 0 < s \le \delta, \quad \rho_\delta(s) = 0, \quad \text{for } s > \delta,$$

and $\rho_\delta(s) = \rho_\delta(-s)$ for $s < 0$.

A direct calculation gives

$$-\frac{d}{dx}\mathbb{G}_\delta^p u(x) = \mathcal{L}_\delta u(x) \tag{4.8}$$

where $\mathcal{L}_\delta$ is given by (4.1). The equation (4.8) is consistent with a derivation of the nonlocal peridynamic stress given in [Lehoucq and Silling, 2008] for a deformation field in multiple space dimensions that has been seen as a consequence of the Noll's lemma, hence the use of superscript p in the notation $\mathbb{G}_\delta^p$. Our formulation adopts a simpler and more conventional representation in the same form as (4.5). we note that for γ_δ satisfying (1.9) and the second moment condition (2.3), the function ρ_δ also shares the same properties as it can be written by

$$\rho_\delta(s) = \frac{2}{s}\int_s^\delta \frac{1}{\delta^3}\gamma(\frac{z}{\delta})dz = \frac{1}{\delta^3}\frac{2\delta}{s}\int_{s/\delta}^1 \gamma(z)dz = \frac{1}{\delta^3}\rho(\frac{s}{\delta}),$$

where for $s \geq 1$, and $\rho(s) = 0$ for $s \in (0,1)$,

$$\rho(s) = \frac{2}{s}\int_s^1 \gamma(z)\ dz, \quad \rho'(s) = -\frac{2}{s^2}\int_s^1 \gamma(z)\ dz - \frac{2}{s}\gamma(s) \leq 0\,.$$

It is also easy to check that

$$\int_{\mathbb{R}} \rho(|\xi|)\xi^2 d\xi = 2\int_0^1 s^2\gamma(s)ds = 1.$$

For the simple 1d linear model (4.2) with a periodic boundary condition (so that boundary effect can be ignored), and the nonlocal solution $u_\delta = u_\delta(x)$ of (4.2) and the local limit solution $u_0 = u_0(x)$ of (4.4) with the same right hand side function $f = f(x)$, it has been shown [Du and Yang, 2016] that the difference between u_δ and u_0 are in general on the order of $O(\delta^2)$, see similar estimates in Theorem 4.3.1 in Section 4.3. However, by taking the first integrals of both the nonlocal and local equations, we can derive from (4.8) the following result.

Theorem 4.1.1. *For the same data $f = f(x)$, let u_δ be the solution of the nonlocal equation* (4.2) *and u_0 be the solution of the local limit* (4.4)*. Then*

$$\mathbb{G}_\delta^p u_\delta(x) = \frac{d}{dx}u_0(x)\,. \tag{4.9}$$

The above relation implies the *superconvergence* or exactness of the nonlocal gradient of the nonlocal solution to the local derivative of the associated local limit

solution. This, of course, is a rather special consequence valid for the 1d problems under consideration. More general multidimensional cases would be studied in the future. For other choices of the kernel β_δ, (4.9) may not hold, and the error $\mathbb{G}_\delta u_\delta - \frac{d}{dx}u_0$ might depend on δ, the nonlocal kernels and the data f. More detailed discussions can be found in later sections.

While $\mathbb{G}_\delta^p$ has nice properties like (4.9), we note that nonlocal gradients given in (4.5) and (4.6) provide us more choices. For instance, the one-sided version may be useful near the boundary in the presence of other boundary conditions. It can also help to model situations that no longer have the forward-backward symmetry [Du *et al.*, 2017b].

4.1.2 Quadrature collocation scheme

For a positive integer N, we set $h = 1/N$ and $\delta = rh + \delta_0$ for a nonnegative integer $r < N$ and $\delta_0 \in [0, h)$. We denote the quadrature points on Ω by $\{x_i = ih\}_{i=0}^N$ and follow the convention that $x_j = x_{mod(j,N)}$. The same periodic extension convention is applied to other relevant vector arrays such as the discrete solutions. A standard continuous piecewise linear *hat* basis function is given by

$$\phi_i^1(x) = \begin{cases} (x - x_{i-1})/(x_i - x_{i-1}) & \text{for } x \in (x_{i-1}, x_i), \\ (x_{i+1} - x)/(x_{i+1} - x_i) & \text{for } x \in [x_i, x_{i+1}), \\ 0, \quad \text{otherwise.} \end{cases} \tag{4.10}$$

We adopt the asymptotically compatible (AC) quadrature collocation scheme studied in [Tian and Du, 2013]: for $i = 1, ..., N$,

$$\begin{aligned} \mathcal{L}_{\delta,1}^h u_i = -2 \sum_{m=1}^{r} \frac{u_{i-m} - 2u_i + u_{i+m}}{(mh)} \int_{I_m \cup I_{m+1}} \phi_m^1(s) s \gamma_\delta(s) ds \\ - \frac{2(u_{i-r-1} - 2u_i + u_{i+r+1})}{(r+1)h} \int_{I_{r+1}} \phi_{r+1}^1(s) s \gamma_\delta(s) ds = f_i \,, \end{aligned} \tag{4.11}$$

where $I_j = ((j-1)h, jh)$ for $1 \le j \le r$, and $I_{r+1} = (rh, \delta)$.

Similar to the approximation to $\mathcal{L}_\delta$, we may consider the following discretization of the nonlocal gradient operator: for $i = 1, ..., N$,

$$\begin{aligned}\mathbb{G}_{\delta,h}u_i = &\sum_{m=1}^{r}(u_{i+m} - u_{i-m})\int_{I_m\cup I_{m+1}} \phi_m^1(s)s\beta_\delta(s)ds \\ &+ \ (u_{i+r+1} - u_{i-r-1})\int_{I_{r+1}} \phi_{r+1}^1(s)s\beta_\delta(s)ds\,.\end{aligned} \tag{4.12}$$

We may also consider the one sided versions of $\mathbb{G}_{\delta,h}$, the details are omitted. In comparison, we let $\mathbb{G}_{0,h}^+$, $\mathbb{G}_{0,h}^-$ and $\mathbb{G}_{0,h}$ denote the local discrete derivative operators with forward, backward and central differences respectively, namely

$$\mathbb{G}_{0,h}^{\pm}u_j = \pm\frac{u_{j\pm1} - u_j}{h}, \quad \text{and} \quad \mathbb{G}_{0,h}u_j = \frac{u_{j+1} - u_{j-1}}{2h}.$$

One may note that the above discretization $\mathbb{G}_{\delta,h}$ also provides an asymptotically compatible approximation to the nonlocal gradient operator and its local limit, as demonstrated through theoretical analysis presented later.

Now, given the freedom in the choices of the kernels for the nonlocal gradient, let us also consider a discrete analog of $\mathbb{G}_\delta^p$. For this, we let $c_m = h^2 b_m$ and S denote the forward shift operator, that is $Su_j = u_{j+1}$, then we have

$$\begin{aligned}-\mathcal{L}_{\delta,1}^h &= \frac{1}{h^2}\sum_{m=1}^{r+1}(S_{-m} - 2I + S_m)c_m \\ &= \frac{1}{h^2}(S-I)(I-S^{-1})\sum_{m=1}^{r+1}c_m(\sum_{k=0}^{m-1}S^k)(\sum_{k=0}^{m-1}S^{-k}) \\ &= \frac{1}{h^2}(S-I)(I-S^{-1})\mathbb{Y}_{\delta,h} \\ &= \frac{1}{h}(S-I)\mathbb{G}_{\delta,h}^{p-} \\ &= \frac{1}{h}(I-S^{-1})\mathbb{G}_{\delta,h}^{p+}\end{aligned}$$

where the operators $\mathbb{G}_{\delta,h}^{p\pm}$ and $\mathbb{Y}_{\delta,h}$ are given respectively by

$$\mathbb{Y}_{\delta,h} = \sum_{m=1}^{r+1}c_m(\sum_{k=0}^{m-1}S^k)(\sum_{k=0}^{m-1}S^{-k})\,, \quad \mathbb{G}_{\delta,h}^{p\pm} = \pm\frac{1}{h}(S^{\pm1} - I)\mathbb{Y}_{\delta,h}\,. \tag{4.13}$$

Then by noting that $(S - I)(I - S^{-1})/h^2$ is in fact the second order central difference of (4.4), we have derived the following special relation.

Theorem 4.1.2. *Let $u_{\delta,h}$ and $u_{0,h}$ be the solutions of* (4.11) *and the central second order difference scheme of* (4.4)*, then*

$$\mathbb{Y}_{\delta,h} u_{\delta,h} = u_{0,h}, \quad \mathbb{G}^{p\pm}_{\delta,h} u_{\delta,h} = \mathbb{G}^{\pm}_{0,h} u_{0,h},$$

and consequently,

$$\mathbb{G}^{p}_{\delta,h} u_{\delta,h} = \frac{1}{2}(\mathbb{G}^{p-}_{\delta,h} + \mathbb{G}^{p+}_{\delta,h}) u_{\delta,h} = \mathbb{G}_{0,h} u_{0,h}\,. \tag{4.14}$$

The above result in particular implies the superconvergence, in fact, the exactness at the discrete level, of the nonlocal discrete gradients of the nonlocal solution to the local discrete gradients (forward, backward and central differences) of the local solution. A further consequence of the exactness of the nonlocal gradient and its discrete approximation to the respective local limits is the error estimate between $\mathbb{G}^{p}_{\delta,h} u_{\delta,h}$ and $\mathbb{G}^{p}_{\delta} u_{\delta}$, which exhibits uniform convergence independent of the parameter δ.

Theorem 4.1.3. *Let u_δ be the solution of the nonlocal equation* (4.2) *and $u_{\delta,h}$ be the solution of quadrature approximation* (4.11)*. Let u_0 and $u_{0,h}$ be the solution of* (4.4) *and the central second order difference approximation. Then,*

$$\mathbb{G}^{p}_{\delta,h} u_{\delta,h} - \mathcal{R}_h \mathbb{G}^{p}_{\delta} u_{\delta} = \mathbb{G}_{0,h} u_{0,h} - \mathcal{R}_h \frac{du_0}{dx}$$

where $\mathcal{R}_h$ denotes the restriction operator with respect to the quadrature points $\{x_i = ih\}_{i=0}^{N}$, that is, $\mathcal{R}_h$ takes a function defined on the interval to a vector whose entries are given by the function values at $\{x_i = ih\}_{i=0}^{N}$.

With the periodic boundary condition, it is easy to see that the order of the above error in h is contingent upon the regularity of the exact solution of the local equation that in fact is determined by the regularity of the right hand side $f = f(x)$. For

nonlocal gradient $\mathbb{G}_\delta$ and the one-sided versions $\mathbb{G}_\delta^\pm$ with a more generic kernel β_δ, the above superconvergence may not always hold. The orders of numerical errors will be examined more closely in the experiments and analysis presented later.

4.2 Numerical experiments

In this section, we present a set of numerical experiments to illustrate the application of nonlocal gradient recovery. For convenience, we work with a simple piecewise constant kernel

$$\gamma_\delta(s) = \frac{3}{2\delta^3}\chi_{[-\delta,\delta]}(s)\,, \tag{4.15}$$

where χ is the characteristic function. We let $\beta_\delta = \gamma_\delta$ in the nonlocal operator $\mathbb{G}_\delta$ and use the AC quadrature discretization discussed earlier. In comparison, we also present nonlocal gradients of the special operator $\mathbb{G}_\delta^p$. In this case,

$$\rho_\delta(s) = \frac{3(\delta - |s|)}{|s|\delta^3}\chi_{[-\delta,\delta]}(s)\,, \tag{4.16}$$

and we adopt (4.13) and (4.14) as numerical discretization. In order to get nonlocal solutions with different regularities, we choose a right hand side f that is characterized by prescribed positive parameters σ and k.

For the first example, we consider $\hat{f}_\sigma(x) = \breve{f}_\sigma(x) - \int_0^1 \breve{f}_\sigma(x)dx$. $\breve{f}_\sigma(x) = (\sigma - |x - 1/2|)/\sigma^2\chi_{[1/2-\sigma,1/2+\sigma]}$, which is piecewise differentiable and often called a hat function or C^0 linear spline. In the second example, we consider some smooth right hand side functions given by Fourier modes $\tilde{f}_k(x) = \sin(kx\pi)$ with k being an even positive integer. We consider the case with a finite and relatively small k and the case where k gets larger as the horizon parameter δ decreases, namely $k = 1/\delta$. The latter case allows us to make observations for oscillatory solutions. In the third example, we use a right hand side given by a box-potential, that is, $f_\sigma(x) = \acute{f}_\sigma(x) - \int_0^1 \acute{f}_\sigma(x)dx$ where $\acute{f}_\sigma(x) = 1/(2\sigma)\chi[1/2 - \sigma, 1/2 + \sigma]$. Note that if we let $\sigma \to 0$, then the sequences $\{\hat{f}_\sigma\}$ and $\{f_\sigma\}$ all converge to the Dirac delta measure $f_\star(x) = \delta(1/2 - x) - 1$, which is

a limiting case that we pay special attention to. We note that the sequence $\{\tilde{f}_\sigma\}$ has the function with constant value zero as the limit in the standard L^2 weak topology.

For all examples considered here, the local solution u_0 can be analytically constructed by solving the corresponding local problems which serves as a convenient benchmark. Similar constructions can be found in [Silling *et al.*, 2003] for various choices of micromudulus or kernel functions. To quantify the errors, we mainly consider the pointwise L^∞ norm in this section but results based on the discrete L^2 norm are also discussed in a number of instances. We adopt (4.11) to get the nonlocal solutions. The asymptotic compatibility of (4.11) has been carefully studied in [Tian and Du, 2013] as well as the convergence of several limiting processes. Thus, the corresponding experimental observations are given only if some potential discrepancies need to be clarified. Our focus, naturally, is to compare the behavior of local and nonlocal discrete gradient operators defined by (4.12) both with fixed $\delta > 0$ (for the solution of nonlocal models) and with $\delta \to 0$ (for bench-marking with well-established local solutions).

Taking $h = \delta/r$ as the mesh size for an integer $r \geq 1$, we consider the following limiting behaviors: 1) let $h \to 0$ with a fixed δ to see if the nonlocal schemes are compatible with the continuum limits; 2) for a sufficiently small h (so that we effectively have the nonlocal solutions available on the continuum level), reduce δ to see the δ-dependence of the convergence of nonlocal solutions to the local limit; 3) let both h and δ go to zero simultaneously with a fixed r, so as to test the asymptotic compatibility.

4.2.1 The case of hat function $\hat{f}_\sigma$ with a given positive σ

In this example, we choose $\sigma = 0.25$. In terms of the limiting behavior of numerical nonlocal solutions as $h \to 0$, we get results that are the same as in [Tian and Du, 2013], namely numerical solutions $u_{\delta,h}$ of the nonlocal problem converge to u_δ at each grid point with an error on the order of $\mathcal{O}(h^2)$. Moreover, if $u_{0,h}$ denotes the numerical

solution of the limiting local model on the same mesh, then

$$\|u_{\delta,h} - u_{0,h}\|_\infty \sim \mathcal{O}(\delta^2),$$

meaning that the discrete nonlocal scheme is asymptotically compatible with the local limit. The error between the discrete solutions of the nonlocal and local problems is on the order of the modeling error. Numerical data are omitted. On the other hand, the data collected on the local derivatives tell us that

$$\|\mathbb{G}_0(u_\delta - u_0)\|_\infty \sim \mathcal{O}(\delta^2),$$

see the columns 2 and 3 of Table 4.1. Note that at the jump discontinuity of $G_0 u_\delta$, the averaged value across the discontinuity is used. The derivative data have not been presented before in [Tian and Du, 2013] since the earlier work was primarily concerned with the numerical solution only, not its derivatives. The second order convergence in the derivatives is due to the regularity pickup resulted from the fact that the local and nonlocal operators under consideration commute with each other for the periodic boundary condition case.

By applying the nonlocal gradient operator $\mathbb{G}_{\delta,h}$, instead of the local one, we find that

$$\|\mathbb{G}_{\delta,h} u_{\delta,h} - \mathcal{R}_h \mathbb{G}_\delta u_\delta\|_\infty \sim \mathcal{O}(h^2),$$

where $\mathcal{R}_h$ is the restriction to the quadrature points $\{x_i = ih\}_{i=0}^N$, as shown in the second and third columns of Table 4.2. Moreover,

$$\|\mathbb{G}_\delta u_\delta - \mathbb{G}_0 u_0\|_\infty \sim \mathcal{O}(\delta^2),$$

as presented in columns 4 and 5 of Table 4.1. The asymptotically compatible property of discrete nonlocal gradient schemes can also be observed, for example, by letting $h \to 0$ with a fixed δ/h. Columns 4 and 5 of Table 4.2 show that the error order as $h \to 0$ with the fixed $\delta/h = 4$ is $\mathcal{O}(h^2)$ as expected. We provide some error estimate of $\mathbb{G}_{\delta,h} u_{\delta,h} - \mathbb{G}_{0,h} u_{0,h}$ in Theorem 4.3.4 of the next section for $\eta \geq 1$ to further substantiate the experimental findings.

δ	$\|\mathbb{G}_0 u_\delta - \mathbb{G}_0 u_0\|_\infty$	Order	$\|\mathbb{G}_\delta u_\delta - \mathbb{G}_0 u_0\|_\infty$	Order
2^{-2}	1.60×10^{-2}	$--$	5.96×10^{-2}	$--$
2^{-3}	3.76×10^{-3}	2.08	1.42×10^{-2}	2.07
2^{-4}	9.25×10^{-4}	2.02	3.54×10^{-3}	2.00
2^{-5}	2.30×10^{-4}	2.00	8.85×10^{-4}	2.00
2^{-6}	5.75×10^{-5}	2.00	2.21×10^{-4}	2.00

Table 4.1: L^∞ errors of local and nonlocal gradient operators as δ decreases with $f = \hat{f}_\sigma$.

	fixed δ=1/4		fixed $\delta/h = 4$	
h	$\|\mathbb{G}_{\delta,h} u_{\delta,h} - \mathcal{R}_h \mathbb{G}_{\delta,\frac{h}{2}} u_{\delta,\frac{h}{2}}\|_\infty$	Order	$\|\mathbb{G}_{\delta,h} u_{\delta,h} - \mathcal{R}_h \mathbb{G}_0 u_0\|_\infty$	Order
2^{-4}	6.85×10^{-4}	$--$	3.41×10^{-3}	$--$
2^{-5}	1.70×10^{-4}	2.01	8.52×10^{-4}	2.00
2^{-6}	4.23×10^{-5}	2.00	2.13×10^{-4}	2.00
2^{-7}	1.06×10^{-5}	2.00	5.32×10^{-5}	2.00
2^{-8}	2.64×10^{-6}	2.00	1.33×10^{-5}	2.00

Table 4.2: L^∞ errors of discrete nonlocal gradient as $h \to 0$ with a fixed δ or a fixed δ/h for $f = \hat{f}_\sigma$.

In comparison, we can also apply the special nonlocal gradient operator $\mathbb{G}_\delta^p$ as well as its discrete forms $\mathbb{G}_{\delta,h}^p$ or $\mathbb{G}_{\delta,h}^{p\pm}$. Since the exactness of nonlocal gradients at the discrete level is guaranteed in Theorem 4.1.2 for any δ, we will focus on the limiting processes of vanishing h with a fixed δ or fixed δ/h. In the second and third columns of Table 4.3, $\mathbb{G}_{\delta,h}^{p+}$ is used and $\mathbb{G}_{\delta,h}^{p+}u_{\delta,h}$ converges to $\mathbb{G}_\delta^p u_\delta = \mathbb{G}_0 u_0$ as shown in Theorem 4.1.1, on the order of $\mathcal{O}(h)$ at each grid point. Moreover, when we use the discrete form $\mathbb{G}_{\delta,h}^p$, in principle we expect second order convergence, the same as the convergence order of local central difference schemes to local models as mentioned in Theorem 4.1.3. However, superconvergence can be observed for the difference approximation of local solutions, yielding exact grid point values of derivatives, see the last column of Table 4.3. One can compare the two kinds of nonlocal gradient operators by Table 4.2 and Table 4.3. Both schemes converge to their continuum nonlocal gradients, $\mathbb{G}_\delta u_\delta$ and $\mathbb{G}_\delta^p u_\delta$, where the former has $\mathcal{O}(\delta^2)$ error from its local limit $\mathbb{G}_0 u_0$ but the latter is exactly the local derivatives.

h	$\|\mathbb{G}_{\delta,h}^{p+}u_{\delta,h} - \mathcal{R}_h\mathbb{G}_\delta^{p+}u_\delta\|_\infty$	Order	$\|\mathbb{G}_{\delta,h}^{p}u_{\delta,h} - \mathcal{R}_h\mathbb{G}_\delta^{p}u_\delta\|_\infty$
2^{-4}	9.38×10^{-2}	$--$	5.55×10^{-17}
2^{-5}	4.69×10^{-2}	1.00	2.22×10^{-16}
2^{-6}	2.34×10^{-2}	1.00	4.44×10^{-16}
2^{-7}	1.17×10^{-2}	1.00	8.88×10^{-16}
2^{-8}	5.86×10^{-3}	1.00	2.66×10^{-15}

Table 4.3: L^∞ errors and error order of the special nonlocal gradient operator as $h \to 0$ with a fixed $\delta = 1/4$ for $f = \hat{f}_\sigma$.

4.2.2 The case of Fourier modes $\tilde{f}_k$

While the first example gives the $O(\delta^2)$ error order of nonlocal gradient recovery, there is no quantitative estimates on how the modeling data affect the error. For

$\tilde{f}_k(x) = \sin(k\pi x)$ with $k = 2$ and let $\delta \to 0$, we expect the second order in accuracy, same as the example 1 (see Columns 2 and 3 of Table 4.4). However, if we let $k = 1/\delta$ and let $\delta \to 0$, we see that the error order of the nonlocal gradient is one order less than that in first example (see columns 4 and 5 of Table 4.4), due to the δ-dependent highly oscillatory right hand side. Such a reduction of error order matches with the analysis in Theorem 4.3.4 corresponding to cases $\eta = 1$ and 0.

	$k = 2$		$k = 1/\delta$	
δ	$\|\mathbb{G}_\delta u_\delta - \mathbb{G}_0 u_0\|_\infty$	Order	$\|\mathbb{G}_\delta u_\delta - \mathbb{G}_0 u_0\|_\infty$	Order
2^{-2}	1.97×10^{-2}	$--$	3.98×10^{-2}	$--$
2^{-3}	4.92×10^{-3}	2.01	1.99×10^{-2}	1.00
2^{-4}	1.23×10^{-3}	2.00	9.95×10^{-3}	1.00
2^{-5}	3.07×10^{-4}	2.00	4.97×10^{-3}	1.00
2^{-6}	7.67×10^{-5}	2.00	2.49×10^{-3}	1.00

Table 4.4: L^∞ errors and error orders between nonlocal gradient of nonlocal solutions and derivatives of the local limits as δ decreases for source terms $\{\tilde{f}_k\}$ with $k = 2$ or $k = 1/\delta$.

4.2.3 The case of box-potential f_σ with a positive σ

The case of discontinuous f_σ with $\sigma = 0.25$ serves to compare the performances of local and nonlocal gradient schemes. Since f_σ is not in H^1, the nonlocal solution u_δ also fails to be in H^1. For a fixed δ and vanishing h, the conventional local gradient operator fails to provide useful information in stress analysis, which is shown in Figure 4.1. This is true regardless which local discrete derivative operator, among forward, backward and central differences, is used. Table 4.5 shows the divergence of local gradient of nonlocal solutions for a fixed δ and vanishing h in the discrete L^2 norm. Hence, for a fixed δ, local gradient schemes are neither effective nor compatible when

the solutions lose regularity.

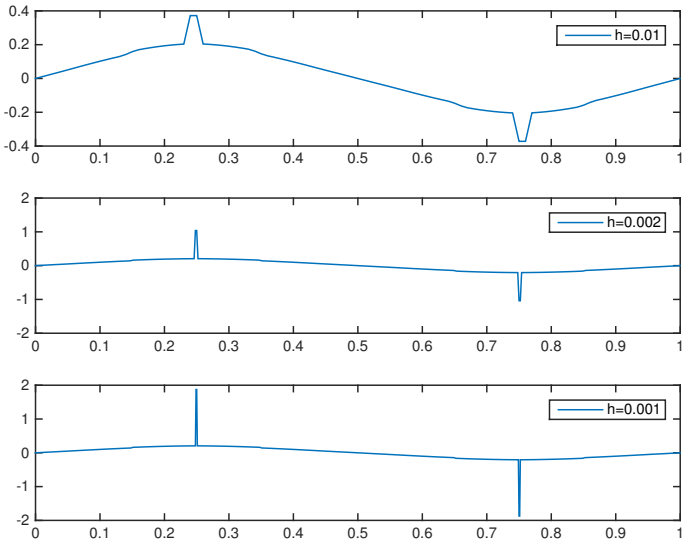

Figure 4.1: The conventional local gradient of nonlocal solutions for discontinuous data with a fixed $\delta = 0.1$ as $h \to 0$. Top: $h = 0.01$; middle: $h = 0.002$; bottom: $h = 0.001$. X-axis: the periodic cell $\Omega = [0, 1]$; Y-axis: values of local gradients.

	central difference	forward/backward difference
h	$\|\mathbb{G}_{0,h}u_{\delta,h} - \mathcal{R}_h\mathbb{G}_{0,\frac{h}{2}}u_{\delta,\frac{h}{2}}\|_{L^2}$	$\|\mathbb{G}^{\pm}_{0,h}u_{\delta,h} - \mathcal{R}_h\mathbb{G}^{\pm}_{0,\frac{h}{2}}u_{\delta,\frac{h}{2}}\|_{L^2}$
2^{-5}	0.118	0.167
2^{-6}	0.167	0.236
2^{-7}	0.236	0.333
2^{-8}	0.333	0.471
2^{-9}	0.471	0.667

Table 4.5: Divergence of discrete local gradient schemes of nonlocal solutions with a fixed $\delta = 0.25$ as $h \to 0$.

As for the nonlocal gradients, one can compare Figure 4.1 with Figure 4.2 to see the differences between the local and nonlocal schemes with a fixed δ and vanishing

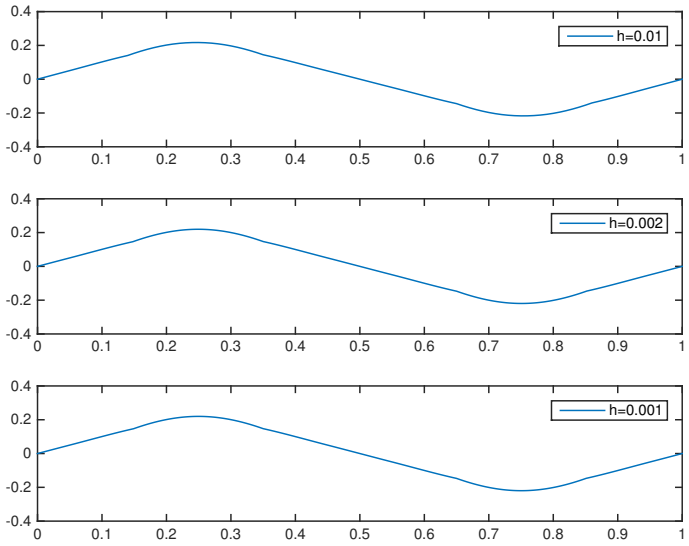

Figure 4.2: The nonlocal gradient recovery of discontinuous data with a fixed $\delta = 0.1$ as $h \to 0$. Top: $h = 0.01$; middle: $h = 0.002$; bottom: $h = 0.001$. X-axis: the periodic cell $\Omega = [0, 1]$; Y-axis: values of nonlocal gradients.

h. Since the nonlocal solutions are only piecewise differentiable in this case, local derivatives blow up at certain grid points as mesh gets refined. Thus, local gradient based stress analysis would not produce useful information. However, if we apply the nonlocal gradient operator on the same nonlocal solution, the corresponding nonlocal gradient not only stays bounded but also, as shown in Figure 4.3, offers compatibility to the local derivative of the local limit as $\delta \to 0$. In this particular case, the maximum stress points coincide with those leading to maximum stress points associated to the local model.

In Figure 4.3, we choose a fixed but a sufficiently small h (so that the modeling error is dominating) and let δ decrease, we can find that the nonlocal gradient of u_δ converges to the local derivative of u_0. In fact, the results in Table 4.6 lead to

$$\|\mathbb{G}_\delta u_\delta - \mathbb{G}_0 u_0\|_\infty \sim \mathcal{O}(\delta)\,,$$

and

$$\|\mathbb{G}_\delta u_\delta - \mathbb{G}_0 u_0\|_{L^2} \sim \mathcal{O}(\delta^{3/2}).$$

The L^2 error order matches with what is stated in Theorem 4.3.4 in the next section corresponding to $\eta = 1/2$.

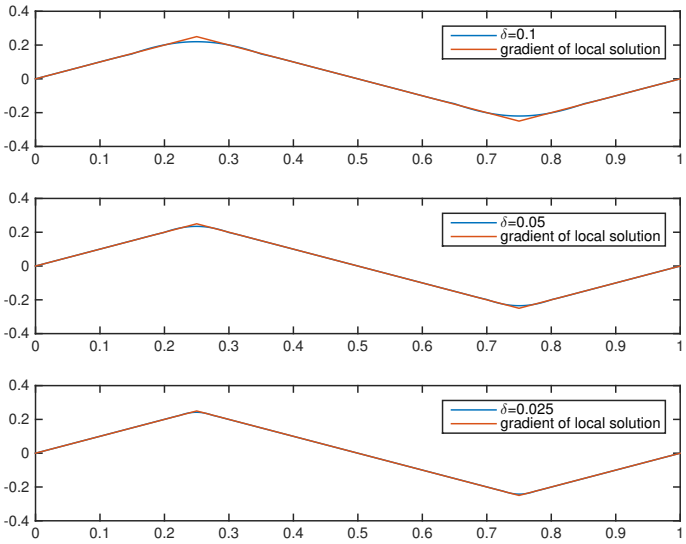

Figure 4.3: The nonlocal gradient recovery for discontinuous data with a sufficiently small $h = 0.001$ as δ decreases. Top: $\delta = 0.1$; middle: $\delta = 0.05$; bottom: $\delta = 0.025$. X-axis: the periodic cell $\Omega = [0, 1]$; Y-axis: values of nonlocal gradients and limiting local gradients.

In addition, we can also compare $\mathbb{G}_{\delta,h}$ with $\mathbb{G}^p_{\delta,h}$ at the discrete level. The results are presented in Table 4.7. Again, both schemes converge to the corresponding nonlocal gradients $\mathbb{G}_\delta u_\delta$ and $\mathbb{G}^p_\delta u_\delta$ on the order of $\mathcal{O}(h)$ at each grid point, but the former has L^∞ error from $\mathbb{G}_0 u_0$ on the order of $\mathcal{O}(\delta)$ as shown in Table 4.6 while the latter is exactly the local derivatives as shown in Theorem 4.1.1.

	L^∞ norm		L^2 norm	
δ	$\|\mathbb{G}_\delta u_\delta - \mathbb{G}_0 u_0\|_\infty$	Order	$\|\mathbb{G}_\delta u_\delta - \mathbb{G}_0 u_0\|_{L^2}$	Order
2^{-2}	7.40×10^{-2}	$--$	2.57×10^{-2}	$--$
2^{-3}	3.72×10^{-2}	0.99	9.14×10^{-3}	1.49
2^{-4}	1.86×10^{-2}	1.00	3.23×10^{-3}	1.50
2^{-5}	9.31×10^{-3}	1.00	1.14×10^{-3}	1.50
2^{-6}	4.66×10^{-3}	1.00	4.10×10^{-4}	1.49

Table 4.6: L^∞ and L^2 errors and error orders between nonlocal gradient of nonlocal solutions and derivatives of the local limits as δ decreases with the right hand side being f_σ.

h	$\|\mathbb{G}_{\delta,h} u_{\delta,h} - \mathcal{R}_h \mathbb{G}_{\delta,\frac{h}{2}} u_{\delta,\frac{h}{2}}\|_\infty$	Order	$\|\mathbb{G}^p_{\delta,h} u_{\delta,h} - \mathcal{R}_h \mathbb{G}^p_\delta u_\delta\|_\infty$	Order
2^{-4}	7.44×10^{-3}	$--$	3.13×10^{-2}	$--$
2^{-5}	3.74×10^{-3}	1.00	1.56×10^{-2}	1.00
2^{-6}	1.90×10^{-3}	0.98	7.81×10^{-3}	1.00
2^{-7}	9.63×10^{-4}	0.98	3.91×10^{-3}	1.00
2^{-8}	4.85×10^{-4}	0.99	1.95×10^{-3}	1.00

Table 4.7: L^∞ errors and error order of two nonlocal gradient operators as $h \to 0$ with a fixed $\delta = 1/4$ for $f = f_\sigma$.

4.2.4 The case of Dirac-Delta function $f_\star$

For the previous example, as $\sigma \to 0$, the right hand side becomes a Dirac delta function, which cannot be interpolated onto grid points directly. We may first mollify the right hand side via a convolution with a kernel also parametrized by δ. Certainly the mollification could in general have a different scaling factor σ, and this will be discussed more in the next section. Different kernels also lead to different mollification $\tilde{f}_\star$. For example, $\tilde{f}_\star$ can be f_δ or $\hat{f}_\delta$ that are identical to f_σ and $\hat{f}_\sigma$ with σ replaced by δ. In this experiment we use these two choices to do mollifications, namely, the right hand side data are the same as in two of the previous examples but are parametrized by the horizon. As δ is reduced, when the mesh is fine enough (so that the discretization error is much less significant than the modeling error), we can make comparisons of the nonlocal solutions with local limits as well as nonlocal gradient with derivatives of its local limit.

First, we use the mollification $\hat{f}_\delta$ and let $\tilde{u}_\delta$ denote the solution of mollified nonlocal problems. Table 4.8 represents the error order of $|\tilde{u}_\delta - u_0|$ in L^2 norm. A theoretical analysis can be found in Theorem 4.3.2 corresponding to $\beta = 0$ and $\eta = -1/2$ where a Gaussian mollifier is used as an illustration. We note that $\hat{f}_\delta$ is regular enough so that it behaves similarly like a Gaussian in the limit.

Now we turn to the two gradient recovery techniques with different mollifications. Since $\hat{f}_\delta \in H^1$, the nonlocal solution of the mollified equation, denoted by $\tilde{u}_\delta$, is also in H^1. Both local and nonlocal gradient schemes converge to the local derivative of u_0 in the sense of L^2 norm. Figure 4.4 shows such limiting behavior of the nonlocal gradient operator as $\delta \to 0$ and Table 4.9 establishes the error orders of the two gradient schemes. Again we refer to Theorem 4.3.4 for related theoretical analysis with $\eta = -1/2$. The maximum nonlocal stress happens at the location of the point load, again the same as the case for local limit.

In comparison, if we pick f_δ as the mollified right hand side, the local gradient operator does not provide useful information as mentioned in the earlier experiment

δ	$\|\tilde{u}_\delta - u_0\|_{L^2}$	Order
2^{-2}	5.73×10^{-3}	$--$
2^{-3}	2.09×10^{-3}	1.45
2^{-4}	7.50×10^{-4}	1.48
2^{-5}	2.67×10^{-4}	1.49
2^{-6}	9.49×10^{-5}	1.50

Table 4.8: L^2 errors and error orders between nonlocal solutions of the mollified equation and the local limits as δ decreases with a Diract-delta function right hand side subject to an H^1 mollification.

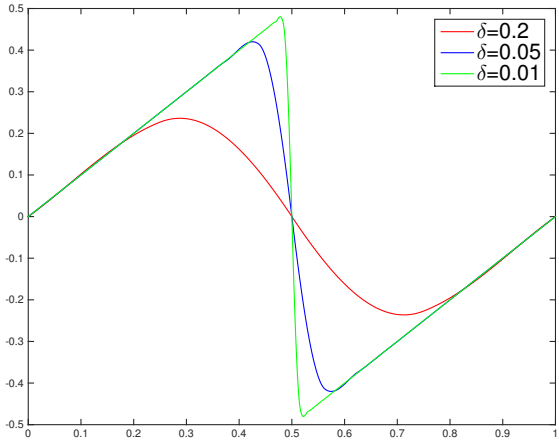

Figure 4.4: The nonlocal gradient recovery for a mollified Dirac-Delta function data as δ decreases. X-axis: the periodic cell $\Omega = [0, 1]$; Y-axis: values of nonlocal gradients with different δ.

	local gradient		nonlocal gradient	
δ	$\|\mathbb{G}_0\tilde{u}_\delta - \mathbb{G}_0 u_0\|_{L^2}$	Order	$\|\mathbb{G}_\delta\tilde{u}_\delta - \mathbb{G}_0 u_0\|_{L^2}$	Order
2^{-2}	1.13×10^{-1}	$--$	1.80×10^{-1}	$--$
2^{-3}	8.02×10^{-2}	0.50	1.27×10^{-1}	0.50
2^{-4}	5.65×10^{-2}	0.50	8.96×10^{-2}	0.50
2^{-5}	4.00×10^{-2}	0.51	6.31×10^{-2}	0.51
2^{-6}	2.79×10^{-2}	0.51	4.43×10^{-2}	0.51

Table 4.9: L^2 errors and error orders between local and nonlocal gradients and derivatives of local solutions as δ decreases with a Dirac-delta function data subject to an H^1 mollification.

due to the lack of regularity of u_δ. However, the nonlocal gradient operator still works and offers the same error order as when we use $\hat{f}_\delta$, see data in Table 4.10.

We omit the case for $\mathbb{G}_\delta^p\tilde{u}_\delta$ as we get the same superconvergence predicted by the earlier theorems.

4.2.5 Discussions on experiments

The numerical experiments reported above use quadrature based approximations and cover various types of data and solutions. We make a brief summary based on the experimental observations. First, by comparing local gradient operators and generic nonlocal gradient operators $\mathbb{G}_\delta$ as well as their discretization, we find that

1. For smooth enough (C^1 or H^1 or better) data where local gradient operators can be directly used to calculate the derivatives of u_δ, nonlocal gradient operators also perform well, especially when both $h \to 0$ and $\delta \to 0$.

2. For H^α data with $\alpha \in [0, 1)$, local gradient fails to provide credible information in nonlocal stress analysis, whereas nonlocal gradient schemes still perform well

δ	$\|\mathbb{G}_\delta \tilde{u}_\delta - \mathbb{G}_0 u_0\|_{L^2}$	Order
2^{-2}	1.83×10^{-1}	$--$
2^{-3}	1.38×10^{-1}	0.41
2^{-4}	1.00×10^{-1}	0.45
2^{-5}	7.19×10^{-2}	0.48
2^{-6}	5.10×10^{-2}	0.49

Table 4.10: L^2 errors and error orders between nonlocal gradients and derivatives of local solutions as δ decreases with the Dirac-delta function subject to an L^2 mollification.

and possess the asymptotically compatible property.

3. For H^α data with $\alpha \in (-1, 0)$, one may mollify the right hand first in order to do quadrature collocation approximations. Then nonlocal gradient operators work well in recovering the derivatives of local limits but whether local gradient operators work or not depends on the regularity of mollified right hand data.

These findings provide motivations to the theoretical analysis given in the next section. While the nonlocal gradient operators performs better than local one for conducting stress analysis, different nonlocal gradient operators, such as $\mathbb{G}_{\delta,h}$ and $\mathbb{G}^p_{\delta,h}$, can also perform differently. On one hand, $\mathbb{G}_{\delta,h}$ gives us the freedom of choosing the kernel β_δ and also works well in other kinds of volume-constrained problems that are nonlocal analog of boundary value problems, see [Du *et al.*, 2012; Du *et al.*, 2013b] for the connections. On the other hand, while $\mathbb{G}^p_{\delta,h}$ is a specialized operator under our considerations of 1d periodic model and quadrature based discretization, it has some unique features. Apart from the AC property, $\mathbb{G}^p_{\delta,h}$ can recover exactly the difference of the local solution as h goes to 0 with any δ, as shown both theoretically in Theorem 4.1.1 and 4.1.2 and numerically in the experiments above.

4.3 Some theoretical analysis

We provide some theoretical insights to the observed convergence results based on numerical experiments. We adopt the Fourier analysis due to the periodic boundary condition, similar to the analysis of spectral methods given in [Zhou and Du, 2010; Du and Yang, 2016].

4.3.1 Preliminaries

Suppose the number of grid points is $2N$ on the interval $[0, 1]$ with spacing $h = \frac{1}{2N}$. Now for a periodic array $\{u_j\}$ defined on the grid, we use the *discrete Fourier transform*: for $j = 1, 2, \cdots, 2N$, and $n = -N+1, \cdots, 1, \cdots, N$,

$$u_j = \frac{1}{2\pi} \sum_{n=-N+1}^{N} e^{i2\pi n x_j} \hat{u}_n \qquad \text{and} \qquad \hat{u}_n = h \sum_{j=1}^{2N} e^{-i2\pi n x_j} u_j \,.$$

Let us take $\delta = rh$ for an integer $r \geq 1$ for simplicity right now. Let $U_N = (u_1, u_2, ..., u_N)^T$ and $F_N = (f_1, f_2, ..., f_N)^T$. For any $\eta \in \mathbb{R}$, we take $\|\cdot\|_\eta$ as the discrete H^η norm and $|\cdot|_\eta$ as the discrete semi-H^η norm defined by

$$|U_N|_\eta^2 = h \sum_{j=1}^{2N} |n|^{2\eta} |u_j|^2 = \frac{1}{2\pi} \sum_{\substack{n=-N+1 \\ n\neq 0}}^{N} |n|^{2\eta} |\hat{u}_n|^2 \quad \text{and} \quad \|U_N\|_\eta^2 = |U_N|_\eta^2 + \|U_N\|_0^2$$

with $\|\cdot\|_0$ being the standard L^2 norm.

First, $\{(e^{i2\pi n x_1}, e^{i2\pi n x_2}, \cdots, e^{i2\pi n x_N})^T\}$ forms an eigenbasis of the discrete operators $\mathbb{A}_\delta^h$, $\mathbb{A}^h$, $\mathbb{G}_{\delta,h}$ and $\mathbb{G}_{0,h}$ introduced before, with eigenvalues given respectively by

$$\lambda_\delta^h(n) = 2 \sum_{j=1}^{r} b_j (1 - \cos(2\pi n j h)), \quad \lambda^h(n) = \frac{2}{h^2}(1 - \cos(2\pi n h)) \,.$$

for integer n between 1 and N where b_j's are given by

$$-b_j := \begin{cases} \frac{4}{h}\sum_{k=1}^{r}\int_{I_k\cup I_{k+1}}\frac{\phi_k^1(s)}{k}s\gamma_\delta(s)ds + \frac{4}{h}\int_{I_{r+1}}\frac{\phi_{r+1}^1(s)}{r+1}s\gamma_\delta(s)ds, & j=0 \\ -\frac{2}{jh}\int_{I_j\cup I_{j+1}}\phi_j^1(s)s\gamma_\delta(s)ds, & 1\le j\le r \\ -\frac{2}{(r+1)h}\int_{I_{r+1}}\phi_{r+1}^1(s)s\gamma_\delta(s)ds, & j=r+1 \\ 0, & \text{otherwise}, \end{cases} \tag{4.17}$$

and

$$\mu_\delta^h(n) = ih\sum_{j=1}^{r} jb_j\sin(2\pi njh), \quad \mu^h(n) = \frac{i}{h}\sin(2\pi nh)\,.$$

As in the experiments corresponding to a non-smooth right hand side $f \in H^\eta$ for $-1 < \eta < 0$, we introduce a mollifier on f to enhance its regularity, and thus u_δ simultaneously. We only consider the Gaussian mollifier here as an illustration and leave more general cases to future discussions. Let $\mathcal{M}_\delta$ be the Gaussian mollifier defined by

$$\mathcal{M}_\delta f(x) = \int_{-\infty}^{\infty} G_\delta(x-\tau)f(\tau)d\tau\,, \quad \text{where} \quad G_\delta(s) = \frac{1}{2\delta\sqrt{\pi}}e^{-(\frac{s}{2\delta})^2}. \tag{4.18}$$

One can define $\tilde{F}_N^\delta$ as: for $j = 1, 2, \cdots, N$,

$$(\tilde{F}_N^\delta)_j = \mathcal{M}_\delta f(x_j) = \frac{1}{2\pi}\sum_{\substack{n=-N+1\\ n\neq 0}}^{N} e^{-4\pi^2n^2\delta^2}e^{i2\pi nx_j}\hat{f}_n\,. \tag{4.19}$$

4.3.2 Convergence analysis of nonlocal numerical solutions with vanishing δ

We first list the asymptotic compatibility properties, similar to the results of [Du and Yang, 2016]. All the proofs can be found in [Du *et al.*, 2016b].

Theorem 4.3.1. *Let $\mathbb{A}_\delta^h U_N^\delta = F_N$ and $\mathbb{A}^h U_N^0 = F_N$, then*

$$\|U_N^\delta - U_N^0\|_0 \le C\delta^2\|F_N\|_0\,, \tag{4.20}$$

for a constant C independent of δ, N and F_N.

Next, if $f \in H^\eta$ for some η such that $-1 \leq \eta < 0$, we consider the mollification operator $\mathcal{M}_\delta$ defined in (4.18). Denote by $\tilde{U}_N^\delta$ and $\tilde{U}_N^0$ the solutions to following mollified equations respectively:

$$\mathbb{A}_\delta^h \tilde{U}_N^\delta = \tilde{F}_N^\delta, \quad \mathbb{A}^h \tilde{U}_N^0 = \tilde{F}_N^\delta,$$

where $\tilde{F}_N^\delta$ is defined in (4.19). Then we have the following theorem with vanishing δ.

Theorem 4.3.2. *Assume that $F_N \in H^\eta$ with $-1 < \eta < 0$. Then for any $0 \leq \beta \leq 2 + \eta$,*

$$\|\tilde{U}_N^\delta - U_N^0\|_\beta \leq C\delta^{2+\eta-\beta}|F_N|_\eta, \tag{4.21}$$

where C is a constant independent of N and δ.

***Remark* 4.3.3.** *We can take different horizon parameters in nonlocal diffusion operators (δ_1) and mollification operators (δ_2). Then instead of* (4.21)*, we can get*

$$\|\tilde{U}_N^{\delta_1} - U_N^0\|_\beta \leq C\left(\delta_1^2\delta_2^{\eta-\beta} + \delta_2^{2+\eta-\beta}\right)|F_N|_\eta.$$

4.3.3 Convergence analysis of nonlocal gradient recovery

We now show the asymptotic compatibility of the nonlocal gradient schemes for the kernel defined in (4.15).

Theorem 4.3.4. *Assume that U_N^δ and U_N^0 are solutions to $\mathbb{A}_\delta^h U_N^\delta = F_N$ and $\mathbb{A}^h U_N^0 = F_N$ respectively. Then*

$$\|\mathbb{G}_{\delta,h}U_N^\delta - \mathbb{G}_{0,h}U_N^0\|_0 \leq C\delta^{\min\{2,1+\eta\}}|F_N|_{\min\{\eta,1\}}, \tag{4.22}$$

where C is a constant independent of N and δ.

Proof. For $\eta \geq 1$, it is easy to verify (4.22). For $-1 < \eta < 1$, we prove the inequality by

$$\|\mathbb{G}_{\delta,h}U_N^\delta - \mathbb{G}_{0,h}U_N^0\|_0 \leq \|\mathbb{G}_{\delta,h}U_N^\delta - \mathbb{G}_{\delta,h}U_N^0\|_0 + \|\mathbb{G}_{\delta,h}U_N^0 - \mathbb{G}_{0,h}U_N^0\|_0.$$

Furthermore, we aim to show

$$\|\mathbb{G}_{\delta,h}U_N^\delta - \mathbb{G}_{\delta,h}U_N^0\|_0 \le C\delta^{1+\eta}|F_N|_\eta, \tag{4.23}$$

and

$$\|\mathbb{G}_{\delta,h}U_N^0 - \mathbb{G}_{0,h}U_N^0\|_0 \le C\delta^{1+\eta}|F_N|_\eta. \tag{4.24}$$

It suffices to show that for all n such that $1 \le |n| \le N$,

$$R_n := \delta^{-1-\eta}|n|^{-\eta}\left|\frac{\mu_\delta^h(n)}{\lambda_\delta^h(n)} - \frac{\mu_\delta^h(n)}{\lambda^h(n)}\right| \le C, \tag{4.25}$$

and

$$T_n := \delta^{-1-\eta}|n|^{-\eta}\left|\frac{\mu_\delta^h(n)}{\lambda^h(n)} - \frac{\mu^h(n)}{\lambda^h(n)}\right| \le C. \tag{4.26}$$

In each part, we separate the cases $\delta|n| \le 1/2$ and $\delta|n| > 1/2$. For R_n, we rewrite it as

$$R_n = \left(\delta^{1-\eta}|n|^{-\eta}\left|\mu_\delta^h(n)\right|\right)\left(\frac{1}{\delta^2}\left|\frac{1}{\lambda_\delta^h(n)} - \frac{1}{\lambda^h(n)}\right|\right).$$

Due to (**??**), it suffices to show

$$\delta^{1-\eta}|n|^{-\eta}\left|\mu_\delta^h(n)\right| \le C. \tag{4.27}$$

When $\delta|n| \le 1/2$, since $|\sin(2\pi njh)| \le 2\pi|n|jh$,

$$|\mu_\delta^h(n)| \le 2\pi|n|\sum_{j=1}^{r} b_j(jh)^2.$$

By the fact that $\sum_{j=1}^r b_j(jh)^2 = 1$,

$$\delta^{1-\eta}|n|^{-\eta}\left|\mu_\delta^h(n)\right| \le 2\pi(\delta|n|)^{1-\eta} \le 2^\eta\pi.$$

When $\delta|n| > 1/2$, one can calculate that

$$b_j = \frac{3h}{\delta^3}, \quad j = 1, 2, \cdots, r-1,$$

and

$$b_r = \frac{h}{\delta^3}\left(\frac{3}{2} - \frac{h}{2\delta}\right).$$

Since $r \geq 1$, $1 \leq \frac{3}{2} - \frac{h}{2\delta} < \frac{3}{2}$. Therefore,

$$|\mu_\delta^h(n)| \leq \frac{Ch^2}{\delta^3} |\sum_{j=1}^{r} j \sin(2\pi njh)|.$$

Moreover, we claim that

$$|\sum_{j=1}^{r} j \sin(2\pi njh)| \leq \frac{C\delta}{nh^2}.$$

Indeed, let $a = 2\pi nh$, our goal is to show

$$|\sum_{j=1}^{r} j \sin(ja)| \leq \frac{Cr}{a} \qquad \forall a \in [0, \pi], \forall r \geq 1 \ .$$

By the formula $2\sin(aj)\sin(a) = \cos(a(j-1)) - \cos(a(j+1))$, we can rewrite $\sum_{j=1}^{r} j\sin(ja)$ as

$$\begin{aligned}
\sum_{j=1}^{r} j \sin(ja) &= \frac{1}{2\sin(a)} \sum_{j=1}^{r} j\big[\cos(a(j-1)) - \cos(a(j+1))\big] \\
&= \frac{1}{2\sin(a)} \Big(\cos(0) + 2\sum_{j=1}^{r} \cos(aj) - (r+1)\cos(ar) - r\cos(a(r+1))\Big) \\
&= \frac{1}{2\sin(a)} \Big(1 + \frac{\sin((r+1/2)a) - \sin(a/2)}{\sin(a/2)} - (r+1)\cos(ar) - r\cos(a(r+1))\Big) \\
&= \frac{1}{2\sin(a)} \Big(\frac{\sin((r+1/2)a)}{\sin(a/2)} - (r+1)\cos(ar) - r\big(\cos(ar)\cos(a) - \sin(ar)\sin(a)\big)\Big) \\
&= \frac{1}{2\sin(a)} \Big(\frac{\cos(a(r+1)) - \cos(ar)}{-2\sin^2(a/2)} - (r\cos(a) + r + 1)\cos(ar) + r\sin(ar)\sin(a)\Big) \\
&= \frac{1}{2\sin(a)} \Big(- (r\cos(a) + r)\cos(ar) + \frac{\sin(a)}{1-\cos(a)}\sin(ar) + r\sin(ar)\sin(a)\Big) \ .
\end{aligned}$$

Hence

$$|\sum_{j=1}^{r} j \sin(ja)| \leq \frac{r(1+\cos(a))}{2\sin(a)} + \frac{|\sin(ar)|}{2(1-\cos(a))} + \frac{1}{2}r|\sin(ar)| \ .$$

Now we split $a \in [0, \pi]$ into two cases. For $a \in [0, 3]$, there exist $c_1, c_2 > 0$ such that

$$\sin(a) \geq c_1 a$$

$$1 - \cos(a) \geq c_2 a^2 \ .$$

Then

$$|\sum_{j=1}^{r} j\sin(ja)| \le \frac{r}{c_1 a} + \frac{ar}{2c_2 a^2} + \frac{1}{2}r \le C\frac{r}{a}.$$

For $a \in [3, \pi]$, there exists $\tilde{c}_1 > 0$ such that

$$\sin(a) \ge \tilde{c}_1(\pi - a)$$
$$1 + \cos(a) \le \frac{1}{2}(\pi - a)^2$$

through Taylor expansions around π. So

$$|\sum_{j=1}^{r} j\sin(ja)| \le \frac{r(\pi-a)^2}{4\tilde{c}_1(\pi-a)} + \frac{ar}{2} + \frac{1}{2}r \le \tilde{C}r \le C\frac{r}{a}.$$

We then can get

$$\delta^{1-\eta}|n|^{-\eta}\left|\mu_\delta^h(n)\right| \le C(\delta|n|)^{-1-\eta} \le 2^{1+\eta}C.$$

For T_n, we first claim that $|\mu_\delta^h(n)| \le |\mu^h(n)|$. Indeed, one can prove by induction that

$$|\sin(2\pi njh)| \le j|\sin(2\pi nh)| \tag{4.28}$$

for any positive integer j. Therefore,

$$\left|\sum_{j=1}^{r} jhb_j\sin(2\pi njh)\right| \le \frac{1}{h}\sum_{j=1}^{r}(jh)^2 b_j|\sin(2\pi nh)| = \frac{1}{h}|\sin(2\pi nh)|, \tag{4.29}$$

which implies our claim. Now, we rewrite T_n as

$$T_n = \delta^{-1-\eta}|n|^{-\eta}\left|\frac{\mu^h(n)}{\lambda^h(n)}\right|\left|\frac{\mu_\delta^h(n)}{\mu^h(n)} - 1\right|. \tag{4.30}$$

We have that

$$\left|\frac{\mu^h(n)}{\lambda^h(n)}\right| \le \frac{C}{|n|} \quad \forall h, \tag{4.31}$$

where C is a constant that is independent of h. This can be verified by the basic inequalities $|\sin(\theta)| \le |\theta|$ and $2(1-\cos(\theta)) \ge \theta^2 - \theta^4/12$. Therefore, it suffices to show

$$(\delta|n|)^{-1-\eta}\left|\frac{\mu_\delta^h(n)}{\mu^h(n)} - 1\right| \le C. \tag{4.32}$$

When $\delta|n| \leq 1/2$, since $\sin(\theta) > \theta - \theta^3/6$, we have

$$1 - \frac{\mu_\delta^h(n)}{\mu^h(n)} \leq 1 - \frac{2\pi n - (2\pi n)^3\delta^2/6}{2\pi n} = (2\pi n\delta)^2/6,$$

thus

$$(\delta|n|)^{-1-\eta}\left|\frac{\mu_\delta^h(n)}{\mu^h(n)} - 1\right| \leq C(\delta|n|)^{1-\eta} \leq C.$$

We can also check the case $\delta|n| > 1/2$ since

$$\left|\frac{\mu_\delta^h(n)}{\mu^h(n)} - 1\right| \leq \left|\frac{\mu_\delta^h(n)}{\mu^h(n)}\right| + 1 \leq 2.$$

□

***Remark* 4.3.5.** *One can choose two different horizon parameters in nonlocal diffusion operator (δ_1) and nonlocal gradient operator (δ_2). Then instead of* (4.22)*, we have*

$$\|\mathbb{G}_{\delta_2,h}U_N^{\delta_1} - \mathbb{G}_{0,h}U_N^0\|_0 \leq C\left(\frac{\delta_1^2}{\delta_2^{\max\{0,1-\eta\}}} + \delta_2^{\min\{2,1+\eta\}}\right)|F_N|_{\min\{\eta,1\}}.$$

4.4 Discussion

Robust algorithms and analysis are essential for predictive multiscale simulations. For complex systems treating defects and cracks such as those modeled by peridynamics, algorithms that are sensitive to changes of parameters may produce results that are unphysical or difficult to verify/validate [Tian and Du, 2013; Tian and Du, 2014]. In this chapter, we have provided both numerical evidence and some preliminary theoretical substantiation to the robustness of the nonlocal gradient recovery using asymptotically compatible discretizations. This, through appropriate constitutive relation, can lead to effective nonlocal stress analysis, Let us now offer some additional discussions on the use of nonlocal gradient operators in nonlocal modeling.

First, the notions of peridynamic nonlocal stress and nonlocal strains have been extensively discussed in [Silling, 2000]. Simple ways are suggested to match nonlocal concepts with their classical local analog. Advantages and limitations have been

further investigated in subsequent works [Lehoucq and Silling, 2008; Bessa *et al.*, 2014; Tupek and Radovitzky, 2014]. Most recently, in [Turner *et al.*, 2015], a nonlocal strain measure was developed for noisy digital image correlation (DIC) measurement. It is formulated as a post-processing technique of measurement or simulation data so that there is no direct link made to the use of such strain measure within nonlocal modeling itself. The computation of such a measure was also made on pixel levels of DIC images that may or may not be tied to the numerical discretizations of the underlying continuum mechanical models. Indeed, it is easy for one to see the advantage of nonlocal gradients on the analysis of noisy images or less regular quantities. Similar observations can also be found in [Buades *et al.*, 2005] for processing noisy images. We note, however, that the work presented here attempts to explore and connect the nonlocality present in both numerical discretizations and the underlying physical processes.

The notion of nonlocal gradient may also be related to the use of kernel-based integral approximations to differential operators in methods like SPH and RKPM [Liu *et al.*, 1996; Monaghan, 2005]. Although many forms of the integral relaxations of differential equations have been around in the literature for a few decades, there are much fewer careful studies of the continuum forms of these nonlocal operators, along with discussions on the appropriate function spaces or domains of definition and properties of these nonlocal integral operators before they get discretized. The situation has started to change recently. [Du *et al.*, 2013b; Mengesha and Du, 2016] attempted to provide a rigorous and systematic framework. Meanwhile, some nonlocal derivatives and gradients discussed in the literature, defined either directly on discrete levels or when discretized, only involve function values of particles within a fixed multiple of typical particle spacings (much like $\delta \leq rh$ for a fixed r in our context). Technically such discrete operators should only be viewed as approximating local differential operators. This is the case even if the defined gradients depend on more than just the nearest neighbors. The discrete nonlocal operators studied

here intrinsically involve two separate length scales, one that characterizes the range of nonlocality on the continuum level while the other serves as a depiction of particle spacing which is dependent on the level of numerical resolution. The concept of asymptotical compatibility is again important in that it allows robust estimations of nonlocal gradients and their local counterpart in respective regimes. It also allows us to delineate the roles of physical scale and level of numerical resolutions.

This chapter demonstrates that while nonlocal gradients may need to be used with caution in correspondence theory [Silling, 2000; Bessa *et al.*, 2014; Tupek and Radovitzky, 2014], they can be utilized as gradient recovery techniques or nonlocal stress analysis. For clarity, we have limited our theoretical illustration to a special nonlocal model problem in one dimension using quadratures based collocation methods, which have close resemblance with the popular particle based meshfree methods used for peridynamics. To make the main point clear, we have considered only the simple one dimensional case with periodic boundary conditions. The techniques can obviously be extended to more complex systems in higher dimensions and under suitable constraints due to the geometric boundary. In such cases, we may adopt the following more general forms of nonlocal gradient operators, as defined in [Mengesha and Du, 2016] with a given third-order odd tensor kernel $\mathcal{K}_\delta$ and a specified scalar kernel β_δ,

$$\mathcal{G}_\delta \mathbf{u}(\mathbf{x}) := \lim_{\epsilon \to 0} \int_{\Omega \setminus B_\epsilon(\mathbf{x})} \beta_\delta(|\mathbf{y}-\mathbf{x}|) \mathcal{K}_\delta(\mathbf{y}-\mathbf{x}) \mathcal{D}(\mathbf{u})(\mathbf{y},\mathbf{x})\, d\mathbf{y}$$

for any vector field $\mathbf{u}$ defined on a bounded domain Ω where $B_\epsilon(\mathbf{x})$ is a ball centered at a point $\mathbf{x}$ with radius ϵ and $\mathcal{D}(\mathbf{u})(\mathbf{y},\mathbf{x}) := (\mathbf{u}(\mathbf{y}) - \mathbf{u}(\mathbf{x}))/|\mathbf{y}-\mathbf{x}|$. This continuum form extends those defined in [Du *et al.*, 2013b]. While it appears to be much more involved than the scalar version (and in the absence of physical boundary), we may draw analogy with the path towards the development of AC schemes.

Chapter 5

Nonlocal models with heterogeneous localization

While nonlocal models have been shown to be effective in simulating material involving fracture or failure, they are computationally more expensive than the traditional local PDEs. Therefore, the study of multiscale models is necessary where nonlocal models are employed when there are discontinuities and traditional PDEs are used otherwise. Due to the nature of finite range of the nonlocal interactions, the treatment of interface between local and nonlocal regions is challenging. Previous works [Seleson *et al.*, 2013b; Seleson *et al.*, 2013a; Seleson and Gunzburger, 2010] have studied such issues with special treatment on the interface when the horizon parameter is fixed to be a constant all over the nonlocal region. However, in [Silling *et al.*, 2015], models with a variable horizon having a positive lower bound over the domain have also been examined. In [Tian and Du, 2017], the variable horizon adopted there is allowed to vanish as the material points approach a co-dimension one hypersurface. With a vanishing horizon, nonlocal models get localized heterogeneously, the corresponding models are thus called nonlocal models with heterogeneous localization [Tian and Du, 2017]. The latter is the topic that we like to further explore here (and also in [Du *et al.*, 2018b]).

In this chapter, we aim to deliver the following messages. First, by introducing the spatially varying horizon, one can allow the nonlocal models to get localized, especially on the boundary or interface. In the latter cases, in contrast to the general theory on nonlocal volumetric constraints for nonlocal problems discussed in [Du *et al.*, 2012] and other related works [Mengesha and Du, 2014a; Mengesha and Du, 2013; Mengesha and Du, 2015; Tian and Du, 2017], we end up with well-posed nonlocal models with local boundary conditions. Furthermore, these local boundary value problems of nonlocal models recovers the local limit as the nonlocal interaction vanishes everywhere in the domain. However, for some horizon functions that have unbounded second order derivative, *e.g.*, a piecewise linear horizon parameter, directly imposing the local boundary conditions might produce nonlocal solutions that fail to accurately capture all the interesting solution properties in the local limit such as the boundary flux associated with local Dirichlet data, which can be seen from the numerical experiments. To address such issues, we discuss two remedies. One is to introduce an auxiliary function approach, which is also mentioned in Chapter 2, to handle the boundary effects for several cases that cover both Dirichlet and Neumann type conditions. Well-posedness results of linear variational problems associated with these nonlocal models are also established. An added advantage, in the case where the constructed auxiliary function is linear, is that one can pass the so called patch test straightforwardly. However, auxiliary functions are not always readily available, especially for the complex geometry in high dimensional spaces. We thus discuss the alternative using a smoother horizon function, *e.g.*, of C^2 class. Although such approach cannot pass the traditional patch test, we demonstrate in the numerical experiments that the effects of ghost forces can be controlled. In addition, we demonstrate that it is possible to seamlessly couple classical local models with nonlocal models with heterogeneous localization through a common interface instead of an overlapping domain of nonzero measure.

5.1 Nonlocal variational problems with heterogeneous localization

We now present a nonlocal variational problem with heterogeneous localization [Tian and Du, 2017]. Given a spatial domain Ω of interest, we let Ω_I denote the corresponding interaction domain. We introduce the following nonlocal energy functional

$$E_\Omega(u) = \frac{1}{2}\int_{\Omega\cup\Omega_I}\int_{\Omega\cup\Omega_I} \rho_\delta(x', x)\left(u(x') - u(x)\right)^2 dx'dx\,, \tag{5.1}$$

where $\rho_\delta(x', x) = \rho_\delta(x, x')$ is a symmetric, nonnegative interaction kernel with more details specified later.

The energy accounting for the contribution due to the work done by a given external force $f = f(x)$ on Ω is given by

$$E_f(u) = E_\Omega(u) - \int_\Omega f(x)u(x)dx\,. \tag{5.2}$$

We consider the constrained minimization problem

$$\min\, E_f(u) \quad \text{subject to} \quad E_c(u) = 0\,, \tag{5.3}$$

where $E_c(u)$ denotes a constraint functional. For homogeneous pure Neumann type problems discussed later, we always assume the compatibility condition

$$\int_\Omega f(x)\,dx = 0\,. \tag{5.4}$$

The weak form of Euler-Lagrange equation for (5.3) and (2.6) with $\Omega_I = \emptyset$ is

$$B_\delta(u, v) := \int_\Omega\int_\Omega \rho_\delta(x, x')\left(u(x') - u(x)\right)\left(v(x') - v(x)\right)dx' = (f, v)\,, \tag{5.5}$$

where

$$(f, v) = \int_\Omega f(x)v(x)dx\,,$$

and $B_\delta(u, v)$ defines a symmetric bilinear form for the solution u and any test function v in suitable function spaces.

5.1.1 Nonlocal kernels, variable horizon and function spaces

Without loss of generality, we focus on the one dimensional scalar version with $\Omega = (0, 1)$. Following [Tian and Du, 2017], we define, for all $x, x' \in \Omega$,

$$\rho_\delta(x, x') = c_\delta(x)\gamma_{\delta(x)}(|x' - x|) + c_\delta(x')\gamma_{\delta(x')}(|x' - x|) \tag{5.6}$$

such that

$$c_\delta(x) \int_\Omega \gamma_{\delta(x)}(|x - x'|)(x' - x)^2 dx' = \frac{1}{2}\,, \tag{5.7}$$

where $\delta(x)$ represents a variable horizon such that $\gamma_{\delta(x)}(|x' - x|) = 0$ for $|x - x'| > \delta(x)$. For example, for a nonnegative function $\hat{\gamma}$ with compact support in the interval $(0, 1)$, we may define

$$\gamma_{\delta(x)}(r) = \hat{\gamma}\left(\frac{r}{\delta(x)}\right)\,. \tag{5.8}$$

For much of this chapter, we restrict to the case that $\hat{\gamma}$ is a constant function but the theory can be readily extended to more singular kernels, following the discussions given in [Tian and Du, 2017] concerning the nonlocal energy spaces corresponding to both the constant and more general kernels.

By heterogeneous localization [Tian and Du, 2017], we are interested in the case where $\delta(x) = 0$ at some isolated points. Here, throughout this section, we consider the case that $\delta(x)$ vanishes as x goes to the end points of $\Omega = (0, 1)$. For example, we can have a piecewise linear $\delta(x)$ given by:

$$\delta(x) = \begin{cases} x & x \le \delta\,, \\ \delta & \delta < x < 1 - \delta\,, \\ 1 - x & x \ge 1 - \delta. \end{cases} \tag{5.9}$$

It is easy to see that $\max \delta(x) = \delta$. Besides (5.9), other forms of the function $\delta(x)$, particularly ones with much more smoothness, will be considered later.

Without loss of generality, we take as a notation convention to use δ representing both the heterogeneously defined horizon function and its maximum value. In this

way, we may use $\delta \to 0$ to represent the localization of the model throughout the domain.

Let us now define some function spaces of interest to us. The space $\mathcal{S}_\delta(\Omega) \subset L^2(\Omega)$ is given by

$$\mathcal{S}_\delta(\Omega) = \left\{ u \in L^2(\Omega) : E_\Omega(u) < \infty \right\} .$$

Now the solution space for the nonlocal homogeneous Dirichlet type problem is defined by the closure of smooth functions in the space of $\mathcal{S}_\delta(\Omega)$. Namely, we define

$$\mathcal{S}_\delta^D(\Omega) = \{ u \in \mathcal{S}_\delta(\Omega) : \exists u_n \in C_c^\infty(\Omega) \text{ such that } u_n \to u \text{ in } \mathcal{S}_\delta(\Omega) \} .$$

It is worth noting that by the trace theorem in [Tian and Du, 2017], any function in $\mathcal{S}_\delta(\Omega)$ has a well-defined trace in the space of $H^{1/2}(\partial\Omega)$. So it is reasonable to impose local boundary constraints in the space of $\mathcal{S}_\delta(\Omega)$. Naturally, the nonlocal Neumann-type constrained energy space can be similarly defined as the space $\mathcal{S}_\delta(\Omega)$ with a normalization condition:

$$\mathcal{S}_\delta^N(\Omega) = \left\{ u \in \mathcal{S}_\delta(\Omega) : \int_\Omega u dx = c_N \right\} ,$$

for some constant c_N. Again, without loss of generality, we assume $c_N = 0$ unless noted otherwise. It is not hard to see that $\mathcal{S}_\delta(\Omega)$ and the constrained energy spaces are real Hilbert spaces with the inner product $(\cdot, \cdot)_s$ defined as $(u, w)_s = B_\delta(u, w) + (u, w)$, see, for example, similar results given in [Mengesha and Du, 2013]. We use $\|u\|_{L^2}$ to denote the L^2 norm of u, $|u|_e$ to denote the energy seminorm $\sqrt{(B_\delta(u, u))}$ of u in $\mathcal{S}_\delta(\Omega)$ and $\|\cdot\|_s$ to denote the norm on $\mathcal{S}_\delta(\Omega)$ defined by $\|u\|_s^2 = \|u\|_{L^2}^2 + |u|_e^2$.

The well-posedness of the nonlocal boundary value problems proposed respectively in sections 5.1.2, 5.1.3 and 5.1.5 can be derived using the conventional Lax-Milgram theorem with the help of a nonlocal Poincaré-type inequality. The latter, shown below, is applicable to any subspace of $\mathcal{S}_\delta(\Omega)$ that intersects $\mathbb{R}$ trivially, including particularly $\mathcal{S}_\delta^D(\Omega)$ and $\mathcal{S}_\delta^N(\Omega)$ as cases of interests here.

Proposition 5.1.1. *Suppose V is a closed subspace of $L^2(\Omega)$ that intersects $\mathbb{R}$ trivially. Then there exists a constant $C = C(\rho_\delta, V, \Omega)$ such that*

$$\|u\|_{L^2} \leq C|u|_e\,, \quad \forall u \in V \cap \mathcal{S}_\delta(\Omega). \tag{5.10}$$

Proof. We prove the inequality by contradiction, which is a standard technique for establishing Poincaré inequality. Suppose the inequality (5.10) is false. Then there exist $\{u_n\} \in V$ such that for all n, $\|u_n\|_{L^2} = 1$, and as $n \to \infty$, $|u_n|_e \to 0$. We claim that in such case $\|u_n\|_{L^2} \to 0$ as $n \to \infty$, resulting in a contradiction. To prove the claim, suppose that u is the weak limit in L^2 of the bounded sequence u_n. Since V is a closed subspace of $L^2(\Omega)$, we have $u \in V$.

Step 1. We show that *the weak limit u is in fact* 0. We claim that $|\cdot|_e$ is L^2-weakly lower semicontinuous, namely

$$|u|_e \leq \liminf_n |u_n|_e\,. \tag{5.11}$$

In fact, since $|\cdot|_e$ is a convex functional, then the weak lower semicontinuity is equivalent to strong lower semicontinuity. So we only need to show (5.11) under the assumption that u_n converges to u strongly in L^2. Indeed, under such assumption, we can extract a subsequence of $\{u\}_{n_k}$ such that it converges to u pointwisely up to a set of measure zero. Then we arrive at (5.11) by applying Fatou's lemma. Now from (5.11) we have $|u|_e = 0$ so that u equals to a constant in Ω. Therefore, u must be identical to zero since the only constant function in V is the zero function by assumption.

Step 2. We show next that, *as $n \to \infty$, $u_n \to 0$ strongly in $L^2(\Omega)$*. First we observe the following fact for $\gamma_{\delta(x)}$ to be of the rescaled type (5.8) and $\delta(x)$ only vanishes on the boundary $\partial\Omega$ continuously. Fix a constant $c > 0$, then for any $\epsilon > 0$, we could choose $M > 0$, such that by defining $\rho_\delta^M = \min(M, \rho_\delta)$, the mass defined by $d(x) := \int_\Omega \rho_\delta^M(x, x')dx'$ has a lower bound c for all x in the interior of Ω characterized

by the distance ϵ to the boundary $\partial\Omega$ (denoted as Ω_ϵ). Then we have

$$\begin{aligned}
|u_k|_e^2 &\geq \int_\Omega \int_\Omega \rho_\delta^M(x,x')(u_k(x)-u_k(x'))^2 dxdx' \\
&\geq 2\int_\Omega \left(\int_\Omega \rho_\delta^M(x,x')dx'\right) u_k^2(x)dx - 2\int_\Omega \left(\int_\Omega \rho_\delta^M(x,x')u_k(x')dx'\right) u(x)dx \\
&\geq 2\int_{\Omega_\epsilon} d(x)u_k^2(x)dx - 2\int_\Omega \left(\int_\Omega \rho_\delta^M(x,x')u_k(x')dx'\right) u_k(x)dx \\
&\geq 2c\|u_k\|^2_{L^2(\Omega_\epsilon)} - \int_\Omega \mathcal{K}u_k(x)u_k(x)dx\,,
\end{aligned}$$

where $\mathcal{K}$ is a Hilbert-Schmidt operator defined by

$$\mathcal{K}u_k(x) = \int_\Omega \rho_\delta^M(x,x')u_k(x')dx'\,,$$

since $\rho_\delta^M \in L^2(\Omega\times\Omega)$. Now since $u_k \rightharpoonup 0$ from the first step, we have $\mathcal{K}u_k \to 0$ strongly in L^2. Thus we have

$$0 = \limsup_k |u_k|_e \geq \sqrt{2c}\cdot \limsup_k \|u_k\|_{L^2(\Omega_\epsilon)}\,.$$

By letting $\epsilon \to 0$ we have $\|u_k\|_{L^2(\Omega)} \to 0$ as $k\to\infty$, which contradicts to $\|u_k\|_{L^2(\Omega)} = 1$. This proves the claim above and completes the proof of the proposition. □

Let $\mathcal{V}_s$ denote a generic subspace $V \cap \mathcal{S}_\delta$ with its dual denoted by $\mathcal{V}_s'$. A standard application of the Lax-Milgram theorem (which is based on the Riesz representation theorem) yields the well-posedness of the variational problems in $\mathcal{V}_s$. The important examples of $\mathcal{V}_s$ considered in this work are the spaces $\mathcal{S}_\delta^D(\Omega)$ and $\mathcal{S}_\delta^N(\Omega)$.

Lemma 5.1.2. *For a given $f \in \mathcal{V}_s'$, there exists a unique $u \in \mathcal{V}_s$ such that*

$$B_\delta(u,v) = (f,v)\,,$$

for all $v \in \mathcal{V}_s$. Moreover, $|u|_e = |f|_{\mathcal{V}_s'}$.

We will study different types of problems in the subsequent sections with different choices of $\mathcal{V}_s$ and f.

5.1.2 Homogeneous Neumann-type problems

Working with $\mathcal{S}_\delta^N(\Omega)$, one can formulate the homogeneous Neumann-type problem in a variational way. For a given $f \in L^2(\Omega)$, find $u_\delta \in \mathcal{S}_\delta^N(\Omega)$, such that

$$B_\delta(u_\delta, v) = (f, v) \quad \forall v \in \mathcal{S}_\delta^N(\Omega)\,. \tag{5.12}$$

Notice that the solution u_δ for any f in the dual space of $\mathcal{S}_\delta^N(\Omega)$ using the Lax-Milgram theory. But in order for the solution to have properly defined homogeneous Neumann data on the boundary and to be valid pointwise in the interior of Ω, we let f in $L^2(\Omega)$, a subspace of the dual of $\mathcal{S}_\delta^N(\Omega)$. Then the nonlocal Neumann problem (5.12) converges as $\delta \to 0$ to the classical local homogeneous Neumann value problem:

$$\text{for } f \in L^2(\Omega), \text{find } u_0 \in H^1(\Omega)\backslash\mathbb{R} \text{ such that } (u_0', v') = (f, v) \quad \forall v \in H^1(\Omega)\,.$$

The strong form of (5.12) is given as

$$\begin{cases} \mathcal{L}_\delta u(x) = f(x) & \text{in } \Omega\,, \\ \displaystyle\int_\Omega u\,dx = 0\,. \end{cases}$$

where $\mathcal{L}_\delta$ is found to be

$$\mathcal{L}_\delta u(x) := -2\int_\Omega \rho_\delta(x, x')(u(x') - u(x))dx'\,,$$

thanks to the Fubini theorem, which can be applied in the case that u has vanishing normal derivatives on the boundary of Ω.

Finally, the strong form of the local limit in our one-dimensional case is given by

$$\begin{cases} \mathcal{L}_0 u := -\dfrac{d^2}{dx^2}u = f & \text{in } \Omega\,, \\ \dfrac{\partial u}{\partial \mathbf{n}} = 0 & \text{on } \partial\Omega\,, \\ \displaystyle\int_\Omega u\,dx = 0\,. \end{cases} \tag{5.13}$$

5.1.3 Inhomogeneous Neumann-type problems

We now extend the study earlier on the homogeneous Neumann-type problems to those involving inhomogeneous Neumann data. Instead of (5.13), we want to get a nonlocal solution which is an approximation of the solution to classical inhomogeneous Neumann problems

$$\begin{cases} \mathcal{L}_0 u = f \quad \text{in } \Omega\,, \\ \dfrac{\partial u}{\partial \mathbf{n}} = g \quad \text{on } \partial\Omega\,, \\ \displaystyle\int_\Omega u\,dx = 0\,, \end{cases} \tag{5.14}$$

for some inhomogeneous boundary data g. This corresponds to the following weak formulation. For any $f \in L^2(\Omega)$ and $g \in L^2(\partial\Omega)$, find $u_0 \in H^1(\Omega)\backslash\mathbb{R}$, such that

$$(u_0', v') = (f, v) + (g, v)_{\partial\Omega} \quad \forall v \in H^1(\Omega)\,. \tag{5.15}$$

Now the nonlocal version of (5.15) is naturally to find $u_\delta \in \mathcal{S}_\delta^N(\Omega)$, such that

$$B_\delta(u_\delta, v) = (f, v) + (g, v)_{\partial\Omega} \quad \forall v \in \mathcal{S}_\delta^N(\Omega)\,. \tag{5.16}$$

We note that (5.16) is a valid problem since by the trace theorem in [**?**], the space $\mathcal{S}_\delta^N(\Omega)$ has $H^{1/2}(\partial\Omega)$ as its trace space, so $(g, \cdot)_{\partial\Omega}$ is a continuous functional on $\mathcal{S}_\delta^N(\Omega)$. We will show numerical experiments on solving (5.16) in Section 5.3. However, the use of (5.16) also leads to some inconveniences. The first is that we lack a proper definition of the strong form of (5.16) since Fubini theorem cannot be applied when the normal derivative of u_δ does not vanish on the boundary. The second is that the horizon function $\delta(x)$ has to be smoothly varying in order for an accurate approximation of the corresponding local problem, as shown in Section 5.3.2. A possible remedy is to consider a relaxed version of (5.16). If the goal is find a proper nonlocal problem that approximates the local Neumann boundary value problem accurately, then one realizes that we do not need to use $(g, v)_{\partial\Omega}$ exactly in (5.16), but some functional (g_δ, v) that approximates $(g, v)_{\partial\Omega}$ in the asymptotic limit. To this end, we introduce

an auxiliary function u_{a} such that $u_{\mathrm{a}} \in C^2(\Omega)$ and $\frac{\partial u_{\mathrm{a}}}{\partial \mathbf{n}} = g$ on $\partial\Omega$. More discussions on choices of less regular u_{a} are given later.

For nonlocal problems with a constant horizon, Chapter 2 discussed suitable strategies to transfer nonlocal inhomogeneous problem to a new homogeneous Neumann problem while maintaining second order consistency with the local limit in terms of δ. The use of auxiliary functions is one of them that we also adopt here. Then instead of (5.16), we consider the solution u_δ to the following variational problem

$$B_\delta(u_\delta, v) = (f + u_{\mathrm{a}}'', v) + B_\delta(u_{\mathrm{a}}, v) \quad \forall v \in \mathcal{S}_\delta^N(\Omega)\,. \tag{5.17}$$

The derivation of (5.17) comes as follows. If we define (g_δ, v) as

$$(g_\delta, v) = (g, v)_{\partial\Omega} + B_\delta(u_{\mathrm{a}}, v) - (u_{\mathrm{a}}', v')\,,$$

then it is obvious that (g_δ, v) will be approximating $(g, v)_{\partial\Omega}$ as $\delta \to 0$, by the consistency of the nonlocal bilinear form to the local bilinear form. Then using integration by parts and the fact that the normal derivative of u_a corresponds to g on the boundary, we arrive at

$$(g_\delta, v) = B_\delta(u_{\mathrm{a}}, v) + (u_{\mathrm{a}}'', v)\,,$$

which leads to the conclusion of (5.17). This modification of (5.16) preserves the limit of u_δ, and as the numerical experiments in Section 5.3, it has optimal accuracy of approximating the local Neumann boundary value problem. Moreover, (5.17) can be written in the following strong from:

$$\begin{cases} \mathcal{L}_\delta(u - u_{\mathrm{a}})(x) = f(x) + u_{\mathrm{a}}''(x) \quad \text{in } \Omega\,, \\ \displaystyle\int_\Omega u\,dx = 0\,. \end{cases}$$

where $\mathcal{L}_\delta$ is defined to be the same operator in Section 5.1.2. For simplicity, a possible choice is to let

$$u_{\mathrm{a}}(x) = -\frac{x^2}{2}\int_\Omega f(x)dx + g(0)x\,.$$

One can easily check that $u_a'(0) = g(0)$ and $u_a'(1) = g(1)$ by the compatibility condition

$$\int_\Omega f(x)dx = g(0) - g(1)\,.$$

Then the strong form reduces to

$$\begin{cases} \mathcal{L}_\delta(u - u_a)(x) = f(x) - \displaystyle\int_\Omega f(x)dx \quad \text{in } \Omega\,, \\ \displaystyle\int_\Omega u\,dx = 0\,. \end{cases} \tag{5.18}$$

5.1.4 Discussion on modeling error

From the experiments presented in Section 5.3, we will see that the solution to nonlocal models with a piecewise linear horizon without the use of auxiliary functions, namely, the problem (5.16), converges to its local limit only in first order.

In principle, there are two ways to improve the convergence behavior. On one hand, introducing the auxiliary function above aims to transfer nonlocal inhomogeneous problem to a new homogeneous Neumann problem, which has the optimal order of consistency in terms of δ. On the other hand, as also proposed in Chapter 2, we can cancel low order terms in the truncation error through modifying the right hand side. Let us elaborate next the second approach in the more general context of heterogeneous nonlocal interactions discussed here.

Assume a function u is smooth enough, say $u \in C^3(\Omega)$. Then if x is close to the left boundary ($x = 0$), we can get from a careful Taylor expansion that

$$\begin{aligned} \mathcal{L}_0 u - \mathcal{L}_\delta u &= 2\int_\Omega \rho_\delta(x,x')(u(x') - u(x))dx' - u''(x) \\ &= 2\int_\Omega \rho_\delta(x,x')(x'-x)u'(x)dx' + \int_\Omega \rho_\delta(x,x')(x'-x)^2 u''(x)dx' - u''(x) + \mathcal{O}(\delta) \\ &= 2\int_\Omega \rho_\delta(x,x')(x'-x)(u'(0) + xu''(x))dx' \\ &\quad + \int_\Omega \rho_\delta(x,x')(x'-x)^2 u''(x)dx' - u''(x) + \mathcal{O}(\delta) \\ &= 2u'(0)\int_\Omega \rho_\delta(x,x')(x'-x)dx' + u''(x)\left(\int_\Omega \rho_\delta(x,x')(x'^2 - x^2) - 1\right)dx' + \mathcal{O}(\delta)\,. \end{aligned}$$

Similarly, when x is close to the right boundary or in the middle of Ω, we can derive the truncation error accordingly. Consequently, similar to the illustration provided in Chapter 2 for the constant horizon case, one may introduce some modified right hand side to the nonlocal model near the boundary to get higher order consistency. For example, when x is close to $x = 0$, we have

$$\mathcal{L}_\delta u(x) = f_\delta(x) := -2u'(0)\int_\Omega \rho_\delta(x,x')(x'-x)dx' + f(x)\int_\Omega \rho_\delta(x,x')(x'^2 - x^2)dx' \,.$$

5.1.5 Dirichlet-type problems

For nonlocal diffusion models with a constant horizon, problems subject to Dirichlet volume constraints have been studied in various earlier works, for example [Du *et al.*, 2013b; Tian and Du, 2013]. The local limiting problem, in one dimensional case, corresponds to

$$\begin{cases} \mathcal{L}_0 u = f & \text{in } \Omega \,, \\ \quad u = g & \text{on } \partial\Omega \,. \end{cases} \tag{5.19}$$

The corresponding weak from is given by: find the solution $u \in \{w \in H^1(\Omega) : w|_{\partial\Omega} = g\}$ such that

$$(u', v') = (f, v) \quad \forall v \in H_0^1(\Omega) \,. \tag{5.20}$$

While intuitively we may use the trace theorem given in [Tian and Du, 2017] to specify a Dirichlet condition on the boundary where the nonlocal interaction gets localized, the derivatives of the resulting solution could develop undesirable oscillations if the horizon function is not sufficiently smooth, which is similar to the inhomogeneous Neumann case and can be observed in Section 5.3.2. It turns out that we can again use the idea of modifying the bilinear form by the use of auxiliary functions. For example, let us assume that the solution to (5.19) satisfies that $u'(0) = a$ and $u'(1) = b$ for some constants a and b to be determined. By compatibility condition, we have

$$b = a - \int_\Omega f(x)dx \,. \tag{5.21}$$

We then introduce an auxiliary function $u_{\rm a}$ such that $u_{\rm a}'(0) = a$ and $u_{\rm a}'(1) = b$. For simplicity, we can let

$$u_{\rm a}(x) = \frac{b-a}{2}x^2 + ax = -\frac{x^2}{2}\int_\Omega f(x)dx + ax \tag{5.22}$$

with an unknown a. Therefore, $\tilde{u} = u - u_{\rm a}$ satisfies the homogeneous Neumann boundary conditions. Consider the following energy functional

$$\begin{aligned} E_f(u;a) =& \frac{1}{2}\int_\Omega\int_\Omega \rho_\delta(x,x')\left(u(x') - u_{\rm a}(x') - (u(x) - u_{\rm a}(x))\right)^2 dx'dx \\ & - \int_\Omega u_{\rm a}'' u\, dx - \int_\Omega f u\, dx\,, \end{aligned} \tag{5.23}$$

and the constrained minimization problem

$$\min E_f(u;a) \quad \text{subject to} \quad u = g \text{ on } \partial\Omega \text{ and } C(u,a) = 0\,, \tag{5.24}$$

where $C(u,a)$ is an appropriate constraint function to be specified later. The solution of u is then defined as

$$\begin{aligned} \tilde{\mathcal{S}}_\delta^D(\Omega) := \big\{ u : u \in \mathcal{S}_\delta(\Omega) \text{ and } u - h \in \mathcal{S}_\delta^D(\Omega) \text{ for a linear function } h \\ \text{such that } h = g \text{ on } \partial\Omega \big\}\,. \end{aligned}$$

The weak form of Euler-Lagrange equation for (5.23) becomes

$$B_\delta(u - u_{\rm a}, v) = (f + u_{\rm a}'', v)\,. \tag{5.25}$$

The space of test functions v should be in $\mathcal{S}_\delta^D(\Omega)$. One can verify that the weak form (5.25) is consistent with (5.20) as $\delta \to 0$. In order to find a suitable constraint $C(u,a)$, we further assume that $\tilde{u}_\delta = u_\delta - u_{\rm a}$ has homogeneous Neumann boundary conditions for all $\delta > 0$, where u_δ solves (5.25) for any $v \in \mathcal{S}_\delta(\Omega)$ and $u_{\rm a}$ is given in (5.22). Therefore, by Fubini's Theorem, (5.25) leads to

$$\mathcal{L}_\delta u - \mathcal{L}_\delta u_{\rm a} = f - \int_\Omega f\, dx\,.$$

Then $C(u,a)$ can be obtained by multiplying a linear function $h(x) = cx$ (taking $c = 1$, for simplicity) on both sides of the above equation and integrate with respect

to x from 0 to 1, which leads to, on the left hand side:

$$\int_\Omega \int_\Omega \rho_\delta(x,x')(x'-x)(u(x')-u_{\mathrm{a}}(x')-(u(x)-u_{\mathrm{a}}(x)))\,dx'dx = B_\delta(u,x) - \frac{a+b}{2}\,,$$

and $g(1)-g(0)-(a+b)/2$ on the right hand side, where the function g is the local Dirichlet boundary data in (5.19). Therefore, we can get

$$C(u,a) = C_g(u) := B_\delta(u,x) + g(0) - g(1) = 0\,, \tag{5.26}$$

which can be viewed as a *nonlocal compatibility condition*. Again by Fubini's theorem, we can get the strong form of Euler-Lagrange equations

$$\begin{cases} \mathcal{L}_\delta(u-u_{\mathrm{a}}) = f - \displaystyle\int_\Omega f\,dx & \text{in } \Omega\,, \\ \qquad u = g & \text{on } \partial\Omega\,, \\ B_\delta(u,x) = g(1)-g(0)\,. \end{cases} \tag{5.27}$$

Similar to the discussion on the Neumann case, we also expect $\|u_\delta - u_0\|_{L^2} \to 0$ as $\delta \to 0$ where u_0 solves (5.19). Note that this serves as a remedy to have better recovery of the local limit from the nonlocal models with a piecewise linear horizon, and it is not necessary when the horizon function is smoothly defined.

5.1.6 Nonlocal models with mixed boundary conditions

The treatment for a nonlocal problem with mixed boundary conditions goes similarly as the discussions previously. We take the example on the domain $\Omega = (0,1)$ with Neumann condition on one side ($x = 0$) and Dirichlet condition on the other ($x = 1$). The auxiliary function then is still given by (5.22) but it is a known function due to the Neumann condition imposed on $x = 0$. By performing similar discussions as in Section 5.1.3 and 5.1.5, the strong form of the mixed boundary problem is given by:

$$\begin{cases} \mathcal{L}_\delta(u-u_{\mathrm{a}}) = f - \displaystyle\int_\Omega f\,dx & \text{in } \Omega\,, \\ \qquad u(1) = g(1)\,. \end{cases} \tag{5.28}$$

5.2 Local-nonlocal coupled problems

While nonlocal modeling has its advantage on complex physical processes, nonlocal model based numerical simulations often incur higher computational cost than those based on traditional local models. Local-nonlocal coupling is a natural approach in practice and various strategies have been proposed [D'Elia *et al.*, 2016; Du *et al.*, 2018a; Du *et al.*, 2016a; Mitchell *et al.*, 2015; Seleson *et al.*, 2015]. In this section, we propose an energy-based seamless coupling approach to define local-nonlocal coupled problems. We first adopt the auxiliary function approach and use a general horizon parameter (one representative could be the piecewise linear horizon (5.9), which is a direct application from what discussed before. However, constructing an auxiliary function in high dimensional spaces may be nontrivial, we then use a smoother variable horizon to solve the coupled problems without the auxiliary functions.

For simplicity, we consider the coupled problem in $\Omega = \Omega_- \cup \Omega_+$ where $\Omega_- = (-1, 0]$ and $\Omega_+ = [0, 1)$. The nonlocal interaction domain Ω_I is defined as

$$\Omega_I = \{y \in \mathbb{R} \setminus \Omega_+ \text{ such that } \rho_\delta(x, y) \neq 0 \text{ for some } x \in \Omega_+\}\,.$$

We define the coupled energy functional as

$$\begin{aligned} E_f(u) =& \frac{1}{2}\int_{\Omega_+\cup\Omega_I}\int_{\Omega_+\cup\Omega_I} \rho_\delta(x, x')(u(x') - u(x))^2 dx'dx \\ &+ \frac{1}{2}\int_{\Omega_-} u'(x)^2\, dx - \int_\Omega f(x)u(x)dx\,. \end{aligned} \tag{5.29}$$

For illustration, we consider the minimization problem of such an energy functional subject to some nonlocal Dirichlet-type volume constraints on Ω_I and a local Dirichlet boundary condition at $x = -1$.

5.2.1 Coupled problems with auxiliary functions for general horizons

Without loss of generality, we still use the same kernel and horizon function mentioned before. For convenience, let us denote the space

$$\mathcal{W}_\delta(\Omega) = \left\{ u \in H^1(\Omega_-) \cap \mathcal{S}_\delta(\Omega_+) \text{ such that } u_- = u_+ \text{ at } x = 0 \right\} ,$$

which is well-defined by the trace theorem given in [Tian and Du, 2017].

As an application of the auxiliary function approach for solving nonlocal Dirichlet problems with heterogeneous localization, we let u_{a} be an auxiliary function and consider the minimizer of the following modified energy functional

$$\begin{aligned} E_f(u;a) =& E_{\Omega_+}(u - u_{\mathrm{a}}) - \int_{\Omega_+} u_{\mathrm{a}}''(x) u(x) dx \\ &+ \frac{1}{2} \int_{\Omega_-} u'(x)^2 \, dx - \int_{\Omega} f(x) u(x) dx \, , \end{aligned} \tag{5.30}$$

subject to the nonlocal Dirichlet boundary conditions and necessary interface condition. The constrained energy space is then given by

$$\widetilde{\mathcal{W}}_\delta(\Omega) = \{ u \in \mathcal{W}_\delta(\Omega), u = g \text{ on } \Omega_I \cup \{x = -1\} \} \, .$$

We further assume that for some auxiliary function u_{a}, the minimizer u_δ of (5.30) satisfies that $u_\delta - u_{\mathrm{a}}$ has a zero Neumann data at $\partial\Omega_+$ for $\delta > 0$. A choice of u_{a} can again be given by (5.22), where Ω should be replaced by Ω_+.

The weak form of Euler-Lagrange equation for the minimization problem becomes

$$B_0(u, v)_{\Omega_-} + B_\delta(u - u_{\mathrm{a}}, v)_{\Omega_+} - (u_{\mathrm{a}}'', v)_{\Omega_+} = (f, v) \, , \tag{5.31}$$

where the subscripts Ω_- and Ω_+ represent the integral domain of the bilinear forms, and the test function v are in $\mathcal{W}_\delta(\Omega)$ but with homogeneous Dirichlet conditions on $\Omega_I \cup \{x = -1\}$. By Fubini's theorem, (5.31) leads to

$$\mathcal{L}_\delta(u - u_{\mathrm{a}}) = f - \int_{\Omega_+} f \, dx \quad \text{in } \Omega_+ \, .$$

In order to find a nonlocal compatibility condition for the coupled problems, we again multiply a linear function $h(x) = cx$ (taking $c = 1$ for simplicity) on both sides and integrate with respect to x from 0 to 1, which leads to

$$\int_{\Omega_+}\int_{\Omega_+} \rho_\delta(x,x')(x'-x)(u(x')-u(x))\,dx'dx - a = \int_{\Omega_+} f(x)(x-1)\,dx\,. \qquad (5.32)$$

5.2.2 Coupled problems with C^2 horizon functions

As demonstrated earlier, constructing suitable auxiliary functions can help retain good consistency of the nonlocal model with the local limit for general kernels and horizons. However, such constructions in general geometry in higher dimensional spaces are challenging. Instead, we now consider the use of a smoother horizon function in the kernel over the domain Ω_+, namely

$$\rho_\delta(x,x') = c_\delta(x)\gamma_{\delta(x)}(|x'-x|) + c_\delta(x')\gamma_{\delta(x')}(|x'-x|)\,,$$

where

$$\gamma_{\delta(x)}(r) = \chi_{\Omega_+}\left(\frac{r}{\delta(x)}\right).$$

Discussion on smooth (and strictly positive) horizon has been made also in [Silling *et al.*, 2015] along with numerical experiments. Here we discuss the case that allows heterogeneous localization with the horizon becoming zero at some interface or boundary points.

Assume that the horizon function $\delta(x)$ in the kernel is second order differentiable. In particular, we use a class of horizon which can be visualized in Fig. 5.1, where the second order derivative $\delta''(x)$ is bounded by some power of the maximum value of $\delta(x)$, denoted by $\delta = \max\delta(x)$ for $x \in \Omega_+$.

Then we consider the minimization problem of the original energy functional (5.29) subject to Dirichlet-type volume constraints on Ω_I (here $\Omega_I = [1, 1+\delta]$) and Dirichlet boundary condition at $x = -1$, so the energy space for u remains as $\widetilde{\mathcal{W}}_\delta(\Omega)$.

The weak form of Euler-Lagrange equation becomes

$$B_0(u,v)_{\Omega_-} + B_\delta(u,v)_{\Omega_+} = (f,v)\,,$$

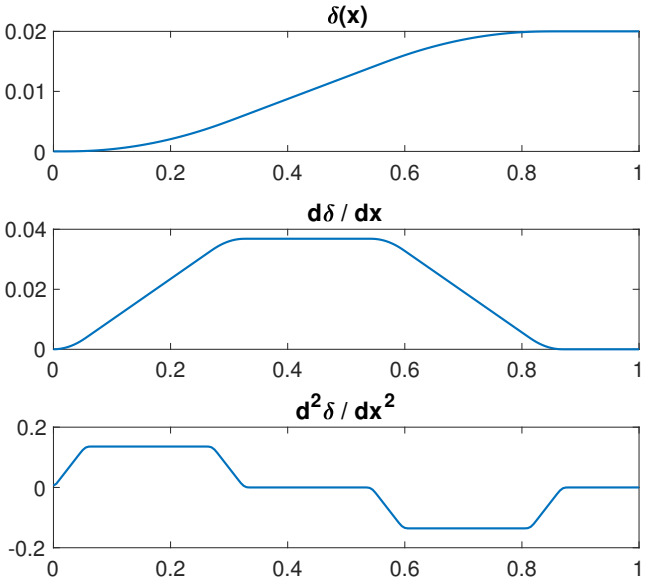

Figure 5.1: horizon as a C^2 function of x.

where the test function v is from $\mathcal{W}_\delta(\Omega)$ with homogeneous Dirichlet condition at $x = -1$ and homogeneous Dirichlet volume constraint in Ω_I.

In the numerical experiments presented in Section 5.3, we can see that the coupled solutions converge to the limiting local solution in an optimal order. Moreover, although the ghost forces do not disappear totally, we demonstrate that they vanish as $\delta \to 0$. We also present numerical experiments on using such a horizon to solve nonlocal problems subject to various constraints. Convergence can again be observed in an optimal order without auxiliary functions.

5.3 Numerical simulations

We now report numerical experiments that on one hand substantiate the analysis given earlier and on the other hand, offer quantitative pictures to the solution behavior (particularly in the local limit) of nonlocal models and coupled local-nonlocal models. We adopt Galerkin piecewise linear finite element methods to do discretization.

5.3.1 Nonlocal homogeneous Neumann problems

After numerical discretization, we get the stiffness matrix $\mathbb{A}$, where $\mathbb{A}$ is assembled by conforming piecewise linear finite element Galerkin approximations, see Chapter 2 for details. For Neumann type problems, however, the matrix is singular without the uniqueness constraint. In principle, we may have several ways to deal with such issue. One possible approach is to modify the stiffness matrix. Let $\mathbf{e}$ be the column vector in the null space of the stiffness matrix $\mathbb{A}$ and define $\mathbb{B} = \mathbb{A} + \mathbf{e}\mathbf{e}^T$, we solve the linear system with coefficient matrix $\mathbb{B}$ to get a solution $\mathbf{U}'$. Then the vector $\mathbf{U}'$ has the property $\mathbf{e}^T\mathbf{U}' = 0$. To get the solutions with different mean values (say to match with suitable benchmark solutions), we need to set $\mathbf{U} = \mathbf{U}' - C_h\mathbf{e}$ for suitably chosen constant C_h.

For numerical experiments, we first fix the horizon δ and calculate the right hand side of the nonlocal equation based on an exact solution $u(x) = x^2(1-x)^2 - 1/30$. This naturally leads to a δ-dependent right hand side $f = f_\delta(x) = \mathcal{L}_\delta u$. Meanwhile, since the integral of u over Ω is zero, which leads to our target weak form:

$$B_\delta(u_\delta, v) = (f_\delta, v) \quad \forall v \in \mathcal{S}_\delta^N(\Omega)\ , \tag{5.33}$$

where $u_\delta \in \mathcal{S}_\delta^N(\Omega)$. We take the kernel

$$\rho_\delta(x', x) = c_\delta(x)\chi_{\delta(x)}(|x' - x|) + c_\delta(x')\chi_{\delta(x')}(|x' - x|),$$

where

$$c_\delta(x) = \frac{3}{4\delta(x)^3}, \quad \delta(x) = \min(\delta, x, 1-x).$$

We solve the nonlocal problem on a uniform mesh with mesh size h and take δ to be constant and reduce h to check the convergence properties. As an illustration we choose $\delta = \frac{1}{4}$ and refine the mesh with decreasing h. For each h, the constant C_h is chosen as the trapezoidal rule of the numerical solution on the grid points for each h which is an approximation of the integral of u.

Table 5.1 shows errors and error rates of the piecewise linear finite element approximations to the solution $x^2(1-x)^2 - 1/30$ with a fixed $\delta = \frac{1}{4}$ while refining mesh

h	$\|\mathbf{U}^h - \mathcal{I}_h u\|_\infty$	Order
2^{-5}	6.14×10^{-4}	–
2^{-6}	1.86×10^{-4}	1.73
2^{-7}	3.64×10^{-5}	2.35
2^{-8}	1.10×10^{-5}	1.73
2^{-9}	2.74×10^{-6}	2.00
2^{-10}	6.25×10^{-7}	2.13
2^{-11}	1.63×10^{-7}	1.94
2^{-12}	3.63×10^{-8}	2.16

Table 5.1: L^∞ errors and error orders of piecewise linear finite element approximations for fixed $\delta = \frac{1}{4}$ to the solution $x^4 - 2x^3 + x^2 - 1/30$ as $h \to 0$.

with a decreasing h, where $\mathcal{I}_h$ denotes the piecewise linear interpolation operator. From the data in the table, we see that the convergence rate for fixed δ is $\mathcal{O}(h^2)$ for finite element approximations.

We now establish the numerical experiments to show the order of convergence as δ and h both go to 0. In this example, we discretize and solve the following equation:

$$B_\delta(u_\delta, v) = (f, v) \quad \forall v \in \mathcal{S}_\delta^N(\Omega)\,. \tag{5.34}$$

We choose the same kernel and the same local limit of the nonlocal solution $u(x) = x^2(1-x)^2 - 1/30$, hence the right hand side would be $f(x) = -12x^2 + 12x - 2$. Let $\mathbf{U}_\delta^h$ denote the numerical solution of (5.34) with mesh size h and horizon δ. Then from the above example, with fixed δ, $\mathbf{U}_\delta^h$ will converge to the interpolant of nonlocal solution u_δ with decreasing h. Therefore, when we keep reducing δ while picking a relative small enough h, the resulting solutions are expected to approximate the local limit. On the other side, we can also fix the ratio between horizon and mesh size: $r = \delta/h$ and refine the mesh, which is also a popular limiting process as it roughly preserves the number of nonzero entries in each row of the stiffness matrix.

	fixed small h		fixed $r = 2$	
δ	$\|\mathbf{U}_\delta^h - \mathcal{I}_h u\|_\infty$	Order	$\|\mathbf{U}_\delta^h - \mathcal{I}_h u\|_\infty$	Order
2^{-2}	7.81×10^{-3}	–	7.88×10^{-3}	–
2^{-3}	3.12×10^{-3}	1.35	3.47×10^{-3}	1.18
2^{-4}	9.46×10^{-4}	1.71	1.14×10^{-3}	1.60
2^{-5}	2.60×10^{-4}	1.86	3.26×10^{-4}	1.81
2^{-6}	6.81×10^{-5}	1.93	8.70×10^{-5}	1.91
2^{-7}	1.74×10^{-5}	1.97	2.25×10^{-5}	1.95
2^{-8}	4.41×10^{-6}	1.99	5.71×10^{-6}	1.98

Table 5.2: L^∞ errors and error orders of piecewise linear finite element method as $\delta \to 0$ to solution $x^4 - 2x^3 + x^2 - 1/30$.

Table 5.2 shows errors and error rates to the local limit of the piecewise linear finite element approximations as δ goes to 0 for a fixed small enough h (Column 2 and 3) and a fixed ratio of horizon size to mesh size (Column 4 and 5). From the table, we can see the convergence rate to the local limit is $\mathcal{O}(\delta^2)$. This example shows the asymptotic compatibility. More thorough discussion can be found in other references, for example [Du *et al.*, 2016b; Tao *et al.*, 2017; Tian and Du, 2013; Tian and Du, 2014].

For further illustration, we can also estimate the derivative of nonlocal solutions to see if it will recover the local Neumann boundary conditions as $\delta \to 0$. Table 5.3 shows that the numerical derivative of the nonlocal solution converges to the derivative of the local limit in the first order, where D_h is the numerical difference quotient operator (forward, backward or central). Moreover, when we only focus on the derivative at the boundary, we can find that for any δ, $u'_\delta(0) = u'_\delta(1) = 0$, which means the nonlocal solutions also satisfy the homogeneous Neumann conditions. For example, we can see this phenomenon in Fig. 5.2, where we fix $\delta = \frac{1}{8}$ and get the

δ	$\|D_h\mathbf{U}_\delta^h - \mathcal{I}_h u'\|_\infty$	Order
2^{-3}	3.83×10^{-2}	–
2^{-4}	2.11×10^{-2}	0.86
2^{-5}	1.11×10^{-2}	0.92
2^{-6}	5.74×10^{-3}	0.97
2^{-7}	2.93×10^{-3}	0.98
2^{-8}	1.47×10^{-3}	0.99

Table 5.3: L^∞ errors and error rates of the numerical derivative of u_δ to derivative of local solution: $4x^3 - 6x^2 + 2x$ as $\delta \to 0$.

corresponding u_δ.

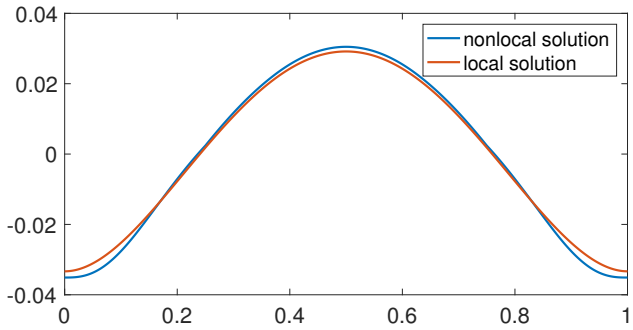

Figure 5.2: The nonlocal solution with $\delta = \frac{1}{8}$ and the local solution.

We would like to remark that we can get the same convergence results when using the smoother horizon shown in Fig. 5.1. The results are omitted here but more interesting examples of solving nonlocal problems by such horizon will be given shortly.

5.3.2 Nonlocal inhomogeneous Neumann problems

In this example, we present the numerical study on inhomogeneous nonlocal Neumann problems by both the smoother horizon shown in Fig. 5.1 with local boundary

conditions and the piecewise linear horizon (5.9) with auxiliary functions, which has been discussed in Section 5.1.3. Before that, we first give an example on the issue when imposing local inhomogeneous Neumann boundary conditions on the nonlocal model with the piecewise linear horizon (5.9). We discretize and solve the following equation:

$$B_\delta(u_\delta, v) = (f, v) + (g, v)_{\partial\Omega}\,, \tag{5.35}$$

where $u, v \in \mathcal{S}_\delta^N(\Omega)$, g is the Neumann boundary condition and $(\cdot,\cdot)_{\partial\Omega}$ denotes the boundary integration. In 1D domain $\Omega = (0, 1)$, it is defined by

$$(g, v)_{\partial\Omega} = u'(1)v(1) - u'(0)v(0)\,. \tag{5.36}$$

For illustration, we take an exact local solution $u = x^4 - 2x^3 + x^2 - 2x + 29/30$. Table 5.4 shows that the nonlocal solution only has first order convergence as $\delta \to 0$. Moreover, there are oscillations of derivatives with length 2δ at the boundary layers. See Fig. 5.3 for example where $\delta = 1/8$.

	numerical solution	
δ	L^∞ error	Order
2^{-3}	3.69×10^{-2}	–
2^{-4}	1.80×10^{-2}	1.03
2^{-5}	8.80×10^{-3}	1.03
2^{-6}	4.34×10^{-3}	1.02
2^{-7}	2.15×10^{-3}	1.01
2^{-8}	1.07×10^{-3}	1.00

Table 5.4: L^∞ errors and error rates of piecewise linear finite element approximations as $\delta \to 0$ to solution $x^4 - 2x^3 + x^2 - 2x + 29/30$ with the piecewise linear horizon function and inhomogeneous Neumann conditions, but without the use of auxiliary function.

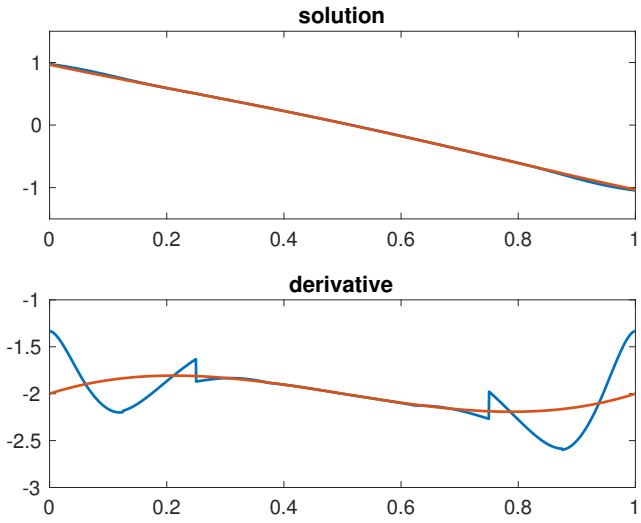

Figure 5.3: Derivatives oscillate around the boundary when imposing local Neumann boundary conditions on nonlocal models with piecewise linear variable horizon.

Instead, we can consider to use the auxiliary functions. Since $g = -2$ on the boundary, we can simply take $u_{\mathrm{a}}(x) = -2x$. Table 5.5 shows that the numerical solution and numerical derivative of the nonlocal case converges to its local limit, which means that this approach works and the boundary condition can still be achieved when the horizon vanishes.

Moreover, we can use the horizon shown in Fig. 5.1 without auxiliary functions and impose the local boundary conditions. As noted before, we use the constant δ to also represent the maximum value of $\delta(x)$. In order to check the asymptotic compatibility of this case, we instead fix $r = \delta/h$ and let $\delta \to 0$. Table 5.6 shows the convergence of numerical solution and numerical derivative to the local limit with a fixed $r = 2$ in L^∞ sense. The order of convergence for numerical derivatives can be confirmed as the optimal order, while the convergence of numerical solutions is close, but not exactly second order. More convincing data on second order convergence for the solutions are presented in Table 5.7, where one can see that the numerical solutions converge in an optimal order in L^2 norm.

	numerical solution		numerical derivative	
δ	L^∞ error	Order	L^∞ error	Order
2^{-3}	2.81×10^{-3}	–	3.82×10^{-2}	–
2^{-4}	9.47×10^{-4}	1.55	2.12×10^{-2}	0.85
2^{-5}	2.64×10^{-4}	1.84	1.13×10^{-2}	0.91
2^{-6}	5.99×10^{-5}	2.14	6.02×10^{-3}	0.91
2^{-7}	1.21×10^{-5}	2.28	3.00×10^{-3}	0.98
2^{-8}	3.12×10^{-6}	2.02	1.50×10^{-3}	0.99

Table 5.5: L^∞ errors and error rates of piecewise linear finite element approximations as $\delta \to 0$ to solution $x^4 - 2x^3 + x^2 - 2x + 29/30$ with the piecewise linear horizon function and inhomogeneous Neumann conditions.

	numerical solution		numerical derivative	
$r = 2$	L^∞ error	Order	L^∞ error	Order
$\delta = 0.02$	3.13×10^{-4}	–	1.96×10^{-2}	–
$\delta/2$	9.06×10^{-5}	1.79	9.90×10^{-3}	0.99
$\delta/4$	2.58×10^{-5}	1.81	4.97×10^{-3}	0.99
$\delta/8$	7.45×10^{-6}	1.79	2.49×10^{-3}	1.00
$\delta/16$	2.20×10^{-6}	1.76	1.25×10^{-3}	1.00

Table 5.6: L^∞ errors and error rates of piecewise linear finite element approximations as $\delta \to 0$ with fixed r to solution $x^4 - 2x^3 + x^2 - 2x + 29/30$ with C^2 horizon function and inhomogeneous Neumann conditions.

$r = 2$	$\|\mathbf{U}_\delta^h - \mathcal{I}_h u\|_2$	Order
δ	1.93×10^{-4}	–
$\delta/2$	4.98×10^{-5}	1.95
$\delta/4$	1.26×10^{-5}	1.99
$\delta/8$	3.19×10^{-6}	1.98
$\delta/16$	8.28×10^{-7}	1.95

Table 5.7: L^2 errors and error rates of piecewise linear finite element approximations as $\delta \to 0$ with fixed r to solution $x^4 - 2x^3 + x^2 - 2x + 29/30$ with C^2 horizon function and inhomogeneous Neumann conditions.

5.3.3 Nonlocal Dirichlet problems

In this example, we still calculate $f = f(x)$ based on the choice of a local limiting solution $u_0(x) = x^4 - 2x^3 + x^2 - 2x + 29/30$. Similar to the example given in Section 5.3.2, we can observe undesirable oscillations of the solution derivative around the boundary when directly imposing local Dirichlet boundary conditions on the nonlocal model with the piecewise linear horizon function. Therefore, we aim to solve the modified variational problem (5.27) with an auxiliary function $u_{\mathrm{a}} = \frac{b-a}{2}x^2 + ax^2$, where a and b are assumed to be the boundary derivatives of the local limiting solution at $x = 0$ and $x = 1$ respectively. In this example, we expect that $a = b = -2$. Table 5.8 shows that the numerical solution and numerical derivative of the nonlocal case again converge in an optimal order. The auxiliary function approach with extra unknowns still work in nonlocal Dirichlet problems. Moreover, from Column 4 of the table we can see that the assumption that $u_\delta - u_{\mathrm{a}}$ has homogeneous Neumann boundary conditions is satisfied for each δ.

Besides, if we use the horizon shown in Fig. 5.1 and impose the local boundary conditions, we can also get convergence of solutions and derivatives both in optimal orders. The results are listed in Table 5.9.

	numerical solution			numerical derivative	
δ	L^∞ error	Order	$u'_\delta(0)$	L^∞ error	Order
2^{-3}	3.09×10^{-3}	–	-2.00	3.80×10^{-2}	–
2^{-4}	9.46×10^{-4}	1.71	-2.00	2.09×10^{-2}	0.86
2^{-5}	2.60×10^{-4}	1.86	-2.00	1.09×10^{-2}	0.94
2^{-6}	6.81×10^{-5}	1.93	-2.00	5.57×10^{-3}	0.97
2^{-7}	1.74×10^{-5}	1.97	-2.00	2.81×10^{-3}	0.99
2^{-8}	4.41×10^{-6}	1.98	-2.00	1.41×10^{-3}	0.99

Table 5.8: L^∞ errors and error rates of piecewise linear finite element approximations as $\delta \to 0$ to solution $x^4 - 2x^3 + x^2 - 2x + 29/30$ as well as the solution derivatives at $x = 0$ (value of a) with the piecewise linear horizon function and Dirichlet conditions.

	numerical solution				numerical derivative	
$r = 2$	L^∞ error	Order	L^2 error	Order	L^∞ error	Order
$\delta = 0.02$	2.76×10^{-4}	–	1.54×10^{-4}	–	1.95×10^{-2}	–
$\delta/2$	7.92×10^{-5}	1.80	3.96×10^{-5}	1.96	9.87×10^{-3}	0.98
$\delta/4$	2.29×10^{-5}	1.79	1.03×10^{-5}	1.95	4.97×10^{-3}	0.99
$\delta/8$	6.78×10^{-6}	1.75	2.73×10^{-6}	1.91	2.49×10^{-3}	1.00
$\delta/16$	2.06×10^{-6}	1.72	7.42×10^{-7}	1.88	1.25×10^{-3}	1.00

Table 5.9: L^∞ and L^2 errors and error rates of piecewise linear finite element approximations as $\delta \to 0$ with fixed r to solution $x^4 - 2x^3 + x^2 - 2x + 29/30$ with C^2 horizon function and Dirichlet conditions.

5.3.4 Local-nonlocal coupled problems

The examples so far have introduced the auxiliary function approach on nonlocal diffusion models with various constraints. Furthermore, the numerical scheme is verified as the asymptotically compatible scheme. We now present how this method can be combined with local PDEs to stimulate coupled local and nonlocal models in a seamless fashion without overlapping domains. In Section 5.2, the coupled problems are presented with two different horizon functions, both cases are explored more in this example.

As a direct application of the last example, we first consider the same variable horizon used in previous examples with an auxiliary function $u_{\mathrm{a}}(x) = \frac{b-a}{2}x^2 + ax$ where $b = a - \int_{\Omega_+} f \, dx$. We discretize and solve the variational problem (5.31) and the compatibility condition (5.32). Table 5.10 shows the convergence of numerical solution and numerical derivative of the coupled case to the local limits. Moreover, we observe that for each δ, we can solve $u'_\delta(0)$ correctly as the mesh size goes to zero.

	numerical solution			numerical derivative	
δ	L^∞ error	Order	$u'_\delta(0)$	L^∞ error	Order
2^{-3}	3.09×10^{-3}	–	-2.00	3.80×10^{-2}	–
2^{-4}	9.46×10^{-4}	1.71	-2.00	2.09×10^{-2}	0.86
2^{-5}	2.60×10^{-4}	1.86	-2.00	1.09×10^{-2}	0.94
2^{-6}	6.81×10^{-5}	1.93	-2.00	5.57×10^{-3}	0.97
2^{-7}	1.74×10^{-5}	1.97	-2.00	2.81×10^{-3}	0.99

Table 5.10: L^∞ errors and error rates of piecewise linear finite element approximations of coupled problem as $\delta \to 0$ to solution $x^4 - 2x^3 + x^2 - 2x + 29/30$ as well as the solution derivatives at $x = 0$ (value of a) with the piecewise linear horizon function.

Another energy-based method is to consider the original energy functional (5.29) but with a smoother horizon function, which is shown in Fig. 5.1. Again we fix

	numerical solution				numerical derivative	
$r = 2$	L^∞ error	Order	L^2 error	Order	L^∞ error	Order
$\delta = 0.02$	2.95×10^{-4}	–	1.74×10^{-4}	–	1.29×10^{-1}	–
$\delta/2$	8.49×10^{-5}	1.79	4.49×10^{-5}	1.95	6.49×10^{-2}	1.00
$\delta/4$	2.43×10^{-5}	1.80	1.15×10^{-5}	1.97	3.25×10^{-2}	1.00
$\delta/8$	7.12×10^{-6}	1.77	2.97×10^{-6}	1.95	1.62×10^{-2}	1.00
$\delta/16$	2.13×10^{-6}	1.74	7.86×10^{-7}	1.92	8.12×10^{-3}	1.00

Table 5.11: L^∞ and L^2 errors and error rates of piecewise linear finite element approximations of coupled problem as $\delta \to 0$ with fixed r to solution $x^4-2x^3+x^2-2x+29/30$ with C^2 horizon function.

$r = \delta/h$ and let $\delta \to 0$ since the model will get localized as the maximum value of horizon vanishes. Table 5.11 shows that the numerical solution and numerical derivative converge to the local limits with a fixed $r = 2$ both in optimal orders. For the convergence of numerical solutions, one can see this more clearly with respect to the L^2 norm.

Although the solution derivatives can converge as $\delta \to 0$, this model does not satisfy the patch test, which could lead to the existence of ghost forces. However, the ghost forces vanishes as $\delta \to 0$. They are also much smaller than those produced in the case with $\delta(x) = \min(x, \delta, 1 - x)$ but without an auxiliary function. In Fig. 5.4, we choose a linear profile $u(x) = -2x + 1$ which implies a zero source term. We can see that the ghost strains vanish as δ decreases. Although we cannot pass the patch test for a fixed $\delta > 0$, the ghost forces do not affect the convergence of solution derivatives and they get reduced with smaller δ.

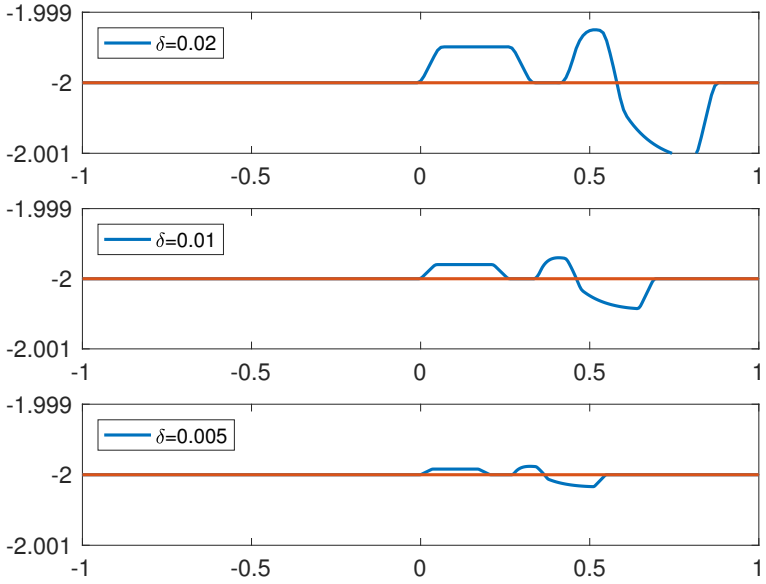

Figure 5.4: In patch test, ghost forces vanish as $\delta \to 0$.

5.4 Discussion

In this chapter, we have developed a linear nonlocal model with a spatially varying horizon that captures a spatial change of scales in nonlocal interactions. Our work has extended existing studies on the nonlocal diffusion and nonlocal peridynamic models, and their finite element discrete approximations.

On the modeling side, we are able to significantly expand the nonlocal modeling technique by allowing heterogeneous localization. The latter in turn offers, in particular, a way to pose local boundary value problems for nonlocal models and provides a seamless coupling of local and nonlocal models. Our studies here, though limited to one space space, are quite extensive as they have covered a number of cases involving piecewise linear or smooth horizons, homogeneous and inhomogeneous, local or nonlocal, and Neumann or Dirichlet constraints.

On the computational side, we have demonstrated that the asymptotically compatible schemes are naturally designed for nonlocal problems with a heterogeneously defined horizon that can be positive and zero in different part of the computational domain. They provide the necessary robustness with respect to the change of length

scales.

We note that the current work is largely based on a simple one-dimensional linear model with a simple representative kernel for the sake of offering insight without being impeded by tedious calculations. In our numerical experiments, the computational mesh is taken to be uniform since a smooth solution is assumed. While these serve the purpose of illustration well, additional complications may arise in practice. It will be interesting to study further extensions to more general models in higher dimensions and more general discretization, as well as more applications in real physical processes.

Bibliography

[Aguiar and Fosdick, 2014] Adair R Aguiar and Roger Fosdick. A constitutive model for a linearly elastic peridynamic body. *Mathematics and Mechanics of Solids*, 19(5):502–523, 2014.

[Aksoylu and Parks, 2011] Burak Aksoylu and Michael L Parks. Variational theory and domain decomposition for nonlocal problems. *Applied Mathematics and Computation*, 217(14):6498–6515, 2011.

[Alali and Gunzburger, 2015] Bacim Alali and Max Gunzburger. Peridynamics and material interfaces. *Journal of Elasticity*, 120(2):225–248, 2015.

[Andreu-Vaillo *et al.*, 2010] Fuensanta Andreu-Vaillo, José M Mazón, Julio D Rossi, and J Julián Toledo-Melero. *Nonlocal diffusion problems*. Number 165. American Mathematical Soc., 2010.

[Askari *et al.*, 2008] E Askari, F Bobaru, RB Lehoucq, ML Parks, SA Silling, and O Weckner. Peridynamics for multiscale materials modeling. In *Journal of Physics: Conference Series*, volume 125, page 012078. IOP Publishing, 2008.

[Barles *et al.*, 2014a] Guy Barles, Emmanuel Chasseigne, Christine Georgelin, and Espen Jakobsen. On neumann type problems for nonlocal equations set in a half space. *Transactions of the American Mathematical Society*, 366(9):4873–4917, 2014.

[Barles *et al.*, 2014b] Guy Barles, Christine Georgelin, and Espen R Jakobsen. On neumann and oblique derivatives boundary conditions for nonlocal elliptic equations. *Journal of Differential Equations*, 256(4):1368–1394, 2014.

[Bessa *et al.*, 2014] MA Bessa, JT Foster, T Belytschko, and Wing Kam Liu. A meshfree unification: reproducing kernel peridynamics. *Computational Mechanics*, 53(6):1251–1264, 2014.

[Bobaru and Zhang, 2015] Florin Bobaru and Guanfeng Zhang. Why do cracks branch? a peridynamic investigation of dynamic brittle fracture. *International Journal of Fracture*, 196(1-2):59–98, 2015.

[Bourgain *et al.*, 2001] Jean Bourgain, Haim Brezis, and Petru Mironescu. Another look at sobolev spaces. 2001.

[Buades *et al.*, 2005] Antoni Buades, Bartomeu Coll, and J-M Morel. A non-local algorithm for image denoising. In *Computer Vision and Pattern Recognition, 2005. CVPR 2005. IEEE Computer Society Conference on*, volume 2, pages 60–65. IEEE, 2005.

[Chen and Gunzburger, 2011] Xi Chen and Max Gunzburger. Continuous and discontinuous finite element methods for a peridynamics model of mechanics. *Computer Methods in Applied Mechanics and Engineering*, 200(9-12):1237–1250, 2011.

[Cortazar *et al.*, 2008] Carmen Cortazar, Manuel Elgueta, Julio D Rossi, and Noemi Wolanski. How to approximate the heat equation with neumann boundary conditions by nonlocal diffusion problems. *Archive for Rational Mechanics and Analysis*, 187(1):137–156, 2008.

[D'Elia *et al.*, 2016] Marta D'Elia, Mauro Perego, Pavel Bochev, and David Littlewood. A coupling strategy for nonlocal and local diffusion models with mixed volume constraints and boundary conditions. *Computers & Mathematics with Applications*, 71(11):2218–2230, 2016.

[Dipierro *et al.*, 2014] Serena Dipierro, Xavier Ros-Oton, and Enrico Valdinoci. Nonlocal problems with neumann boundary conditions. *arXiv preprint arXiv:1407.3313*, 2014.

[Du and Yang, 2016] Qiang Du and Jiang Yang. Asymptotically compatible fourier spectral approximations of nonlocal allen–cahn equations. *SIAM Journal on Numerical Analysis*, 54(3):1899–1919, 2016.

[Du *et al.*, 2012] Qiang Du, Max Gunzburger, Richard B Lehoucq, and Kun Zhou. Analysis and approximation of nonlocal diffusion problems with volume constraints. *SIAM review*, 54(4):667–696, 2012.

[Du *et al.*, 2013a] Qiang Du, Max Gunzburger, RB Lehoucq, and Kun Zhou. Analysis of the volume-constrained peridynamic navier equation of linear elasticity. *Journal of Elasticity*, 113(2):193–217, 2013.

[Du *et al.*, 2013b] Qiang Du, Max Gunzburger, Richard B Lehoucq, and Kun Zhou. A nonlocal vector calculus, nonlocal volume-constrained problems, and nonlocal balance laws. *Mathematical Models and Methods in Applied Sciences*, 23(03):493–540, 2013.

[Du *et al.*, 2016a] Qiang Du, Robert Lipton, and Tadele Mengesha. Multiscale analysis of linear evolution equations with applications to nonlocal models for heterogeneous media. *ESAIM: Mathematical Modelling and Numerical Analysis*, 50(5):1425–1455, 2016.

[Du *et al.*, 2016b] Qiang Du, Yunzhe Tao, Xiaochuan Tian, and Jiang Yang. Robust a posteriori stress analysis for quadrature collocation approximations of nonlocal models via nonlocal gradients. *Computer Methods in Applied Mechanics and Engineering*, 310:605–627, 2016.

[Du *et al.*, 2017a] Qiang Du, Yunzhe Tao, and Xiaochuan Tian. A peridynamic model of fracture mechanics with bond-breaking. *Journal of Elasticity*, pages 1–22, 2017.

[Du *et al.*, 2017b] Qiang Du, Jiang Yang, and Zhi Zhou. Analysis of a nonlocal-in-time parabolic equation. *Discrete & Continuous Dynamical Systems-B*, 22(2):339–368, 2017.

[Du *et al.*, 2018a] Qiang Du, Xingjie Helen Li, Jianfeng Lu, and Xiaochuan Tian. A quasi-nonlocal coupling method for nonlocal and local diffusion models. *SIAM Journal on Numerical Analysis*, 56(3):1386–1404, 2018.

[Du *et al.*, 2018b] Qiang Du, Yunzhe Tao, and Xiaochuan Tian. Nonlocal models with heterogeneous localization and their application to seamless local-nonlocal coupling. *Submitted*, 2018.

[Du *et al.*, 2018c] Qiang Du, Yunzhe Tao, Xiaochuan Tian, and Jiang Yang. Asymptotically compatible discretization of multidimensional nonlocal diffusion models and approximation of nonlocal green's functions. *IMA Journal of Numerical Analysis*, 2018.

[Du, 2016] Qiang Du. Local limits and asymptotically compatible discretizations. In *Handbook of Peridynamic Modeling*, pages 125–146. Chapman and Hall/CRC, 2016.

[Du, 2018] Qiang Du. An invitation to nonlocal modeling, analysis and computation. In *Proceedings International Congress of Mathematicians*, volume 3, pages 3523–3552, 2018.

[Du, 2019] Qiang Du. *Nonlocal modeling, analysis and computation*. SIAM, 2019.

[Emmrich and Puhst, 2013] Etienne Emmrich and Dimitri Puhst. Well-posedness of the peridynamic model with lipschitz continuous pairwise force function. *Communications in Mathematical Sciences*, 11(4):1039–1049, 2013.

[Emmrich and Puhst, 2016] Etienne Emmrich and Dimitri Puhst. A short note on modeling damage in peridynamics. *Journal of Elasticity*, 123(2):245–252, 2016.

[Emmrich *et al.*, 2007] Etienne Emmrich, Olaf Weckner, et al. On the well-posedness of the linear peridynamic model and its convergence towards the navier equation of linear elasticity. *Communications in Mathematical Sciences*, 5(4):851–864, 2007.

[Ha and Bobaru, 2010] Youn Doh Ha and Florin Bobaru. Studies of dynamic crack propagation and crack branching with peridynamics. *International Journal of Fracture*, 162(1-2):229–244, 2010.

[Hu *et al.*, 2012] Wenke Hu, Youn Doh Ha, and Florin Bobaru. Peridynamic model for dynamic fracture in unidirectional fiber-reinforced composites. *Computer Methods in Applied Mechanics and Engineering*, 217:247–261, 2012.

[Lehoucq and Silling, 2008] Richard B Lehoucq and Stewart A Silling. Force flux and the peridynamic stress tensor. *Journal of the Mechanics and Physics of Solids*, 56(4):1566–1577, 2008.

[Lehoucq *et al.*, 2008] Richard B Lehoucq, Stewart Andrew Silling, Steven James Plimpton, and Michael L Parks. Peridynamics with lammps: a user guide. Technical report, Sandia National Laboratories, 2008.

[Lipton, 2014] Robert Lipton. Dynamic brittle fracture as a small horizon limit of peridynamics. *Journal of Elasticity*, 117(1):21–50, 2014.

[Liu *et al.*, 1996] Wing Kam Liu, Y Chen, S Jun, JS Chen, T Belytschko, C Pan, RA Uras, and CT Chang. Overview and applications of the reproducing kernel particle methods. *Archives of Computational Methods in Engineering*, 3(1):3–80, 1996.

[Mengesha and Du, 2013] Tadele Mengesha and Qiang Du. Analysis of a scalar peridynamic model with a sign changing kernel. *Discrete Contin. Dynam. Systems B*, 18:1415–1437, 2013.

[Mengesha and Du, 2014a] Tadele Mengesha and Qiang Du. The bond-based peridynamic system with dirichlet-type volume constraint. *Proceedings of the Royal Society of Edinburgh Section A: Mathematics*, 144(1):161–186, 2014.

[Mengesha and Du, 2014b] Tadele Mengesha and Qiang Du. Nonlocal constrained value problems for a linear peridynamic navier equation. *Journal of Elasticity*, 116(1):27–51, 2014.

[Mengesha and Du, 2015] Tadele Mengesha and Qiang Du. On the variational limit of a class of nonlocal functionals related to peridynamics. *Nonlinearity*, 28(11):3999, 2015.

[Mengesha and Du, 2016] Tadele Mengesha and Qiang Du. Characterization of function spaces of vector fields and an application in nonlinear peridynamics. *Nonlinear Analysis*, 140:82–111, 2016.

[Mitchell *et al.*, 2015] John Mitchell, Stewart Silling, and David Littlewood. A position-aware linear solid constitutive model for peridynamics. *Journal of Mechanics of Materials and Structures*, 10(5):539–557, 2015.

[Monaghan, 2005] Joe J Monaghan. Smoothed particle hydrodynamics. *Reports on progress in physics*, 68(8):1703, 2005.

[Oterkus and Madenci, 2012] Erkan Oterkus and Erdogan Madenci. Peridynamic analysis of fiber-reinforced composite materials. *Journal of Mechanics of Materials and Structures*, 7(1):45–84, 2012.

[Palatucci *et al.*, 2013] Giampiero Palatucci, Ovidiu Savin, and Enrico Valdinoci. Local and global minimizers for a variational energy involving a fractional norm. *Annali di matematica pura ed applicata*, 192(4):673–718, 2013.

[Seleson and Gunzburger, 2010] Pablo Seleson and Max Gunzburger. Bridging methods for atomistic-to-continuum coupling and their implementation. *Communications in Computational Physics*, 7(4):831, 2010.

[Seleson *et al.*, 2013a] Pablo Seleson, Samir Beneddine, and Serge Prudhomme. A force-based coupling scheme for peridynamics and classical elasticity. *Computational Materials Science*, 66:34–49, 2013.

[Seleson *et al.*, 2013b] Pablo Seleson, Max Gunzburger, and Michael L Parks. Interface problems in nonlocal diffusion and sharp transitions between local and nonlocal domains. *Computer Methods in Applied Mechanics and Engineering*, 266:185–204, 2013.

[Seleson *et al.*, 2015] Pablo Seleson, Youn Doh Ha, and Samir Beneddine. Concurrent coupling of bond-based peridynamics and the navier equation of classical elasticity by blending. *International Journal for Multiscale Computational Engineering*, 13(2), 2015.

[Silling and Lehoucq, 2010] Stewart A Silling and RB Lehoucq. Peridynamic theory of solid mechanics. In *Advances in applied mechanics*, volume 44, pages 73–168. Elsevier, 2010.

[Silling *et al.*, 2003] STEWART A Silling, Markus Zimmermann, and Rohan Abeyaratne. Deformation of a peridynamic bar. *Journal of Elasticity*, 73(1-3):173–190, 2003.

[Silling *et al.*, 2007] Stewart A Silling, M Epton, O Weckner, J Xu, and E Askari. Peridynamic states and constitutive modeling. *Journal of Elasticity*, 88(2):151–184, 2007.

[Silling *et al.*, 2010] SA Silling, O Weckner, E Askari, and Florin Bobaru. Crack nucleation in a peridynamic solid. *International Journal of Fracture*, 162(1-2):219–227, 2010.

[Silling *et al.*, 2015] Stewart Silling, David Littlewood, and Pablo Seleson. Variable horizon in a peridynamic medium. *Journal of Mechanics of Materials and Structures*, 10(5):591–612, 2015.

[Silling, 2000] Stewart A Silling. Reformulation of elasticity theory for discontinuities and long-range forces. *Journal of the Mechanics and Physics of Solids*, 48(1):175–209, 2000.

[Tao *et al.*, 2017] Yunzhe Tao, Xiaochuan Tian, and Qiang Du. Nonlocal diffusion and peridynamic models with neumann type constraints and their numerical approximations. *Applied Mathematics and Computation*, 305:282–298, 2017.

[Tian and Du, 2013] Xiaochuan Tian and Qiand Du. Analysis and comparison of different approximations to nonlocal diffusion and linear peridynamic equations. *SIAM Journal on Numerical Analysis*, 51(6):3458–3482, 2013.

[Tian and Du, 2014] Xiaochuan Tian and Qiang Du. Asymptotically compatible schemes and applications to robust discretization of nonlocal models. *SIAM Journal on Numerical Analysis*, 52(4):1641–1665, 2014.

[Tian and Du, 2017] Xiaochuan Tian and Qiang Du. Trace theorems for some nonlocal function spaces with heterogeneous localization. *SIAM Journal on Mathematical Analysis*, 49(2):1621–1644, 2017.

[Tian *et al.*, 2015] Hao Tian, Lili Ju, and Qiang Du. Nonlocal convection–diffusion problems and finite element approximations. *Computer Methods in Applied Mechanics and Engineering*, 289:60–78, 2015.

[Tian, 2017] Xiaochuan Tian. *Nonlocal models with a finite range of nonlocal interactions*. Columbia University, 2017.

[Tupek and Radovitzky, 2014] MR Tupek and R Radovitzky. An extended constitutive correspondence formulation of peridynamics based on nonlinear bond-strain measures. *Journal of the Mechanics and Physics of Solids*, 65:82–92, 2014.

[Turner *et al.*, 2015] Daniel Z Turner, Richard B Lehoucq, and Phillip L Reu. A nonlocal strain measure for digital image correlation. Technical report, Sandia National Lab.(SNL-NM), Albuquerque, NM (United States), 2015.

[Wang and Tian, 2012] Hong Wang and Hao Tian. A fast galerkin method with efficient matrix assembly and storage for a peridynamic model. *Journal of Computational Physics*, 231(23):7730–7738, 2012.

[Zhou and Du, 2010] Kun Zhou and Qiang Du. Mathematical and numerical analysis of linear peridynamic models with nonlocal boundary conditions. *SIAM Journal on Numerical Analysis*, 48(5):1759–1780, 2010.

[Zienkiewicz and Zhu, 1992] Olgierd Cecil Zienkiewicz and Jian Zhong Zhu. The superconvergent patch recovery and a posteriori error estimates. part 2: Error estimates and adaptivity. *International Journal for Numerical Methods in Engineering*, 33(7):1365–1382, 1992.